Chem Soc Rev

Developing High Safety Li-Metal Anode for Future High-Energy Li-Metal Batteries: Strategies and Perspectives

Journal:	*Chemical Society Reviews*
Manuscript ID	CS-SYN-09-2019-000636.R3
Article Type:	Review Article
Date Submitted by the Author:	03-May-2020
Complete List of Authors:	Liu, Daihuo; Henan Normal University, Key Laboratory of Green Chemical Media and Reactions, Ministry of Education, Collaborative Innovation Center of Henan Province for Green Manufacturing of Fine Chemicals, School of Chemistry and Chemical Engineering Bai, Zhengyu; Henan Normal University, Key Laboratory of Green Chemical Media and Reactions, Ministry of Education, Collaborative Innovation Center of Henan Province for Green Manufacturing of Fine Chemicals, School of Chemistry and Chemical Engineering Li, Matthew; University of Waterloo, Chemical Engineering Yu, Aiping; University of Waterloo, Chemical Engineering Luo, Dan; University of Waterloo, Chemical Engineering Liu, Wenwen; University of Waterloo, Yang, Lin; Henan Normal University Lu, Jun; Argonne National Laboratory, Chemical Science and Engineering Division Amine, Khalil; Argonne National Laboratory, Chen, Zhongwei; University of Waterloo, Chemical Engineering

Developing High Safety Li-Metal Anode for Future High-Energy Li-Metal Batteries: Strategies and Perspectives

Dai-Huo Liu,[a,e] Zheng-Yu Bai,[a]* Matthew Li,[e] Aiping Yu,[e] Dan Luo,[e] Wenwen Liu,[e] Lin Yang,[a] Jun Lu,[b] Khalil Amine [b,c,d]* and Zhongwei Chen[e]*

a Key Laboratory of Green Chemical Media and Reactions, Ministry of Education, Collaborative Innovation Center of Henan Province for Green Manufacturing of Fine Chemicals, School of Chemistry and Chemical Engineering, Henan Normal University, Xinxiang 453007, Henan, P. R. China. Email: baizhengyu@htu.cn

b Chemical Sciences and Engineering Division, Argonne National Laboratory, 9700 South Cass Avenue, Lemont, Illinois 60439, United States, Email: amine@anl.gov

c Department of Material Science and Engineering, Stanford University, Stanford, CA 94305, USA

d Institute for Research and Medical Consultations (IRMC), Imam Abdulrahman Bin Faisal University (IAU), Dammam, 34212 Saudi Arabia

e Department of Chemical Engineering, Waterloo Institute for Nanotechnology, Waterloo Institute for Sustainable Energy, Waterloo University, 200 University Avenue West, Waterloo, Ontario N2L 3G1, Canada. E-mail: zhwchen@uwaterloo.ca

Developing high-safety Li-metal Anode (LMA) is extremely important for the application of high-energy Li-metal batteries (LMBs), especially Li-S and Li-O_2 batteries systems. However, the notorious Li-dendrite growth problem results in serious safety concerns for any energy storage application. Through a recent combination of interface-based science, nanotechnology-based solutions and characterization methods, LMA is now primed for a technological boom. In this review, we summarize recent emerging strategies and perspectives on LMA, followed by highlighting the current huge evolution in interface chemistry regulation, optimizing electrolyte components, designing a rational 'host' for lithium metal, optimal strategies "solid-state electrolytes" and other emerging strategies for developing high-safety LMA. Furthermore, several state-of-the-art in situ/operando synchrotron-based X-ray techniques for high safety LMBs research are introduced. With the further development on LMA in the future, subsequent application in high energy LMBs are to be expected.

1. Introduction

Using metallic lithium as a battery anode has been one of the most promising direction towards high-energy Li-metal batteries (LMBs). This is mostly due to its ideally host-less nature and low redox potential.[1-7] Accordingly, LMA has been indispensable for next-generation high-energy Li-S and Li-air systems, both of which are highly investigated future energy storage devices (ESDs).[8-11] Unfortunately, the development of Li-metal anode (LMA) has be hindered due to the formation of dendritic lithium during the charge/discharge processes, which result in severe and sporadic safety concerns.[1, 2, 12, 13] Therefore, developing high safety and high-energy-density LMBs beyond Li-ion batteries (LIBs) is extremely urgent to better satisfy the increasing demands for high safety and high energy density ESDs.

In recent decades, great efforts have been devoted to solve the aforementioned safety problems. Several emerging strategies are used in suppression lithium dendrite growth such as regulating the interface of LMA, optimizing electrolyte formulations, designing nanostructured LMA and developing solid-state electrolytes (SSEs) among others. Firstly, strategies of interfacial chemistry regulation, including artificial solid electrolyte interphase (SEI)/metallic Li interface,[5, 14-22] artificial lithium protective layer,[23-33] dual-layered film protected LMA,[34] and controlling the dendrite growth direction by interfacial regulation[12, 35-38] can improve the interfacial stability of SEI layer. Secondly, strategies of optimizing electrolyte, including altering the electrolyte components,[39-41] suitable salts and electrolyte concentrations,[42-46] introducing electrolyte additives[47, 48] and pretreatment of the electrodes in ionic liquid electrolytes before battery assembly[49] can also stabilize the interface of LMA and restrain the formation of lithium dendrite. Thirdly, strategies of engineering LMA, including nanostructured three dimensional (3D) conducting scaffolds of Li/carbon composite anodes,[50-65] directing lateral growth of Li-dendrites,[66, 67] design particular current collector skeleton,[57, 68-70] vertical-aligned nanochannels,[71] glass fiber modified Cu foil electrode[72] and overlithiation of mesoporous AlF_3 framework[73] have also been shown to be able to delay or suppress dendrite growth. Lastly, the optimal solution should be SSEs instead of liquid electrolytes, which benefits from the comparatively low amount of combustible chemicals in the cell.[13, 74-79] With the development of nanotechnology and advanced characterization techniques, LMA appears to be approaching a commercial reality.

To develop and revive high safety LMA for future high-energy LMBs, this review aims to provide some emerging strategies for improving safety problems caused by dendritic lithium growth and to summarize some of the recent methodologies, novel composites and emerging characterization techniques. Firstly, the formation and growth mechanisms of Li dendrites are described detailedly. Secondly, the main development roadmap of LMA in LMBs is presented in detail. We will then summarize recently emerging strategies and perspectives for developing high-safety LMA, which can be classified into five categories: (i) interfacial chemistry regulation; (ii) optimizing electrolyte components; (iii) designing a rational 'host' for LMA; (iv) optimal strategy "SSEs" and (v) other emerging strategies for developing high energy LMA. We next specify the realization channels of high safety LMA via the evolution of characterization techniques and nanotechnology progress from primeval liquid electrolytes to ultimate solution "SSEs". In brief, this review aims to present some recently emerging strategies and offer a few foresightedness perspectives for improvement safety concerns caused by lithium dendrite growth, which can offer a farsighted guidance to achieve the practical application of high safety LMBs.

2. The formation and growth mechanisms of Li dendrites

Recent progress indicates that an electric double layer would be formed at the electrode/electrolyte interface before any interfacial chemistry happens or during the initial charging, which foreknows the eventual interfacial chemistry.[1, 2] Particularly, a dense, thin and inorganic inner SEI layer would be formed due to the negatively charged electrode surface repels the salt anions (e.g. F^- etc.) from the inner layer, which is responsible for insulating electrons and conducting Li-ions.[67] Thereafter, the organic-rich and electrolyte-permeable outer layer begin occurrence.[67] Finally, a heterogeneous SEI layer on the surface of LMA was formed by the self-assembly of electrolyte solvent molecules (Fig. 1a, SEI formation).[67] The next process is lithium nucleation where some sphere-like lithium nucleuses appeared at the SEI/LMA interface during the charging process or Li deposition, and the grew diameter of nucleus's is proportional to the square root of time (Fig. 1a, Li nucleation).[2, 80-83] To follow, some lithium dendrites (such as needle-like, moss-like, whisker-like or branch-like dendrites) begin to grow from their root driving the nucleuses away from the LMA at a big rate.[2, 80, 84, 85] The morphologies of Li dendrites are affected by pressure, temperature, current density, electrolyte composition and interface physical/chemical properties.[2, 80, 84-88] Once the dendrite sprouts out, the growing dendrite drives the Li particles upwards (Fig. 1a, dendritic growth).[2, 84] Finally, a lot of dendrites stop grew longitudinally along with the used voltage increased, but are usually bent to collapse in an abrupt manner, which has been attributed to the large axial compressive load on the tenuous dendrite (Fig. 1a, dendritic collapse or pulverization).[2, 84, 89, 90] After a long-term cycle, a porous lithium electrode with some inactive/dead Li and dendrites are formed, in which the long dendrite can easily cause cell short circuit.[2, 13, 80, 84, 85]

To solve this issue of uncontrollable dendrite growth, there is a need for improving the fundamental understanding to the growth mechanism and electro-chemo-mechanical behaviour of lithium dendrites. Recently, Wang[84] and Huang[2]

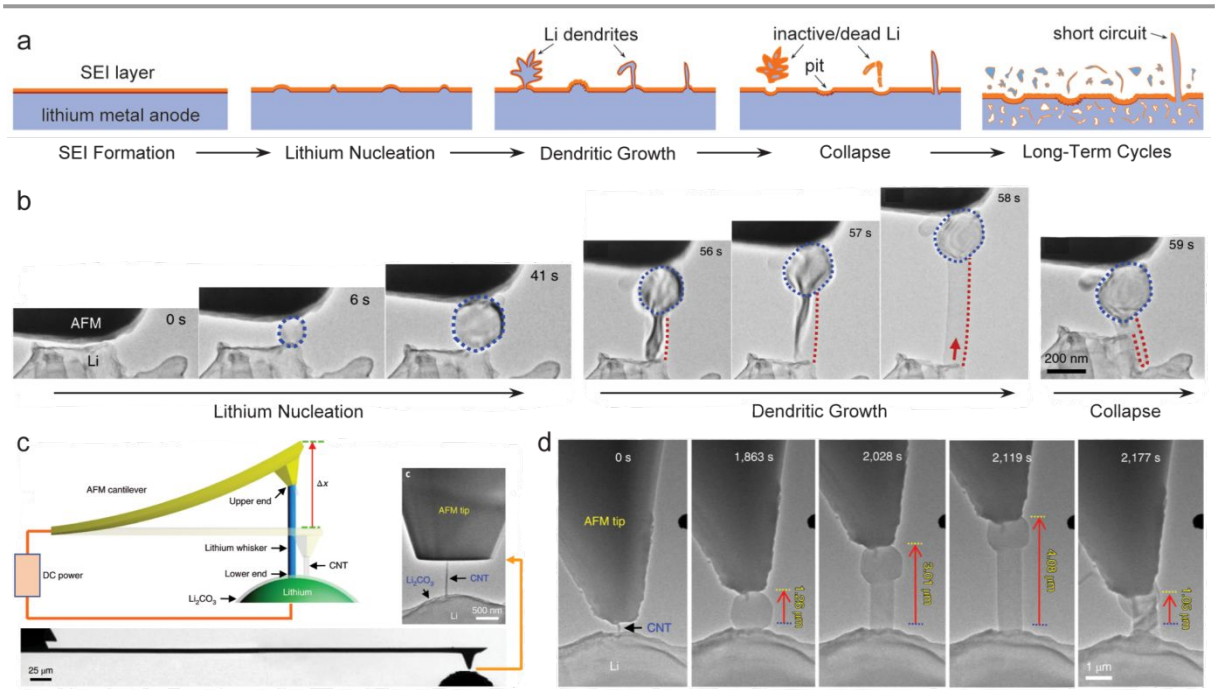

Fig. 1 a) The evolution schematic of the formation and growth of Li dendrites. b) In situ TEM images of lithium nucleation, whisker growth and collapse processes (the red arrow shows the growth direction of Li whisker, blue dotted ring is lithium nucleus).[84] b) Reproduced with permission from ref. 84. Copyright 2019, Nature Publishing Group; c) Schematic of the AFM–TEM configuration applied for the survey of lithium dendrite growth, and d) real-time TEM images of dendrite growth.[2] c and d) Reproduced with permission from ref. 2. Copyright 2020, Nature Publishing Group.

directly observe the nucleation and dendrite growth behaviour of lithium whiskers by coupling an in situ atomic force microscopy (AFM) cantilever into an open-cell device in transmission electron microscopy (TEM, Fig. 1b-d). Wang and co-workers[84] found that a single crystalline lithium particle slowly nucleates during lithium deposition without any preferential growth orientation as shown in Fig. 1b, and the lithium nucleation process was dominated by the surface energies. Once the whisker sprout, the whisker will push the nucleation upwards, which shows a tip-growth behaviour and promotes a local lithium deposition at the whisker/SEI interface. The continuous growth whisker will eventually collapse because the AFM cantilever exerts an incremental counterforce. Huang and co-workers[2] recently also observed these same phenomena by using the similar technique (Fig. 1d), they analysed in detail the three stages of nucleation, growth and collapse of lithium whisker and obtained the strength of whiskers under mechanical loading (~244 MPa). These quantitative data are beneficial to design of lithium dendrite restrain strategies in high energy LMBs. Furthermore, the sluggish interface transport of lithium is very crucial to the subsequent lithium deposition morphology.[84]

In terms of dendrite growth mechanisms, García and co-workers[88] report three unreported dendrite growth mechanisms based on the thermodynamically consistent theory: i) The stress is relaxed near to the base, and the electrodeposited surface is electrochemically shielded, where no electrodeposition/electrodissolution occurs; ii) stress-induced electrodeposition/electrodissolution on these interfaces firsthand facing each other, forming a self-sustained overpotential that shoves the lithium dendrites towards the cathode; iii) the local, lateral extrusion can be seen in those side branches undergoing non-hydrostatic stresses. Meanwhile, six regimes of lithium dendrite growth are proposed (thermodynamic repression regime, incubation regime, base-controlled regime, tip-controlled regime, mixed regime, and Sand's regime).[88] These theories offer a roadmap to understand the structural evolution mechanisms suppressing dendrite growth.

3. Emerging strategies and perspectives for improving safety concerns of LMA

On the basis of the previous mechanistic and theoretical research, Li have a tendency to plate in a non-uniform manner. Li plating in commercial LIBs have been identified as one of the leading causes for well-reported battery fires.[91] Therefore, researchers hope to develop a high-safety dendrite-free LMA without dead-Li formation during lithium plating/stripping as shown in Fig. 2, the former can well address the safety concerns, while the latter can effectively improve the utilization of

Li during the Li plating/stripping, and hence improve Coulombic efficiency (CE) and cycle lifespan of LMBs, both of which play a decisive role to the application of future high-safety LMBs. Various emerging strategies have been proposed to develop dendrite-free deposition and restrain Li dendrite growth[92, 93]: 1) the homogeneous Li-ion flux distribution on the surface of LMA via optimizing electrolyte is crucial for the uniform nucleation of Li and dendrite-free growth on the surface of LMA; 2) Reconstructing LMA via designing a lithiophilic Li-matrix composites could allow effective Li entrapment and decrease the volume fluctuations of LMA during discharging/charging; 3) a robust artificial SEI film with strong mechanical strength, uniformly distributed channel for Li^+ diffusion, and low interfacial resistance is also expected to suppress Li dendrites growth above the LMA; 4) the CE can be easily enhanced by reactivating the dead-Li or improving the utilization of Li; 5) the problematic lithium dendrite can be further suppressed by regulating the interface chemistry between electrode and electrolyte. Recently emerging strategies and perspectives to develop and characterize LMA are elaborately summarized.

3.1. Strategies of interfacial chemistry regulation

Li metal is an extremely reactivity and reacts readily with most electrolytes.[91] The reaction products were first found by

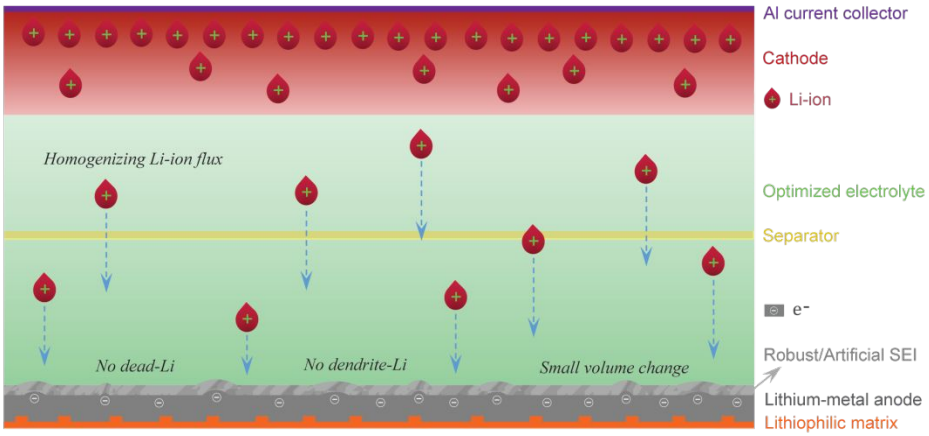

Fig. 2 The schematic illustration of an ideal high-safety LMA without dendrite-Li and dead-Li for future high-energy LMBs.

Dey[94] in 1970 and called as SEI film by Peled[95] in 1979. In contrast to the SEI on graphite (commercially established anode for LIBs), the thin SEI films on the surface of LMA are generally unstable, heterogeneous and fragile during repeated discharging/charging and the associated volume changes. This results in an adverse effect on the electrochemical performance and cycle life of LMBs.[91, 96, 97] Probing into the causes of dendrite formation, the uneven electric field distribution, rough surface, microscopic protrusions, and non-uniform supply of Li-ion flux are harmful factors that accelerate dendrite formation.[15, 98] Therefore, the dynamic stability of SEI film is extremely critical to achieve superior energy storage performance and long cycle life. Currently, many researchers have devoted much effort to the engineering and construction of robust SEI films *via* interfacial chemistry regulation, including artificial SEI/metallic Li interface,[5, 14-21] artificial lithium protective layer,[23-33] dual-layered film protected LMA,[34] and controlling the dendrite growth direction by interfacial regulation.[12]

3.1.1. An armored mixed conductor interphase

There are many approaches have been presented to develop dendrite-free LMA by in/ex situ formation of robust SEI.[14, 15, 23-25, 27, 34, 99] The robust SEI should possess strong mechanical strength,[25] low interfacial resistance[100, 101] and uniformly distributed channel for Li-ion diffusion[15]. These features are also the key strategies in the interfacial chemistry regulation of LMA, which could effectively suppress the Li dendrites growth and hence greatly extend the lifespan of LMBs.[74, 75, 102]

Recently, a new strategy was put forward where a mixed ionic/electronic conductor interface (abbreviated as MCI) was constructed on the surface of LMA via a facile displacement reaction at room temperature.[25] The armored LiF/Cu protective MCI membrane on the LMA surface is derived from a controllable displacement reactions ($CuF_2 + 2Li \rightarrow 2LiF + Cu$), the rough surface of the routine LMA is fully smoothed by the replacement reaction, which is beneficial for homogenizing Li-ion flux (Fig. 3a). In addition, the LiF reinforced hybrid MCI exhibits much higher Young's modulus (12.9 GPa) than the routine SEI (0.63 GPa) on the surface of LMA obtained by atomic force microscope, far more than the 6.0 GPa to restrain dendritic lithium growth. These features indicate that armored MCI can well stabilize the interphases of LMA and suppress the growth of Li dendrite (Fig. 3b). Therefore, the armored MCI film endow the cells with a decreased

resistance, small polarization (0.18 V in the symmetrical Li cells), high ionic conductivity, long life (for example, the lifespan of $LiNi_{0.5}Co_{0.2}Mn_{0.3}O_2$ Li with armored MCI on LMA is much longer than the batteries with a fresh LMA), homogeneous Li-ion flux and stable Li-storage performance, all of which offers superior lithium plating/stripping (Fig. 3c-e). In Li Li symmetrical electrodes, no dendrite can be seen on LMA surface with MCI *via* operando optical microscopy (Fig. 3d), while the pristine SEI begins to form mossy lithium (Fig. 3c). In addition, the electronic (2.03×10^{-3} S cm^{-1}) and ionic conductance (1.79×10^{-4} S cm^{-1}) of lithiated armored MCI increased compared with pristine armored MCI. This implies faster transport of both electrons and ions in the armored MCI. These superior properties are also testified by the measurement of cycle stability of symmetric cells (Fig. 3e).

Another effective strategy is employing conformal and ultrathin mixed ionic/electronic ceramic conductor (abbreviated as MIEC) to protect and stable LMA. For example, Ding and co-workers[93] proposed using ultrathin $Li_{3x}La_{2/3-x}Ti$

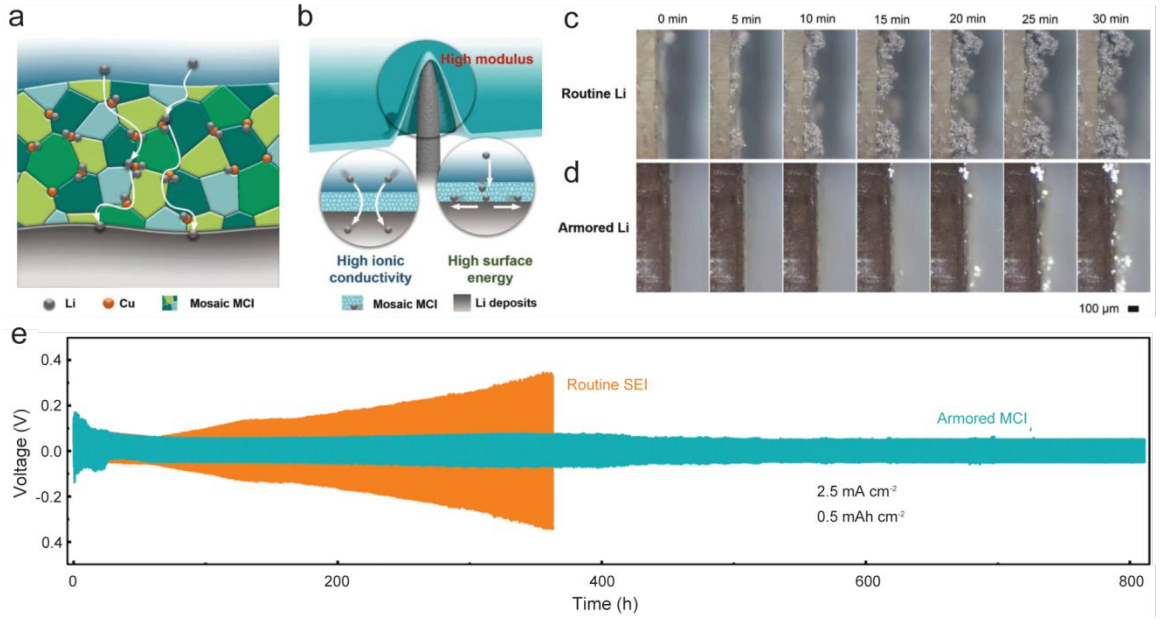

Fig. 3 Schematic of robust MCl and its effects on lithium depositing: a) the improved Li-ion transport by introducing Cu atoms in composite MCI, b) schematic of functionalized MCI, the deposition behaviour of c) routine Li and d) MCI-modified Li, e) theelectrochemical stability of Li Li batteries.[25] a-e) Reproduced with permission from ref. 25. Copyright 2018, Wiley-VCH.

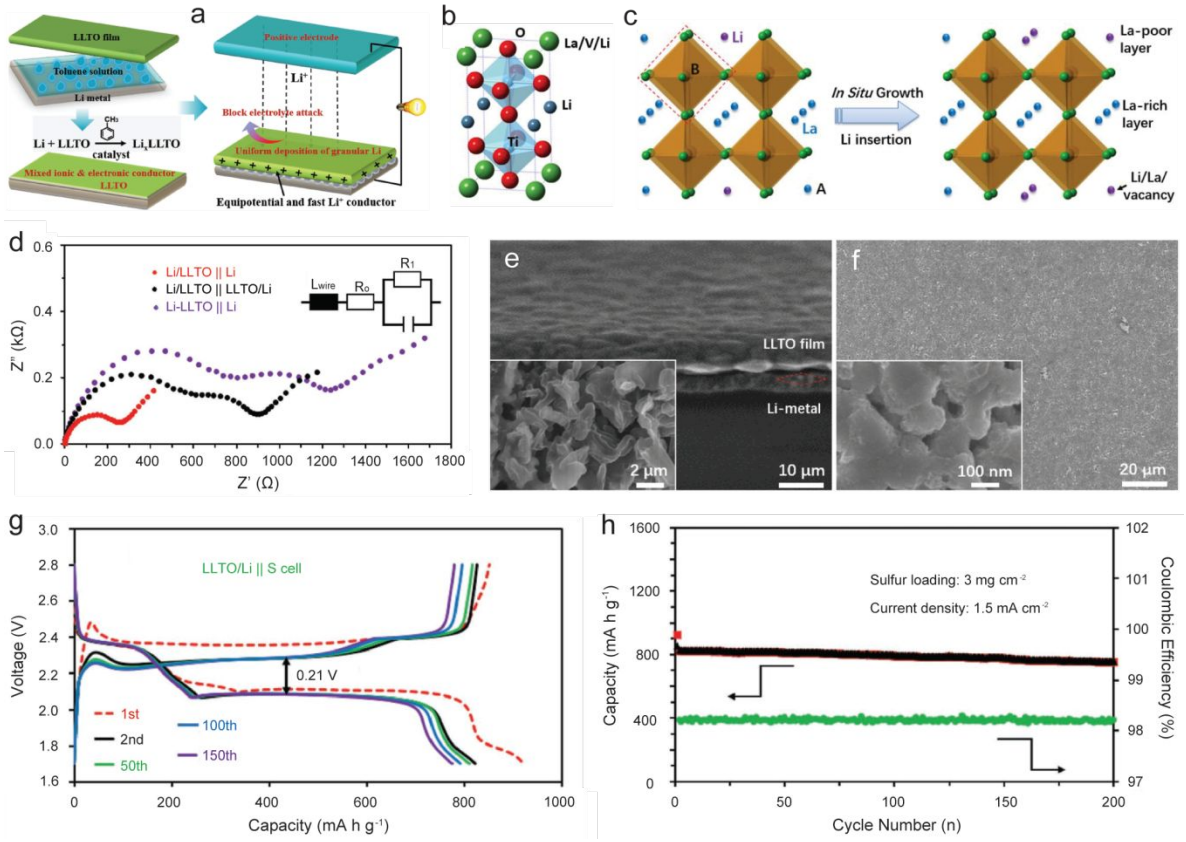

Fig. 4 a) Schematic of reaction mechanism of LLTO and LMA, b) the molecular structures of the LLTO and c) Li-insertion LLTO, d) Nyquist diagram of three cells, e) cross-section of the Li/LLTO, f) top surface of the LLTO over 200 cycles, g) galvanostatic curves of LLTO/Li S cell, h) cycling capability and CE of the LLTO/Li S cell.[103] a-h) Reproduced with permission from ref. 103. Copyright 2018, Wiley-VCH.

O_3 (LLTO) film with MIEC property to stabilize LMA by preparing a composite LLTO/Li anode with a stable and robust interface (Fig. 4a). During this in situ integration process between LMA and LLTO, the toluene served as catalyst, which facilitated the generation of a denser and hybrid LLTO/Li interphase after the voltilization of toluene. Meanwhile the formation of hybrid LLTO/Li alloy layer (see the equation in Fig. 4a) can greatly decrease the interfacial resistance (Fig. 4d) between LMA and LLTO and improve the electronic conductivity of LLTO films (from LLTO-Li of 8.2 x 10^{-6} to hybrid LLTO/Li of 9.5 x 10^{-4} S cm^{-1}). Moreover, the thickness of densely packed LLTO ceramic filmis controllable, and the ionic conductivity of the LLTO membrane can be further enhanced by calcining these LLTO nanoparticles (NPs) with LiCl.

From the viewpoint of structures of the single-crystal LLTO NPs, the Perovskite-type LLTO crystals with lithium, lanthanum and vacancies are presented in Fig. 4b, the site A and site B are occupied by Li/La and TiO_6, respectively. During an in situ growth process, Ti of B-site is reduced from Ti^{4+} to Ti^{3+}, resulting in an improved electronic conductivity of composite LLTO/Li (Fig. 4c). In addition, the ordering of La-poor and La-rich sites can boost the kinetics of Li^+ that diffuse from site A to the next site, these properties endow LLTO with superior Li-conductor and fastest ionic conductivity in SSEs, the high shear modulus can block the large volume fluctuation during lithium intercalation. As a result, the hybrid LLTO/Li anode on blocking Li-dendrite is effective, which is demonstrated by analyzing microstructures of LMA over 200 cycles (Fig. 4e and f). Li-depositions and lithium nucleated under the LLTO membrane exhibited granular morphology, and the LLTO film was well-preserved. Meaningfully, the assembled LLTO/Li S cell exhibits low voltage difference during cycling, high reversibility (Fig. 4g), high CE of over 98% and capacity at 3 mA cm^{-2} (Fig. 4h). Therefore, the application of MIEC as a Li-conductor interphase layer may be a promising strategy to achieve high-energy Li-S cells.

3.1.2. A smart SEI membrane with self-adapting interface regulation

A smart SEI film with high flexibility is needed to better accommodate the volume fluctuation and the interfacial stability of LMA during the repeat Li deinsertion/insertion.[14, 104, 105] Most importantly, the flexible SEI layer should better adapt and regulate the interfacial deformation of LMA during the Li plating/stripping processes, which is defined as self-adapting interface regulating.[14]

The polyacrylic acid (PAA) was chosen wisely as an important component of the flexible SEI layer due to its strong adhesive properties and its capability towards forming a homogeneous Li-ion conductive coating (Fig. 5a).[14] The LiPAA polymer was obtained easily via redox reaction between PAA and lithium, and the LiPAA gel polymer exhibits 582% strain

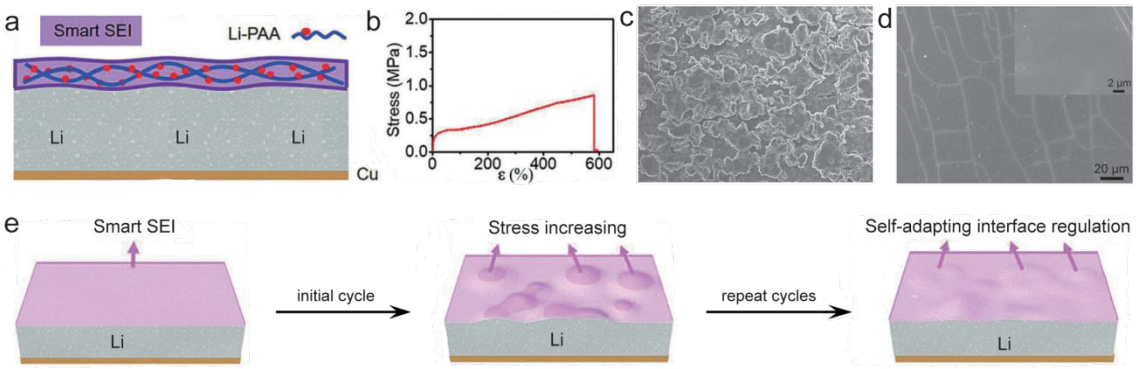

Fig. 5 a) The designed LMA with a flexible SEI layer, b) the stress-strain profile of Li-PAA layer, top surface of c) fresh Li and d) LiPAA-Li over 10 cycles, e) the schematic of self-adapting interface regulation.[14] a-e) Reproduced with permission from ref. 14. Copyright 2018, Wiley-VCH.

based on its stress-strain curve (Fig. 5b). In a symmetrical cell, the untreated Li metal shows a highly porous nature with mossy lithium depositions after 10 cycles (Fig. 5c), while the LiPAA-Li anode remain original morphology (Fig. 5d), which is due to the self-adapting interface regulation of the flexible SEI layer. These results indicate that the smart LiPAA coating dynamically changes its stress based on its current strain conditions, which allows for the accommodation of Li deformation suppressing non-uniform Li plating, reduce side reactions and realize stable Li stripping/plating (Fig. 5e).

In recent years, the reactive polymeric composite layers are widely employed to enhance the SEI layers and endow stable cycling of LMA.[18, 30, 106] For example, the organo(poly)sulfide can enhance the flexibility and withstand the large volume fluctuations during cycling, which are beneficial to enabling a dendrite-free Li deposition.[18, 107] Unfortunately, the insolubility of the S-rich polymer leads to poor dispersibility in a liquid electrolyte and precipitation continually during Li deposition, and the low conductivity of the organo(poly)sulphide is unfavourable for Li^+ diffusion on the interface. In order to overcome abovementioned issues, Wang and co-workers[108] proposed an effective strategy for protecting LMA via a composite Li polysulfidophosphate and polymer film. The designed strategy of an in situ cross-linked, MSCP are presented in Fig. 6a, the MSCP protective film was obtained by a reaction between PCEA and LiPSP. The hybrid MSCP protective film possesses a high hardness (0.06 ± 0.011 GPa) and elastic modulus (1.585 ± 0.223 GPa), which can contribute to relieve the volume change and reinforce the hybrid SEI layer. The multiple components of hybrid SEI derived from the MSCP (including inorganic Li_3PS_x, Li salts, lithium sulphides and polymer-tethered organo(poly)sulfide), enables the robust SEI film durable

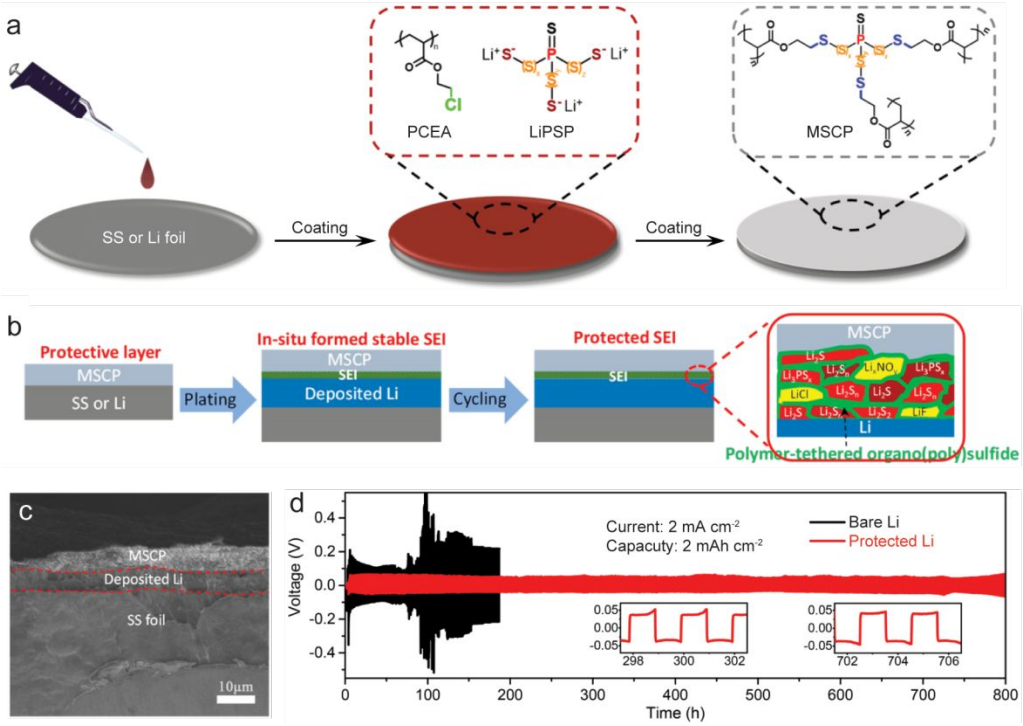

Fig. 6 a) Schematic of preparing MSCP/SS or MSCP/Li, b) schematic of forming organic/inorganic composite SEI film, c) cross-section of MSCP/SS film after 10 cycles, d) cycling capability of both symmetric cells.[108] a-d) Reproduced with permission from ref. 108. Copyright 2018, American Chemical Society.

to accommodate the volume change and prevent the dendrite formation (Fig. 6b). In addition, the MSCP layer on the top surface and cross-section keep intact and uniform after 10 cycles. Even after 10 cycles, a sandwich cross-section structure remains intact (Fig. 6c), which indicate that the MSCP layer can offer well protection for LMA and hence realize long-term cycling stability. In comparison to the bare LMA, the MSCP protected LMA achieved a longer cell life and lower voltage overpotential (< 120 mV) in a symmetric battery (Fig. 6d). Therefore, the designed concept of multicomponent composite layer can stimulate novel ideal in development of reactive polymer-based composite for LMA.

3.1.3. Tailored multi-layered interface film protected LMA

Generally, the formation of dendrites is caused by the rough surface and inhomogeneous SEI, the mosaic-like SEI on the uneven surface of LMA accelerate the dendrite growth through the collaps of the SEI, which limits its lifespan in LMBs (Fig. 7a).[34, 109] The ideal SEI films for LMA should be chemically and mechanically stable and Li ion-conductive for LMBs to operate. They possess a fine structure both in vertical and lateral directions with hybrid mechanical nature of elasticity and rigidity to relieve the volume fluctuation during Li stripping/plating (Fig. 7a). Therefore, constructing a multi-layered, ultra-smooth and ultra-thin (abbreviated as USUT) SEI film beyond the formation of inorganic/organic component is crucial to restrain Li dendrite rigidity and elasticity (Fig. 7c). These strategies provide novel insights into LMA protection and realize excellent electrochemical performance.[15, 34, 98, 109] Here, the USUT-SEI is obtained by adjusting inorganic-rich (abbreviated as I) and organic-rich (abbreviated as O) composite multi-layered structure in appropriate electrolytes, the preparation strategies of the Li-rich USUT with the I-O-I and O-I multi-layered growth obtained an ultra-long life of LMBs, the mechanical properties of USUT interface on flat Li surface are based on the electrochemical stripping/plating (ESP) method (Fig. 7b). The near-perfect lithium, sodium and potassium metal anodes with designable multi-layered USUT-SEI structures can be created through the aforementioned ESP method.[15] These representative multi-layer SEI architectures are different from the mosaic model, and can possess good mechanical properties of both elasticity and rigidity. Therefore, the electrochemically polished metal anodes with these features exhibited significantly improved cycling stability even at a high-rate with high depth of discharge.[15, 34, 109]

A dual-layered film with both organic and inorganic layers can be obtained by the spontaneous reaction between LMA and fluoroethylene carbonate (FEC) solvent (Fig. 7c).[34] The FEC decomposes is prior to pristine solvents on the surface of LMA according to the first-principles calculations,[110, 111] which is similar to the FEC additive in solvents.[111] Finally, the LiF

component (inorganic layer) is formed by the Li-F interaction because of the electrostatic attraction both Li and F atoms, the organic composition (organic layer, such as CH_2CHOCO_2Li and CH_2CHOLi) is also formed on the anode surface

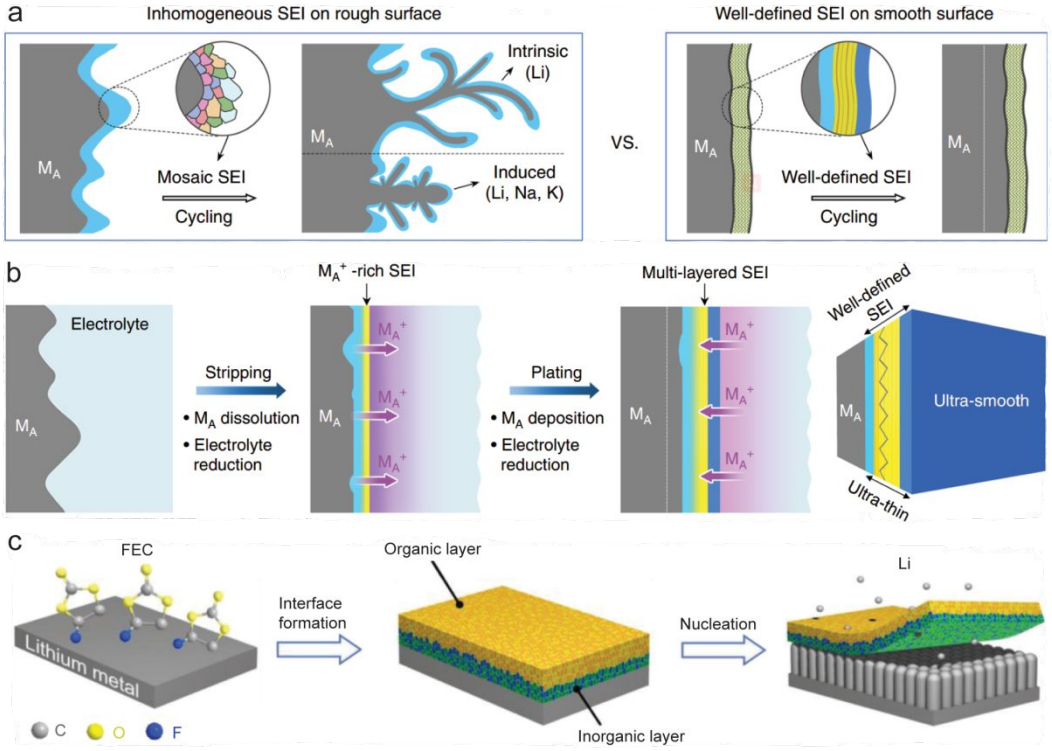

Fig. 7 a) Schematic of a rough surface and a smooth surface during cycling, b) scheme of the formation of an ultra-smooth SEI interface.[109] a and b) Reproduced with permission from ref. 109. Copyright 2018, Nature Publishing Group; c) The composite organic/ inorganic film grows on the LMA via the reactions between FEC and LMA.[34] Reproduced with permission from ref. 34. Copyright 2018, Wiley-VCH.

simultaneously (Fig. 7c). In this strategy, the dual-layered interphase on the surface of LMA can uniformly distribute nucleation seeds of Li^+, generate a dendrite-free plane and finally achieve a long-term cycling stability.[34]

3.1.4. Li-alloy anodes

A variety of decorations have been reported to improve the stability and homogeneous of the LMA surface, such as 3D current collectors,[50, 66, 68] 3D skeleton of carbon nanostructures[5, 52, 53] and Li-alloy anode.[99, 101] In these strategies, a better strategy is to construct a Li-alloy surface film that offers uniform sites for Li-reaction, and create a buffer layer in electrochemical potential between the organic electrolyte and the highly reducing LMA.[99]

In order to decrease the interface resistance between garnet and LMA, a new methodology for decreasing the interfacial resistance of garnet/LMA were proposed by forming a 20 nm thick Ge layer over garnet-type material (Fig. 8a).[101] Indeed, their interfacial resistance decreases through this approach from ~900 to ~115 Ω cm^{-2}, this technique yielded highly stable cycling of a Li-metal full-cell at room temperature. Aligning with experimental results, first-principles calculation demonstrates the enhanced wetting at the LiGe/garnet interfacial.

In addition to LiGe-alloy has been reported to enhance the wettability and reduce the Li-garnet interfacial resistance. Loh and co-workers[99] demonstrated much improved uniform lithium dissolution/deposition on the Li_xSi-modified LMA (Fig. 8j). In this work, the ion-conducting Li_xSi layer on top of lithium foil was formed through a radio frequency-magnetron sputtering system at room temperature and subsequently alloying process at 250 ^oC (Fig. 8b-g). The pristine Si (Fig. 8c, d) and uniform Li_xSi (Fig. 8e and f) layers are well formed, which are critical to achieve better rate ability, more homogeneous utilization of lithium and long cycling life. In order to demonstrate the effect of the Li_xSi layer, the electrochemical deposition behaviour of lithium in a symmetric cell is monitored by an in situ optical microscopic (Fig. 8h). Obviously, the

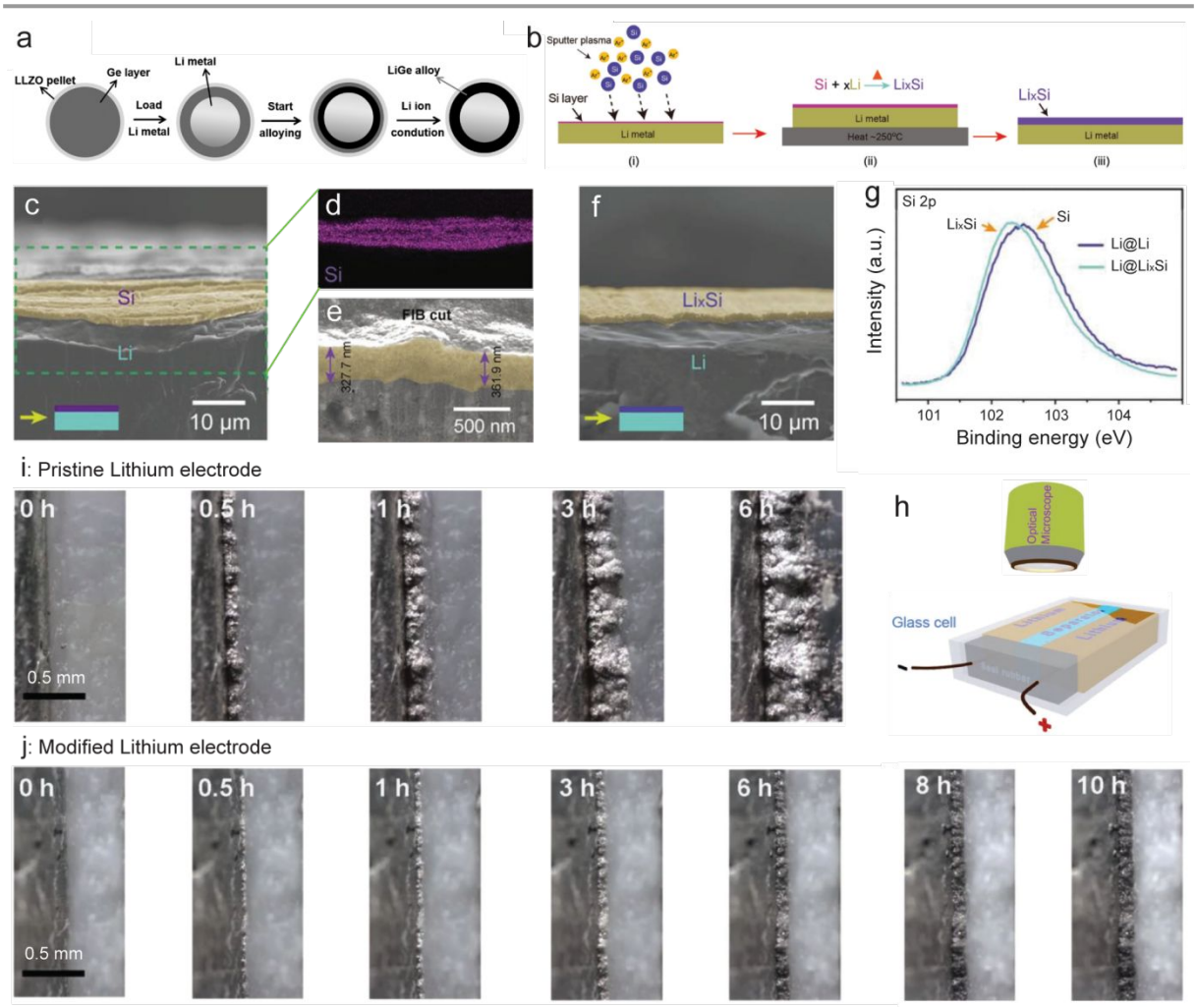

Fig. 8 a) Schematic of the designed LLZO/LiGe alloy.[101] Reproduced with permission from ref. 101. Copyright 2017, Wiley-VCH; b) The preparation procedure of Li_xSi-decorated LMA, c) the side view and d) EDS mapping of Si-coated LMA, e) cross-section of Li_xSi-modified LMA obtained by FIB method, f) the side view of Li_xSi-decorated LMA, g) XPS of Li@Si and Li@LixSi, h) a symmetric cell and a visual optical configuration, Li plating behaviour of i) pristine Li and j) decorated LMA.[99] b-j) Reproduced with permission from ref. 99. Copyright 2018, Wiley-VCH.

surface of the Li_xSi-decorated lithium maints a smooth and dense surface even after 10 h of charging (Fig. 8j). On the contrary, the morphology of pristine lithium deposition is uneven, porous and obvious dendrite appearance at 6 h (Fig. 8i). The depositing thickness of the Li_xSi-decorated Li foil is much thinner than that on the pristine lithium due to the Li_xSi layer improves the uniformity of Li dissolution/deposition.

3.1.5. Creating a "water-defendable" and "dendrite-free" LMA

It is widely accepted that LMA is the highest energy density anode for a lithium-ion charge carrier-based battery such as Li-S and Li-air batteries have been widely researched in the past decade.[74, 75, 112] Unfortunately, the Li-dendrite growth, water attack and instable interfacial SEI film have impeded its application, especially for open-system Li-O_2 battery.[112-114] Recently, He and co-workers[26] demonstrated a highly scalable method for the protection of LMA by building a Ge composite protective layer on the LMA surface (Fig. 9a). The Ge composite protective layer possesses three advantages (Fig. 9b): (i) Ge layer can reduce the interfacial resistance and stabilize LMA due to its high conductivity; (ii) the in situ generated Li-Ge alloy could be used as a Li^+ conductor on the interface between liquid electrolyte and LMA; (iii) Ge is mechanically stiff and insoluble in water, which is beneficial to form "water-defendable" and "dendrite-free" LMA.[26] These properties make a potential Ge layer and excellent candidate for Li metal protection. In addition, the Ge composite protective layer consisted of amorphous Ge (Ge and GeO_x) and Li compounds (LiOH, LiCl, LiO_2 and Li_2CO_3) with a quality ratio of 4:6 based on the analysis of XPS and Raman spectra (Fig. 9c), which could effectively improve the cycle life of Li-O_2 system and H_2O-

containing Li-symmetrical cells due to a “water-defendable” role of the Ge composite protective layer in LMB systems (Fig. 9d-f). It is obvious that the symmetrical cells with the Ge composite protected LMA (Fig. 9i and j) exhibit more robust and more homogeneous Li-plating/stripping behaviour than pristine LMA (Fig. 9g and h) at a high current density of 3 mA cm^{-2}. Besides, the Li-O_2 cell can maintain stable discharging/charging over 150 cycles in a humid O_2 with the relative humidity of 45%. These advantages demonstrate the feasibility and superiority of the Ge composite protective layer on the surface of LMA.

3.1.6. A hopeful lithiophilic–lithiophobic gradient strategy

The interface protective layer strategy is a hopeful direction to suppress dendritic growth and enable massive fabrication and practical application.[23-26, 34, 99] Various ceramics (fluoride,[25, 34] nitride[17] and phosphate[20]), polymers,[14, 18] carbon materials[5] and their composite interfacial layers[29, 101, 115] have been demonstrated in optimizing the dissolution/deposition of Li and finally suppressing dendrite growth. Nevertheless, the mechanism interpretation and design guidelines of the reported interface protective layers are elusive.[24] We will discuss in this section the school of thought of lithiophilicity and lithiophobicity. The different interface protective layers possess different chemical/physical properties, including mechanical strength, porosity, ionic and electronic conductivity, lithiophilicity and interfacial resistance.[23-26, 34, 99] The

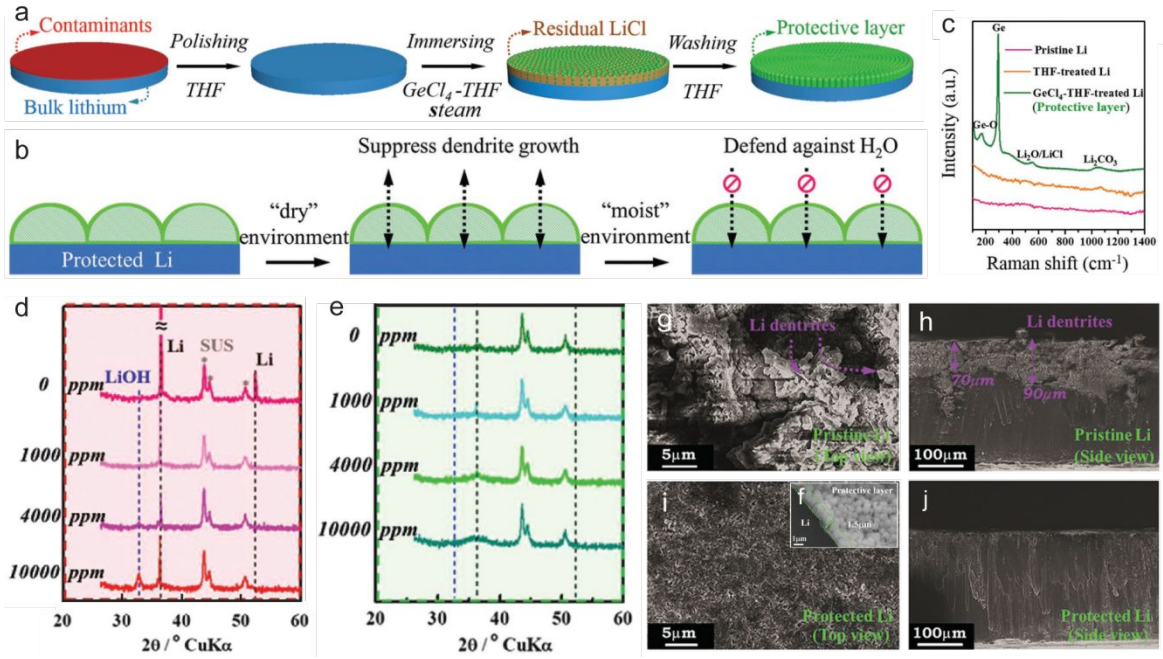

Fig. 9 a) Schematic of the preparation process of $GeCl_4$-THF-treated LMA, b) schematic of the Li plating/stripping behaviour in the Ge-modified layer, c) Raman spectra of fresh Li and protected LMA, d) XRD patterns of fresh LMA (red region) and e) protected LMA (green region), f) the protective layer on the LMA surface, the top/side views of the g, h) untreated LMA and i, j) protected LMA in normal electrolyte over long-cycle life.[26] a-j) Reproduced with permission from ref. 26. Copyright 2018, Wiley-VCH.

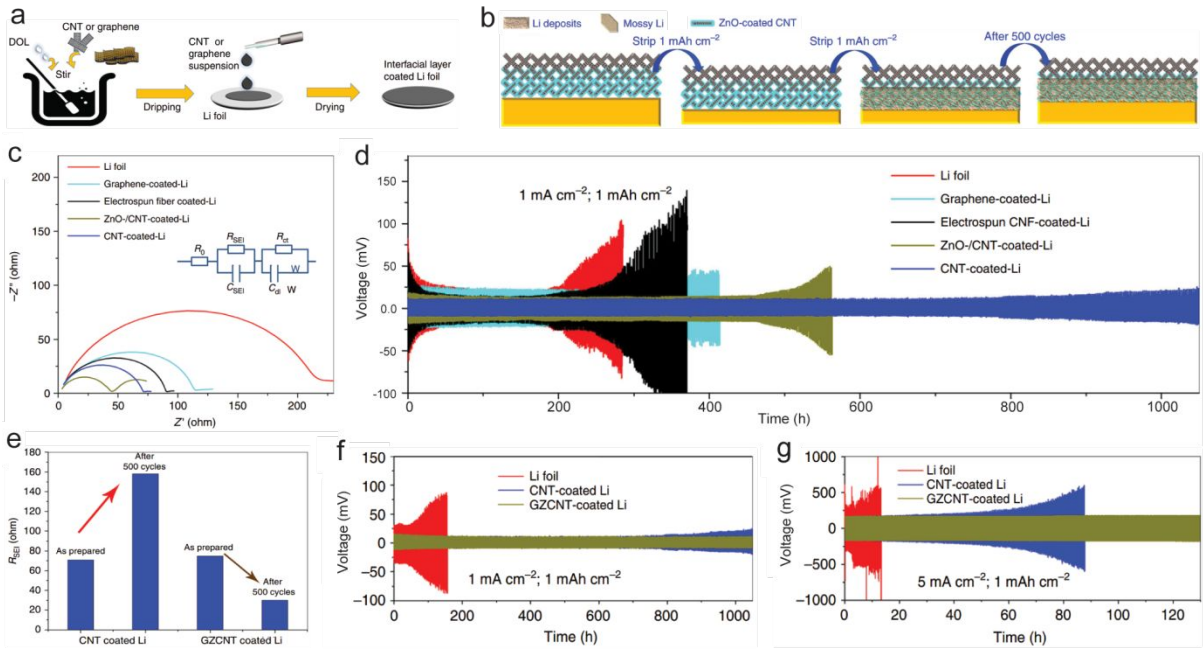

Fig. 10 a) Schematic of the gradient interface preparation, b) lithium stripping/plating behaviour in the designed GZCNT layer, c) EIS of fresh and protected Li, d, f and g) comparison of the electrochemical stability in different conditions, e) caparison of R_{SEI} of CNT-modified Li and GZCNT-modified Li.[24] a-g) Reproduced with permission from ref. 24. Copyright 2018, Nature Publishing Group.

benefit of these layer go beyond their mechanical properties but also include the nucleation and controlled growth of Li.

Given the abovementioned viewpoints, Mai and co-workers[24] put forward a lithiophilic-lithiophobic gradient (LLG) strategy by coating carbon nanotube (CNT) with different ZnO layer by layer to Li-foil (thereafter named GZCNT) (Fig. 10a, b), which can effectively restrain dendrite growth and achieve ultralong-term stable lithium deposition/dissolution even at a high current density of 5 mA cm^{-2}. The design guidelines and mechanism interpretation of the LLG strategy are detail illustrated by contrast experimentation and electrochemical characterization (Fig. 10c-g). Firstly, the prepared CNT, ZnO/CNT, graphene, electrospun fiber coated-Li exhibit different R_{SEI} due to the different wettability at the electrode/electrolyte interface (Fig. 10c), which are directly related to cycle stability of the symmetric cells (Fig. 10d). Secondly, the obvious necking behaviour (the overpotential decreases at first, and then increases) of both bare Li and electrospun fiber coated-Li electrodes during cycling indicate the stability of the SEI in the initial stage and succedent SEI incrassation from the incessant growth of dendrite-Li. In contrast, the CNT-coated Li shows a lower overpotential and better cycling stability due to it high porous and mechanical strength feature and lithiophobic property. On the contrary, the grapheme presented far fewer mesopores, which may prevent Li diffusion in the interfacial layer and lead to the Li deposits on the upper surface. Therefore, an ideal interfacial layer can be designed by an experimental discovery of the guidelines, the interface protective layer should be lithiophobic and robust to stop the penetration of Li dendrites and possibly improve the diffusion kinetic of Li-ion.[24] Lastly, the R_{EIS} and cycling stability of CNT- modified Li during cycling can be further improved through designing a LLG GZCNT layer, in which the lithiophobic CNT framework can blocks dendrites, the lithiophilic ZnO/CNT can promote diffusion of Li-ion into the porous layer, facilitating the generation of a robust SEI film, and prevent the formation of mossy lithium (Fig. 10e-g). These results are well consistent with the R_{SEI} fitting results and cycling stability of both a symmetric cell and Li-S cells, indicating the lithiophilic-lithiophobic interface is a potential strategy for future high-safety LIBs fields such as Li-S, Li-O_2, Li-intercalation oxides, and Li-polymer batteries.[24]

Recently, there has been an increased interest on the wetting behaviour of molten liquid lithium. Among various wetting strategies, Li-matrix composites exhibit promise in the aspect of suppression dendrite growth, stabilization SEI and accommodation volume fluctuations during discharging/charging processes.[116, 117] However, most available matrices possess poor wettability (Fig. 11a), which hinder the progress of Li-matrix composites. Moreover, it is still a challenge to prepare the thin lithium with proper capacity (e.g. 3-6 mA h cm^{-2}, 15-30 μm) via rolling commercially thick lithium-foil. Casting molten Li on lithiophilic-matrix might be a potential way to achieve the large-scale of rollable thin Li and solve the wettability problem. Certainly, the poor surface wettability of substrates can be improved via organic coating of abietic resin on the surface of substrates (Fig. 11b-m). So the poor wettability of substrates can be improved either by coating the lithiophobic substrates with lithiophilic materials (Fig. 11a), or by increasing the temperature to reduce the viscosity of

liquid-Li.

Generally, the preferential deposition orientation is top-growth on the surface of LMA during Li plating, which increases the danger of cell short circuits.[92, 117] In order to alleviate the risk of short circuits, a good strategy is to design a

Fig. 11 a) The electronegativities, wettability and ΔG of various elements. The wettability behaviour between molten-Li and various substrates: b) Cu, c) Cu-foam, d) Fe-foam, e) Ni-foam, f) carbon fibre and g) GO; h) The contact angle is ~140° on the Cu surface, the interfacial wettability of i) Cu-foam, j) Fe-foam, k) Ni-foam, l) carbon fiber and m) GO are improved via abietic resin-coated substrates.[116] a-m) Reproduced with permission from ref. 116. Copyright 2019, Nature Publishing Group.

conductivity and lithiophilicity gradients substrate to guide lithium deposition at the bottom of substrate.[117] The deposition behaviours of lithium metal are closely related to its conductivity and wettability because the interface/electrode resistance and lithiophilicity play key roles in dendrite-induced short circuits (Fig. 12a-c). Therefore, the preferential deposition position of lithium metal can be tuned by engineering a conductivity/lithiophilicity gradients substrate material (Fig. 12c), which will induce lithium deposition away from the dangerous anode/separator interface. The conductivity and lithiophilicity gradient-substrate can be obtained by a template method combined with subsequently deposition, etch and sputter processes, the presented 3D deposition-regulating scaffold (DRS) is composed of a low conductivity top and a superlithiophilicity bottom, the both are beneficial to deposit preferentially at the bottom of substrates during Li plating (Fig. 12d and g). On the contrary, the preferential deposition orientation is top-growth in the bare nickel scaffold (BNS) or conventional electrodes during Li plating (Fig. 12e and f). More importantly, the DRS with conductivity and lithiophilicity gradients also exhibit the best low temperature property (down to -15 °C) and highest capacity (40 mA h cm^{-2}) in a symmetric cells among three matrixes (Fig. 12h). Based on the abovementioned advantages, the deposition-regulating strategy may be an effective channel to relieve the risk of cell short circuit.

3.2. Strategies for optimizing electrolyte components

The nature of the Li deposition is highly correlated to the passivation layer on the LMA.[39, 42, 43] Because of the highly cathodic environment provided by Li,[39, 118] electrolyte constituents (including additive,[43, 115] salts,[42, 45] solvents[39, 118] and other impurities etc.[115]) are easily decompose and thermodynamically instable, which leads to surface passivation of LMA. These complications could ultimately lead to a poor cycle life, terrible safety, low CE, and low rate for LMBs.[115, 103] Therefore, another promising strategy is to optimize the electrolyte components to generate a stable interphase between electrolyte and LMA.

3.2.1. A facile route by altering the electrolyte components

The spontaneous reactions of both LMA and electrolyte would generate SEI film, adjusting the stability of the SEI film by optimizing the electrolyte components is a simple and feasible route.[42, 115] For example, Matsumoto and co-workers[119] found that the high concentration lithium bis(trifluoromethanesulfonyl)imide (abbreviated as LiTFSI) electrolyte can effectively suppress the aluminum current collector corrosion due to the low solubility of $Al(TFSI)_3$. In addition, researchers[120] discovered that the electrochemical oxidation stability of certain ether-base electrolytes can be enhanced to ~5 V on the Pt electrode. Unfortunately, when the $LiCoO_2$ Li systems charged to 4.2 V, severe capacity fade is observed

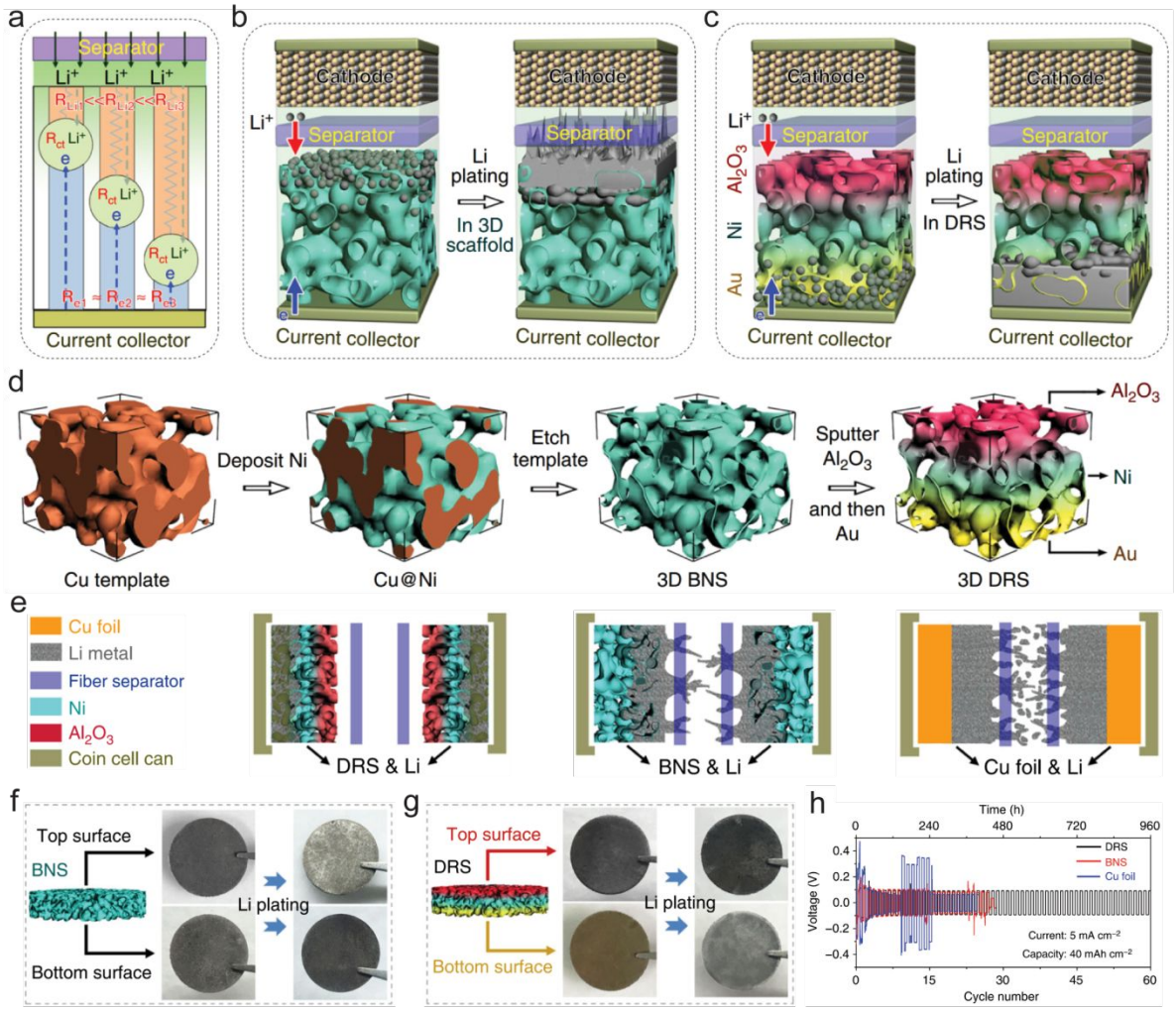

Fig. 12 a) The resistance evolution of the Li-ion, electron and R_{ct} in the anode, b) the top-growth pattern at the interface between anode and separator, c) the bottom–growth pattern in the DRS-modified anode, d) the DRS preparation procedure, e) schematic of three Li-deposition patterns in cells, the top and bottom surface images of f) BNS and g) DRS before and after lithium plating, h) the cyclability of three substrates.[117] a-h) Reproduced with permission from ref. 117. Copyright 2019, Nature Publishing Group.

within 200 cycles. Therefore, the exhibition of LMB in ether-based electrolyte is generally got with cathodes under 4.0 V.[120]

Recently, Zhang and co-workers[42] offered a strategy to obtain excellent cyclability of both a high-voltage (> 4 V *vs.* Li^+/Li) cathode $LiNi_{1/3}Mn_{1/3}Co_{1/3}O_2$ (NMC333) and LMA in an ether electrolyte by simply using appropriate electrolyte concentrations and salts. The observed improvements were based on the fact that free ether molecules are very limited in concentrated electrolyte, rendering them difficult to be oxidized. Furthermore, Li-ion can significantly reduce the reactivity of the electron lone of the ether. In addition, the interfacial layers between cathode and electrolyte in thickness are distinct due to the difference in electrolyte components (Fig. 13a-d). The thickness of cathode electrolyte interface (CEI) in the 4M dual-salt ether electrolyte is the thinnest among electrolytes, which indicate that the lithium difluoro(oxalato)borate (abbreviated as LiDFOB) endows effective protection on the ternary cathode, the electrolyte decomposition can be further restrained during cycling. In addition to the CEI, the interface layer between electrolyte and LMA in the 4M dual-salt ether electrolyte also exhibits much better compactly integrated, higher Li CE and lower Li volume

fluctuations during repetitive cycling than those in 3M LiTFSI or 4M LiDFOB electrolytes, respectively (Fig. 13e-h). The corrosion of the LMA in 3M LiTFSI-DME electrolyte is very serious (100 μm in thickness, Fig. 13e), which indicates that the surface layer can't prevent the further reaction between LMA and electrolyte. The obvious corrosion of LMA is also seen in the 4M LiDFOB-DME electrolyte (about 120 μm, Fig. 13f), many isolated "dead-Li" are found, which directly result in low Li CE and quick capacity fade of the LMA. Recently, Dasgupta and co-workers[121] also demonstrated the formation mechanism of dead lithium which have been related to quick capacity attenuation of Li anodes. The LMA corrosion can be greatly suppressed in the 4M dual-salt electrolyte (only 22 μm, Fig. 13g) due to the synergistic effect of high-concentration dual-salt and the protection of LiDFOB. Accordingly, the stability of LMA is highly correlated to the ability of the SEI film to accommodate for cyclic volume changes.

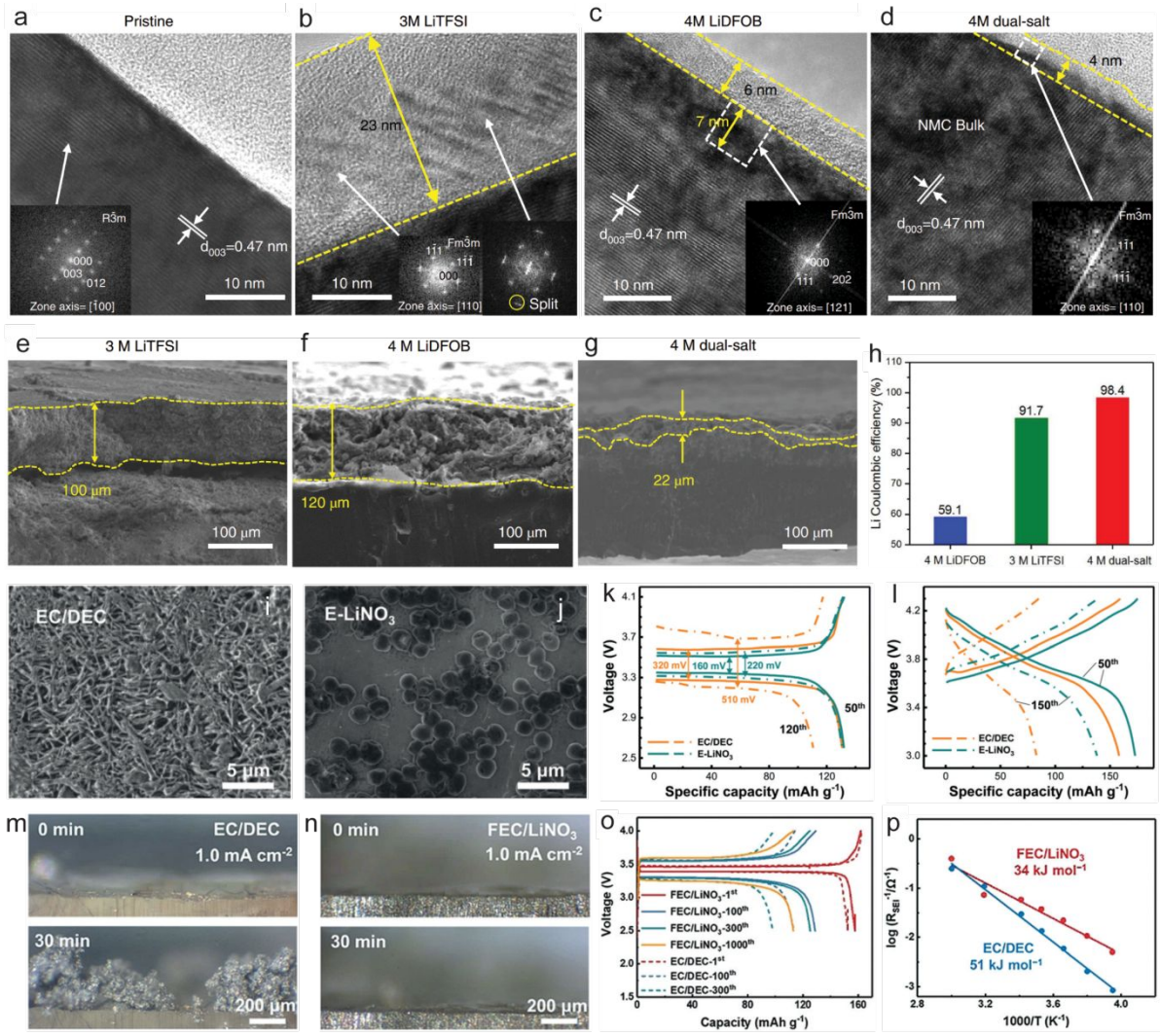

Fig. 13 a) The fresh NMC333 cathode, the cycled NMC333 in various ether-based electrolytes: b) LiTFSI, c) LiDFOB and d) dual-salt, e-g) the side view of LMA after 50 cycles in three electrolytes, h) CE of LMA in three electrolytes.[42] a-h) Reproduced with permission from ref. 42. Copyright 2018, Springer Nature; Top surface of the LMA in i) EC/DEC and j) E-$LiNO_3$, voltage curves of k) Li//LFP and l) Li//NCA cells.[39] i-l) Reproduced with permission from ref. 39. Copyright 2018, Wiley-VCH; The side view of Li-deposition in m) EC/DEC and n) FEC/$LiNO_3$ electrolytes, o) electrochemical curves of Li//$LiFePO_4$ in various electrolytes, p) the activation energy of the SEI generated in two electrolytes.[118] m-p) Reproduced with permission from ref. 118. Copyright 2018, Wiley-VCH.

3.2.2. Regulating the solvation of Li-ion by introducing additives

In addition to alter the electrolyte concentration and components,[42] another efficient improvement strategy is introduction additives[115] in the electrolytes. Various additives for improving the interface stability of LMA have been investigated: FEC,[103] lithium nitrate ($LiNO_3$),[39] ethylene sulfite (ES)[115] and vinylene carbonate (VC)[115, 122] and so on. In all additives, $LiNO_3$ and FEC are widely used at additives amounts in ether-based system to improve the quality of the passivation layer over

Li.[103] It should be noted that the normally poor solubility of $LiNO_3$ can be enhanced by the addition of trace amounts of CuF.[103] It is also regarded as an important additive in lithium sulfur battery systems and can effectively restrain the polysulfide shuttle effect and limit Li dendrites by passivating the Li surface.[39 103] For example, the morphology of Li deposits on copper foil in the $LiNO_3$-containing electrolyte is spherical structures, while its morphology in without $LiNO_3$ additive EC/DEC is needle-like dendritic structures (Fig. 13i and j), the abovementioned results demonstrate that the growth and nucleation of Li metal can be controlled by introducing additives. From comparison, the LMBs cells in the E-$LiNO_3$ electrolyte shows a higher CE, a lower hysteresis voltage and a slower capacity decline than that of EC/DEC electrolyte Fig. 13k, l). The poor CE and the capacity decay rapidly are mainly caused by the higher hysteresis voltage and the irreversible electrolyte decomposition.

Very recently, Zhang and co-workers[103] found that the SEI is rich in lithium fluoride and LiN_xO_y can be obtained by introducing simultaneously the FEC and $LiNO_3$ into an electrolyte. The Li plating in the carbonate is mossy and dendritic with a porous surface after repeated cycling, while the morphology of Li deposition in FEC/$LiNO_3$ electrolyte is smooth, dendrite-free and dense (Fig. 13m and n). Furthermore, in contrast to EC/DEC electrolyte, the Li $LiFePO_4$ coin or pouch cells with FEC/$LiNO_3$ electrolyte exhibit higher CE and lower hystersis potential during long-term cycling due to the low activation energy for Li-ion diffusion (34 kJ mol^{-1}) and large amounts of lithium fluoride and LiN_xO_y in the SEI (Fig. 13o and p). These results offer insight into understanding the key role of the solvation of Li-ion in reconstructing the SEI and developing an effective strategy to optimize electrolytes for future high-safety LMBs.

3.2.3. Synergistic effects of ionic liquid

Room-temperature ionic liquid (IL) electrolytes are potentially a promising alternative to conventional organic electrolytes due to their tailored-made nature.[123] More meaningfully, IL can be nonvolatile and nonflammable. Both cation and anion are widely researched additives that restrain Li dendrite growth.[124] For example, Basile and co-workers showed that when N-propylN-methylpyrrolidinium bis(fluorosulfonyl)imide was added into the electrode, the interface between electrode and LMA bacame stabilized, realizing 1000 cycles with CE of over 99.5% in a full-cell coupled with an $LiFePO_4$ cathode.[123] Very recently, Passerini and co-workers found that the [DEME][TFSI] IL electrolyte exhibits good performances for application in Li-O_2 cell, including a low-polarization cycling with a capacity of ~13 Ah g^{-1} and CE approximating 100%, besides, the increase in temperature would increase the energy efficiency of Li-O_2 battery.[125]

In all IL electrolytes, imidazolium IL are very attractive as electrolyte due to its good thermal stability, wide redox stability, high ionic conductivity and ultralow vapor pressure.[126] Archer and co-workers[126] report a new class of solventless electrolytes prepared by tethering IL to hard ZrO_2 nanostructures (hereafter defined as IL-nanoscale ionic materials, IL-NIMs), the fluids show unique redox stability, robust interfacial stability and more reversible Li-ion transference numbers on the surface of LMA in an appropriate ionic conductivities. Song and co-workers[127] demonstrate that the Dawson-type polyoxomolybdate $(NH_4)_6P_2Mo_{18}O_{62}$ (abbreviated as PMO) with $P_2Mo_{18}O_{62}^{6-}$ anion can be coupled on the graphene oxide-ionic liquid (GO-IL) via an anion exchange with PF_6^-, the formed GO-IL-PMO composite exhibits improved charge-transfer efficiency at the interface between electrolyte and electrode and a synergistic effect both the POM and GO-IL, and delivers a high specific capacity of 903.9 mA h g^{-1} over long cycles.[121] These researches presented a step forward to the progress of IL-based cells for future high energy density ESDs.[123, 125, 128, 129]

3.2.4. Optimizing the electrolyte's electrochemical/physical properties through computational method

Electrolyte, as one of the key components of LIBs, not only acts a role in conducting inner circuit and conducting Li-ion, but also decides the cycle stability and rate capacity of cell. An excellent electrolyte should possess some special characteristics, including superior chemical stability during cycling, fast Li-ion transport dynamics, electronic insulation property, excellent interfacial compatibility with cathode or LMA electrodes, eco-friendly and low-cost.[130] However, the current commercial liquid organic electrolytes (LOEs) can not satisfy the abovementioned requirements. Therefore, screening and optimization of electrolyte composition may be an effective pathway to optimize the performance of battery.

The fundamental understanding of the electrochemical features and physical properties of electrolyte composition is very significant for the design and optimize of electrolyte system.[131] Some of the electrochemical behaviors of electrolyte systems can be predicted via advanced modeling techniques and atomistic molecular dynamics simulations (MDS), which provide molecular scale the relationships between the structure and property and simulate design of novel electrolytes.[131, 132] For example, Garcia and co-workers[133] found that IL electrolytes could present better electrochemical properties than conventional LOEs. After that, more IL electrolytes are developed due to their high thermal stability, non-volatility, negligible vapor pressure and good ionic conductivity.[130, 134, 135] Some typical IL electrolytes and Li-salt are widely used in various metal-based second batteries (Fig. 14a). Recently, Zhang and co-workers[130] investigated the effect of Li-salt concentration on the electrochemical properties of four IL by combining the computational simulation techniques and

experimental data, the atomistic MDS indicate that the viscosity and density of four IL electrolytes will increase with the increase of the LiTFSI concentration. In addition, the increased LiTFSI concentration would result in a more compact and closed structure, with both the transport of Li-ion and the residence time have a strong coupling/correlation (Fig. 14b). Ohba and co-workers[136] studied the decomposition reaction of electrolyte at the graphite electrode/electrolyte interface by a hybrid quantum-classical (QC) MDS technique. They found that the desolvated Li-ion could be quickly inserted into the graphite layer when an electric field of about 0.3 V $Å^{-1}$ was used in the QC MDS, the electric field decreased to 0.2 V $Å^{-1}$, the Li-ion would catalyze the decomposition of the ethylene carbonate into Li-CO_3 and C_2H_4. Therefore, the information of interfacial reaction and formation of SEI layer can be predicted by the hybrid QC MDS method, which can further guide the optimization of the electrolyte system.

The lithium dendrite growth is a serious problem during cycling, the understanding to the formation and growth behavior of Li dendrite is critical to develop high safety LMBs.[84] Recently, Seminario and co-workers[137] analyze the dendrite formation and growth behavior via an atomistic MDS technique (Fig. 14c), the computational data show that the electrolyte reaction will postpone the Li dendrite formation and the dendrite cannot uniformly grow in a spatially even i.e. homogeneous manner but instead tends to deposit preferentially at a specific areas of LMA. In order to avoid the dendrite formation with structural damage at 67 °C, the electrolyte should be able to bear big compressive stress (≥ 2 GPa).

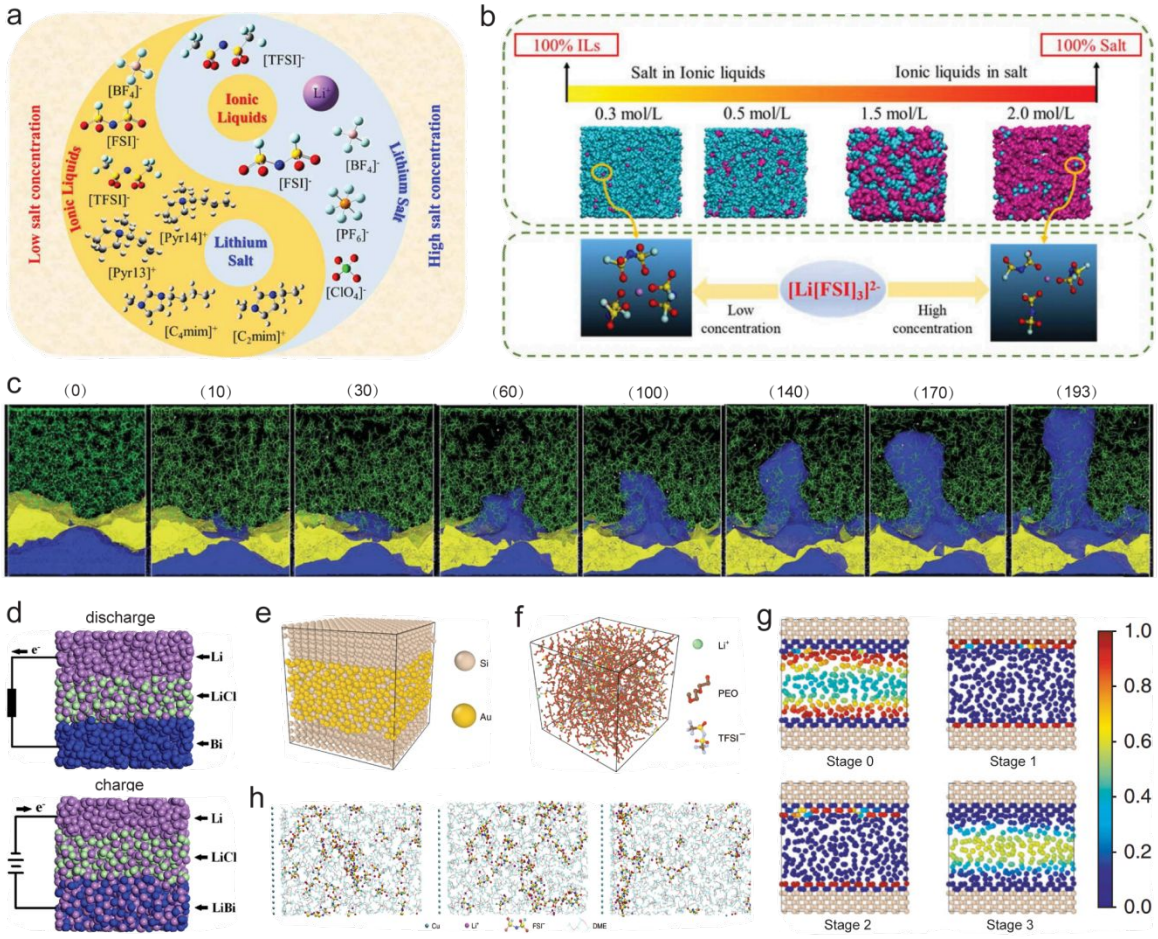

Fig. 14 a) The molecular structure of IL and Li salt, and b) the snapshots with different Li-ion concentration of the IL system (blue: IL, pink: Li salt).[130] a and b) Reproduced with permission from ref. 130. Copyright 2019, Frontiers Media S.A.; c) The dendrite growth processes (blue: Li, pink: Li^+, green: EC and PF_6, yellow: LiF).[137] Reproduced with permission from ref. 137. Copyright 2019, Royal Society of Chemistry; d) The discharge/charge processes of liquid LMBs.[138] Reproduced with permission from ref. 138. Copyright 2020, Elsevier; The microstructure of e) the Si-Au diphase system and f) the molecular structure of PEO/LiTFSI PSSEs, g) side view of the Si-Au system in various states.[139] e-g) Reproduced with permission from ref. 139. Copyright 2019, Nature Publishing Group; h) Simulation snapshots from the MDS at 0 V (left), 1.0 V (middle) and 2.8 V (right).[134] Reproduced with permission from ref. 134. Copyright 2020, Nature Publishing Group.

Furthermore, they also found that the high current density prefer the dendrite formation compared with the low current density. As a result, a moderate current density could relieve the dendrite formation in some extent.

As a powerful computational simulation technique, various MDS methods are widely applied in the field of energy storage materials. The pivotal structural and dynamical information of electrolyte system (eg. electrolyte/electrode interface,[134, 136] electrode or electrolyte polarization,[131] structural correlations[130, 139] and interfacial Li-diffusion[140]) can be predicted in advance by the MDS technique, which helps us screen the ideal electrolyte and hence optimize the electrolyte system. For instance, He and co-workers[138] calculated the thermodynamic, Li-ion transport and electronic properties of the LiBr, LiF and LiCl electrolytes in LMBs by applying first principles and MDS techniques, the calculated results indicate that the LiBr electrolyte possesses the highest Li-ion diffusion coefficient (LDC) and melting point among three electrolytes. The LDC in the LiBr will further increases when a certain amount of F and Cl are doped into LiBr electrolyte. The energy storage mechanisms and structural evolution during discharging/charging processes is vividly depicted in Fig. 14d (here take the Li Bi cell as the example). Besides, Grossman and co-workers[139] develop graph dynamical networks, which can learn the key dynamical information for all kinds of multicomponent system in each stage (Fig. 14e-g). Firstly, an equilibrium system is constructed at the simulated for 25 ns applying MDS. The first 12.5 ns trajectory is used to verify the four-state models, the last 12.5 ns trajectory confirms the atomic dynamics of Si (Fig. 14g). In addition, the Li-ion transport behavior can be understood by analyzing the eigenvectors and solvation environments (Fig. 14f). Very recently, Zhu and co-workers[134] verified the formation of an electric double layer in the SEI by MDS (Fig. 14h), which agree with the result of real-time mass spectrometric characterization on the SEI. These abovementioned results show that the electrochemical/physical properties of electrolyte system can be further optimized through various MDS techniques.

3.3. Strategies for designing a rational 'host' for LMA

The dendrite deposition and the infinite relative dimension change of LMA during charging/discharging processes severely hinder its applications.[62, 64] Many approaches adopted previously as below: i) optimizing electrolyte systems for the interfacial stabilization of SEI;[39, 42, 141] ii) constructing mechanically and electrochemically robust SEI films by in/ex situ technologies for dendrite suppression and SEI stabilization;[5, 23-25, 99] iii) designing high-modulus SSEs to suppress dendrite penetration.[63, 91, 113, 115] These abovementioned strategies are effective to some extent for alleviating SEI collapse and suppressing dendrite growth. However, they cannot solve the dimensional changes of the electrodes induced by the 'hostless' Li deposition/dissolution.[64] The stability of between electrodes and SEI interface are closely related to electrode dimension stability.

3.3.1. Constructing a 3D flexibility conducting skeletons host for metallic Li

In all host candidates for LMA, carbon-based materials are the perfect host candidates for metallic lithium.[54, 62] Carbon is widely applied in energy storage field because of its lightweight and high flexibility available for one/two/three dimension skeleton construction, such as spherical carbon,[58, 65] carbon foam,[53, 54] CNT,[52] carbon nanofibers (CNFs),[57] graphene.[51, 56, 61, 62, 64] It is not only an ideal host for LMA as a composite anode for future high energy density Li-O_2 and Li-S systems, but also reserves the space for adapting the dimension changes during cycling.[62]

In order to seek ideal host materials for Li metal, Guo and co-workers[53] design that the 3D N-doped graphitic carbon foams (NGCFs) can realize uniform lithium nucleation/growth (Fig. 15a). The well-distributed Li nucleation sites on the surface of NGCFs might benefit from N-containing functional groups of NGCFs and low local current density. The 3D porous NGCF is beneficial to remit the volume change, form homogeneous Li nucleus seed layer and enhance the electrochemical performances (such as high CE of 99.6%, ultralong lifespan of 1,200 h and dendrite-free Li formation) during the Li plating/stripping. Lai and co-workers[51] designed a hierarchical 3D porous silver-nanowire-graphene framework (abbreviated as 3D-SGF) as the host for LMA (Fig. 15b), the unique hierarchical binary scaffold provides ultrafast, successive and fluent electron transportation channel. It also shows superior mechanical strength and flexibility to support Li deposition and relieve volume expansion during repeated Li deposition/dissolution. In addition, the superior high rate performance and long cycle life in symmetric half-cell and full-cell indicate the hierarchical 3D-SGF host can better restrain the Li dendrite formation and bear the infinite relative dimension change. Zhu and co-workers[54] controlled the Li amount infused into a hollow 3D graphene foam host while maintaining the well-defined 3D network intact (Fig. 15c). The hollow hierarchical porous structure with tubular shape shows many advantages as follows: i) it offers both inner and outer surfaces ion transfer path; ii) improves ion diffusion kinetics and reduces the local current density; iii) provides a well-defined structure to accommodation dimension change and promotes the dendrite-free Li deposition. Based on the above superiority, the particular morphology of hollow 3D Li foam composite anode showed excellent performance in a full cell. For example, a high capacity of 138 mA h g^{-1} at 0.2 C can be obtained using 3D Li foam composite as anode and $LiFePO_4$ as cathode, with high CE of about 99.5% after 200 cycles at 1C.

CNT paper is also used as a high mass loading host for Li metal. Ji and co-workers[52] designed and prepared a lightweight but mechanically robust and highly conductive CNT paper host for metallic Li, the freestanding skeleton can

infuse Li metal with a lithium mass fraction of 80.7% (Fig. 15d). Furthermore, the highly conductive 3D Li/CNT electrode consist of the expandable 1D CNT with sp2-hybridized carbon and uniform Li loading on the surface of CNT, which can effectively impedes formation of Li dendrites and achieves a good CE of over 97.5%. The Li/CNT scaffolds can also be well maintained throughout cycling even after long cycles at 10 mA cm^{-2}. These features demonstrate that CNT paper is robust and expandable in nature, allowing it to withstand large volume change. Consequently this design offered stable voltage hysteresis at high gravimetric/areal capacities with high Li utilization. In addition, Luo and co-workers[50] also develop a 3D MIEC network as a superior host for Li metal (Fig. 15e). The $Li_{6.4}La_3Zr_2Al_{0.2}O_{12}$ (LLZO) NPs was incorporated into 3D CNFs skeleton as a MIEC host for metallic Li, which the LLZO can reduce the interface energy between CNFs and electrolyte, hence enhancing the electrolyte wettability on the surface of 3D scaffolds. Besides, the LLZO also can compensate Li^+ depletion near the interface of electrode and homogenize Li^+ flux during repetitive Li stripping/plating processes. As a result, the 3D MIEC skeleton shows outstanding electrochemical performance, homogeneous Li deposition on MIEC CNFs and retained morphology.

Many carbon-based substrates are not well-wetted by metallic lithium, which result in the melted lithium didn't infiltrate this carbon layer.[106, 142] Recently, a facile strategy was provided to endow carbon hosts from Li metal nonwetting to superwetting through ammonia treatment, and hence achieve self-smoothing behavior on the surface of carbon film during cycling, which benefited from the mesoporous functionalized carbon (Fig. 16a).[143] The results of density functional theory (DFT) simulation of the strong interaction between amine and lithium indicate that a more negative segregation energy (E_{seg}) value can be obtained on the ammonia functionalized carbon surface, which is beneficial to get more thermodynamically favourable lithium segregation and form two dimensional lithium clusters round the –NH locations.[144, 145] Therefore, the surface chemistry of the pristine carbon with non-wetting host can transform into superwetting through amine functionalization, the molten-lithium also can infiltrate the functionalized-C film spontaneously (Fig. 16b). In contrast, lithium often prefers the vertical orientation growth on the pristine carbon surface, which would induce the

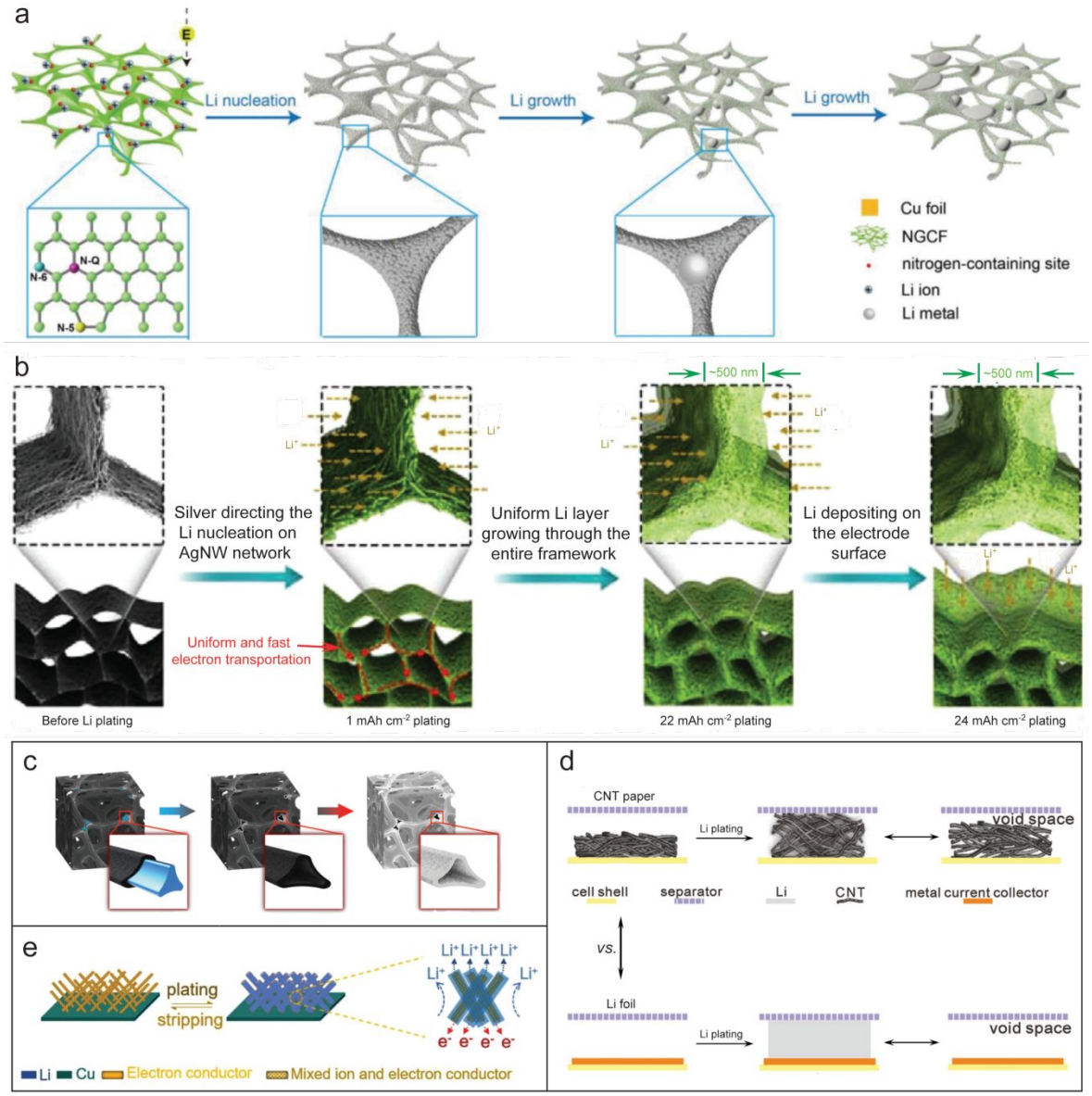

Fig. 15 a) Schematic of the nucleation/growth of lithium on the NGCF.[53] Reproduced with permission from ref. 53. Copyright 2018, Wiley-VCH; b) Schematic of the lithium depositing processes in the 3D-AGBN.[51] Reproduced with permission from ref. 51. Copyright 2018, Wiley-VCH; c) Schematic of the preparation process of hollow Li-foam.[54] Reproduced with permission from ref. 54. Copyright 2018, Wiley-VCH; d) Schematic of volume change of CNT-coated lithium and LMA during cycling.[52] Reproduced with permission from ref. 52. Copyright 2018, Wiley-VCH; e) 3D MIEC framework can homogenize Li^+ flux, inducing homogeneous Li depositing on the MIEC.[50] Reproduced with permission from ref. 50. Copyright 2018, Wiley-VCH.

generation of Li dendrites and large Li particles aggregated on the carbon surface. The wetting, self-smoothing and nucleation behavior of both can be observed by in situ TEM technologies (Fig. 16c), which agree with DFT. Based on the previous nucleation theory,[146] the relationship of the free energy barrier between heterogeneous nucleation ($\Delta G^{\star}_{\mathrm{het}}$) and homogeneous nucleation barrier ($\Delta G^{\star}_{\mathrm{hom}}$) in the solution is presented in equation (1):

$$\Delta G^{\star}_{\mathrm{het}} = S(\theta) \times \Delta G^{\star}_{\mathrm{hom}} \quad (1)$$

where *S* is related to the contact angle θ, which is shown in equation (2):

$$S(\theta) = \frac{(2+\cos\theta)(1-cos\theta)^2}{4} \quad (2)$$

Obviously, the surface wettability of functionalized carbon hosts can be improved when the $S(\theta)$ reduces monotonically with the reducing of the θ, which benefits the heterogeneous nucleation of lithium. When the sum of the θ of the nucleus and the $\phi/2$ of the cavity is low than 90°, the nucleation energy barrier would be zero in a functionalized

mesopore/cavity surface (Fig. 16d). As a result, the mesopore channels and cavities are often prior nucleation sites for metallic lithium, which is also beneficial to self-smoothing behavior during cycling.[98, 146] Based on the above advantages, the functionalized 3D carbon film with high electronic conductive, mesoporous and huge surface area can well decrease

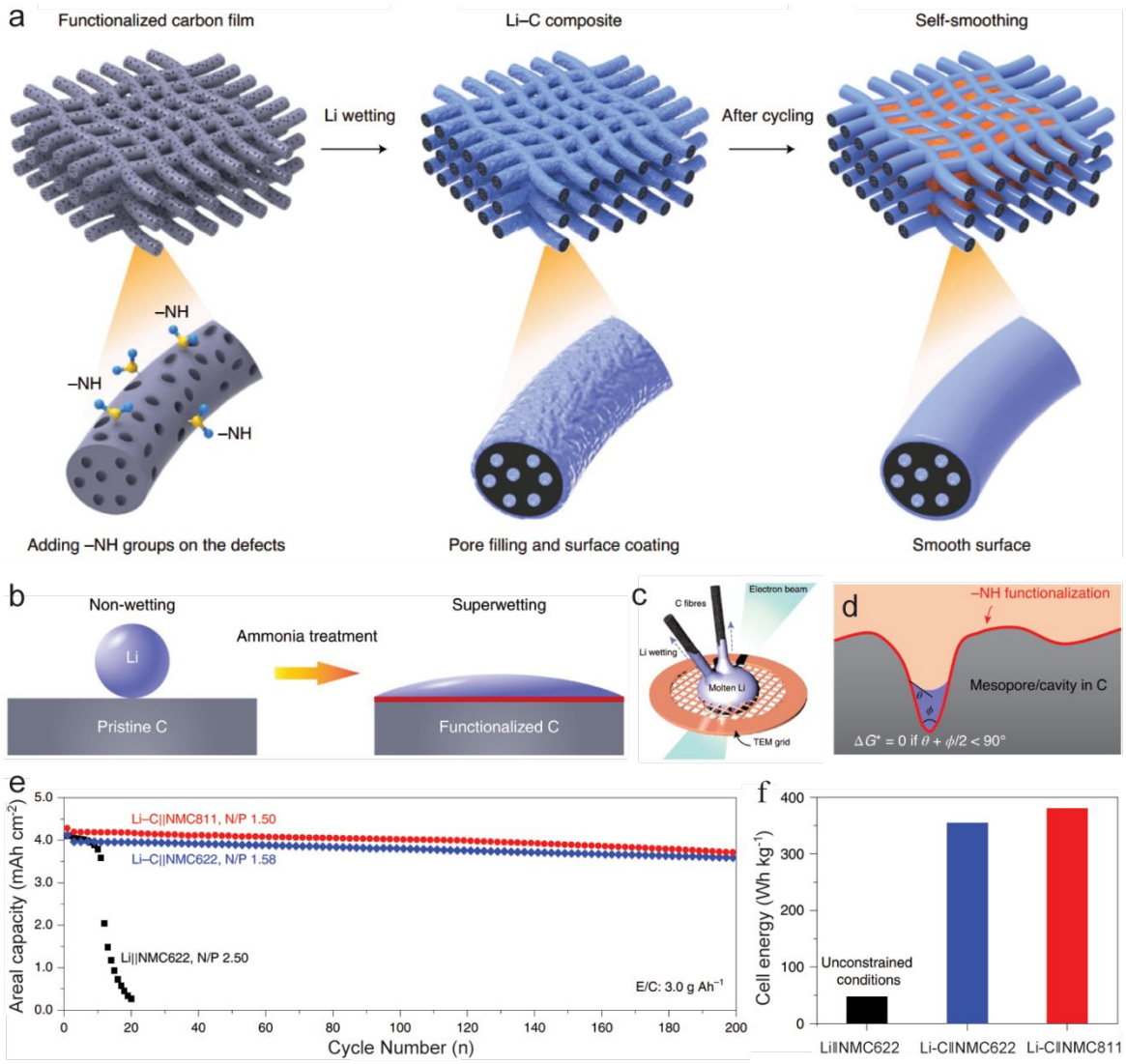

Fig. 16 a) Schematic of self-smoothing behavior on the Li–C surface, b) schematic of wettability of LMA on the functionalized-C surface, c) the wettability of carbon fiber is investigated by an in situ TEM, d) the nucleation behavior of lithium on the functionalized-C surface, e) cycling capability of three LMBs in different N/P ratios, f) estimated specific energy for the three LMBs.[143] a-f) Reproduced with permission from ref. 143. Copyright 2019, Nature Publishing Group.

the electrolyte consumption, alleviate the SEI or impedance build-up and hence retard the production of 'dead' Li. Therefore, when the Li-C was coupled with the $LiNi_{0.6}Mn_{0.2}Co_{0.2}O_2$ (NMC622) and $LiNi_{0.8}Mn_{0.1}Co_{0.1}O_2$ (NMC811) in a Li-C NMC622 (the capacity ratio of negative/positive electrodes (abbreviated as N/P) is 1.58, the ratio of electrolyte mass to cathode capacity (abbreviated as E/C) is 3.00 g Ah^{-1}) and Li-C NMC811 (N/P is 1.50 and E/C is 3.00 g Ah^{-1}) cells under the constrained conditions, respectively, a good cycling beyond 200 cycles was obtained with a high capacity retention at 0.20C charge and 0.33C discharge (Fig. 16e). Importantly, the Li-C NMC622 and Li-C NMC811 full-cells exhibited a high specific energy of 353 and 381 Wh kg^{-1} under realistic conditions, respectively, which are obvious superior to the constrained conditions Li NMC622 (Fig. 16f). These advantages indicate good prospect for the self-smoothing anode in high-energy LMBs.

3.3.2. Designing a rational current collector host for Li metal

An ideal LMA should be dendrite-free, but in reality dendrite growth is unavoidable. If the direction of dendrite growth is

perpendicular towards the cathode, unfortunately it would finally penetrate the separator and induce an inner short circuit.[66] In the development of stable LMA for LMBs, the current collector (CC) is regarded as an important component to regulate Li plating.[68, 70] The CC influences the nucleation at the initial stage of lithium plating, which is crucial for the morphology of the plated-Li during cycling.[70] Most of the CC applied in LMBs are planar, which is prone to non-uniform lithium deposition.[70] On planar copper CC (P-Cu), the direction of electric field is perpendicular to the cathode, but the distribution of the electric field occurs inside the polyimide-clad copper grid CC (E-Cu). In this design, the electric field

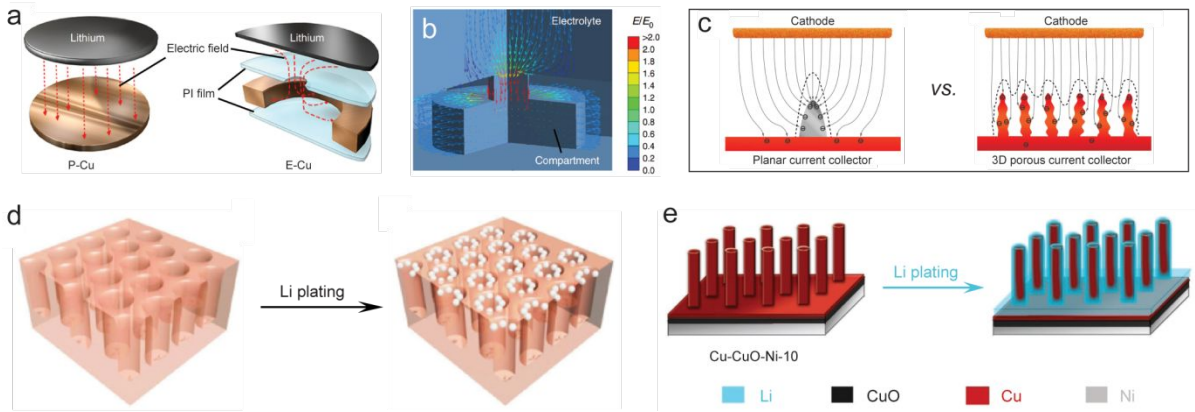

Fig. 17 a) Schematic diagrams of the electric field transport, b) schematic of the simulated electric field transport.[66] a and b) Reproduced with permission from ref. 66. Copyright 2018, Nature Publishing Group; c) Illustration of the Li^+/electrons distribution on planar/3D current collector during Li deposition.[70] Reproduced with permission from ref. 70. Copyright 2015, Nature Publishing Group; d) The simulated lithium plated preferentially on the holey Cu matrix.[67] Reproduced with permission from ref. 67. Copyright 2017, Wiley-VCH; e) Li depositing behavior on the lithiophilic Cu-CuO-Ni.[68] Reproduced with permission from ref. 68. Copyright 2018, Wiley-VCH.

spreads from the LMA, through the pinhole, and extends laterally to the E-Cu skeleton surface (Fig. 17a), which can be confirmed via a numerical simulation employing an electrical conduction model (Fig. 17b).[66] In addition, the phenomenon of charge accumulation at sharp ends in the electric field can be eliminated by designing a 3D porous Cu CC, the electric field and charges are uniform dispersion along the 3D porous Cu scaffold (Fig. 17c).[70]

In order to achieve stable and homogeneous lithium plating, designing a rational CC host for metallic Li is a feasible strategy. Guo and co-workers[67] design a porous Cu CC with vertically aligned microchannels (VAMCs) host for metallic Li plating (Fig. 17d). Lithium is uniform plated into the microchannels by adjusting the current density of the lithium plating/stripping processes. In comparison to the conventional planar Cu CC, the VAMCs Cu CC show great advantage in suppressing lithium dendrite growth. Cui and co-workers[71] also provided a new strategy to restrain the dendritic growth by a polymer-coating layer with vertical nanoscale channels (VNCs) of high specific surface area. The modified Cu CC achieved greatly improved CE and long-term cycle life compared with the bare planar CC. Additionally, the host scaffold with lithiophilic coating layer of a polyimide could permit complete Li entrapment. Therefore, the lithium dendrite growth could be restrain by manipulating Li^+ flux uniform distribution through VNCs confinement, the unique nanoarchitecture provides a major step towards dendrite-free LMA.

Recently, Zhang and co-workers[68] developed a lithiophilic Cu-CuO-Ni composite structure with low lithium nucleation overpotential compared with the bare Cu CC during Li plating process (Fig. 17e). The CuO provided lowered lithium nucleation overpotential than that of Cu during Li deposition while the Cu layer on the surface of Cu-CuO-Ni played the key role of a conductive and protecting layer. Besides, the lithiophilic nature is beneficial to form a well interface contact and achieve uniform Li-deposition. Therefore, the lithiophilic Cu-CuO-Ni nanowire arrays show evenly distributed electric field and lithium-ion flux, and finally achieve dendrite-free lithium plating.

As we all known that the uncontrollable Li dendrites especially under deep plating/stripping hinder its applications in LMBs.[147] In order to address this issue caused by deep Li plating/stripping, Yang and co-workers[148] develop an vertically oriented Li-Cu-Li arrays, which can uniform the distributions of both Li-ion flux and electric field, efficiently inducing the regular stripping/plating of Li during cycling. The preparation procedures of vertically oriented Li-Cu-Li arrays via controllable rolling or repeated stacking methods are presented in Fig. 18a. The deep Li stripping/plating processes of Li-Cu-Li in a cell are intuitively observed via a 3D video microscope (Fig. 18b-d), the lithium will be stripped from the Li-Cu-Li arrays after a deep stripping at 30 mAh cm^{-2}, forming deep and regular valleys (Fig. 18c). Reversibly, the lithium will be homogeneously plated between the Cu arrays and on the top during the deep plating, the plating Li gradually filled the valleys, leaving a flat and smooth surface without visible dendrites (Fig. 18d). The superior deep Li stripping/plating capabilities of Li-Cu-Li arrays also were verified by using a two-dimensional (2D) model to calculate the concentration

distribution of Li-ion (Fig. 18e-g). Based on the Fick's law ($J = \frac{d_m}{Ad_t} = -\frac{DC}{x}$) and Poisson equation, the transport flux of Li-ion is closely related to the distribution of electric field and the concentration gradient of Li-ion.[67, 149, 150] For the vertically oriented Cu arrays, the valleys are beneficial to homogenize the distributions of electric field and Li-ion flux, and facilitate Li-ion fill valleys (Fig. 18f). Additionally, according to "lightning rod theory", the electric field is preferentially concentrated at the top (white circles in Fig. 18g) of the Cu arrays, which result in the continuous deposition of Li and subsequently dispersion uniformly on the top of the copper arrays.[151] Therefore, the prepared Li-Cu-Li arrays showed better rate capabilities, longer cycle life and lower overpotential (91 mV for Li-Cu-Li arrays, 447 mV for bare lithium) than bare Li in a symmetric cells (Fig. 18h). In addition, the assembled Li-Cu-Li $LiCoO_2$ full cells exhibited good cycling stability and a high initial capacity, which is almost same to conventional LMBs (Fig. 18i). These superior electrochemical properties demonstrate that the vertical current collector arrays should be an effective strategy to control the dendritic growth.

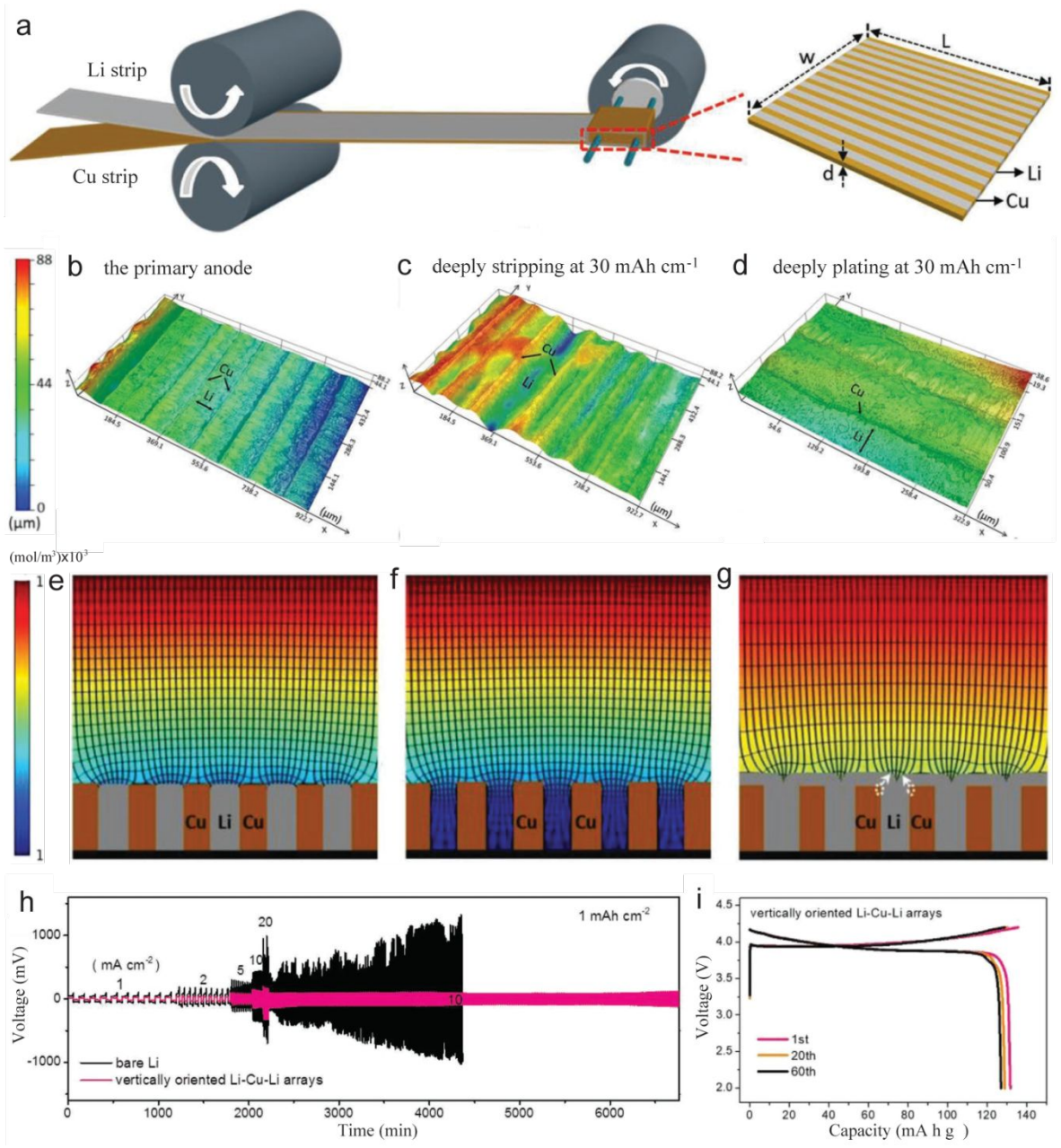

Fig. 18 a) Schematic of the preparation process of Li-Cu-Li electrodes, b-d) the evolution of top surface of Li-Cu-Li arrays in different charging states, simulation results of e) the initial Li-Cu-Li electrodes, f) the deep stripping and g) deep plating, h) the cycle stability of symmetric cells in different rates, i) charge/discharge curves of Li-Cu-Li $LiCoO_2$ full-cell.[148] a-i) Reproduced with permission from ref. 148. Copyright 2019, Wiley-VCH.

3.3.3. Developing nanostructured Li-alloy composite anode

High energy density alloy anode materials are one potential option for future high energy density LMBs, especially Si anode (the theoretical capacity is 4,200 mA h g^{-1}). However, the whole energy density of full cell is limited by using alloy without pre-stored lithium as anode. In such situations, Cui and co-workers[64] provide a universal strategy to prepare Li_xM (M = Si, Sn, or Al) alloy NPs encapsulated into a flexible 2D graphene network (Fig. 19a), the Li_xM/graphene foils inherit the desired properties possessed by both alloy anodes and LMA. For example, the volumetric capacity of Li_xSi/graphene membrane is 1,800-2,000 mA h cm^{-3}, approximating the theoretical value of LMA (2,061 mA h cm^{-3}). The prepared foil can effectively relieve the huge volume expansion by the confined effect of the graphene protection layer. Moreover, it is also stable when exposed to different air conditions due to the impermeable graphene layer to gases and good against oxidation (Fig. 19b). The long cycle stability and high CE of Li_xM/graphene V_2O_5 full cells show that Li-alloy composite anode is a promising high-energy anode for LMBs.

3.4. Optimal strategies "Solid-state electrolytes"

Numerous commercial LIBs use LOEs, where fast Li-ion transport kinetics is important to achieve high rate performance.[101]

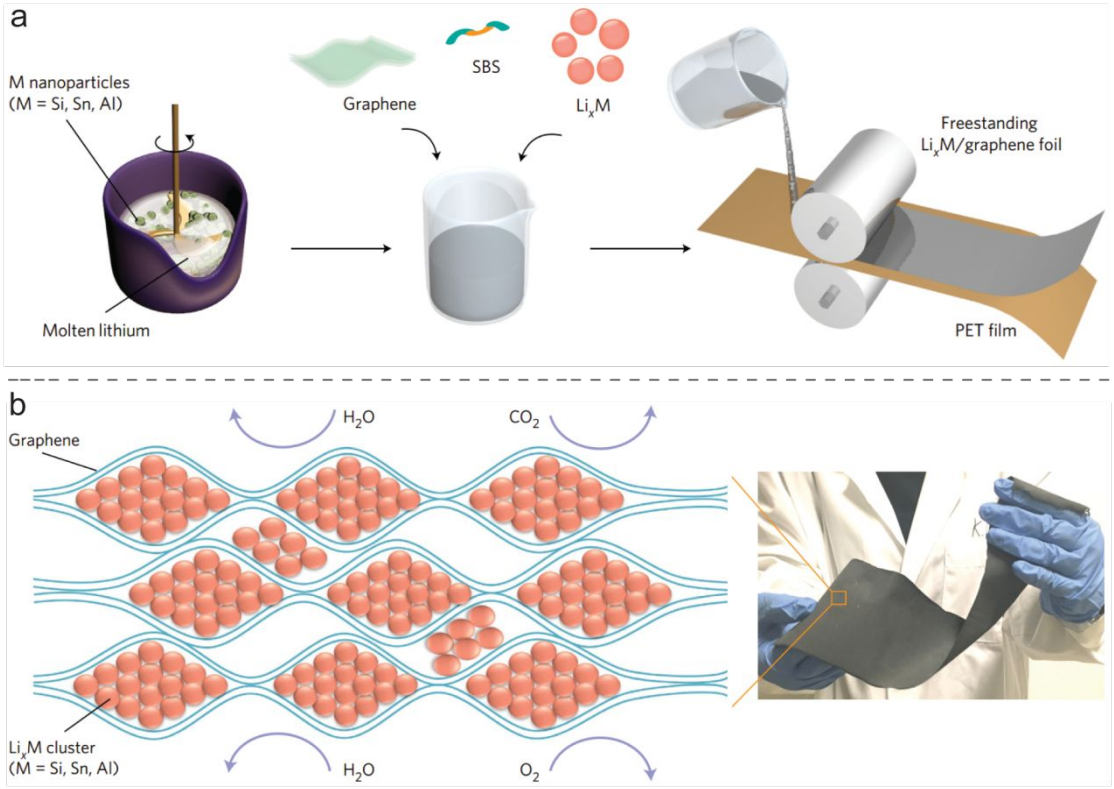

Fig. 19 a) Schematic of the preparation procedure of Li_xM/graphene composites, b) schematic of air-stable, flexible and freestanding Li_xM/graphene composites.[64] a and b) Reproduced with permission from ref. 64. Copyright 2017, Nature Publishing Group.

Unfortunately, its application has been frustrated by safety concerns arising from the lithium dendrite growth during Li plating.[152] In contrast, SSEs show great advantages beyond LOEs in term of impeding lithium dendrite growth and enhancing the safety issues of LMBs due to their high mechanical rigidity and nonflammable nature.[63] Therefore, the great efforts have been devoted to building the ideal high-safety solid-state LMBs (SLMBs) as shown in Fig. 20, in which the SSEs is critical to realize the future high-energy SLMBs. The ideal SSEs should possess high Li-conduct ability, sufficient rigidity, good interface contact, and low interface resistance. The seamless/compact interface contact between electrode and SSEs can well decrease the interface resistance and improve electrical connection, which should contribute to the fast ion diffusion kinetics.[87, 152] The sufficient rigidity of SSEs can effectively restrain the Li dendrite growth owe to its high elastic modulus and accommodate the large volume fluctuations of LMA during discharging/charging processes.[91] It is probably necessary that constructing a specific interface modification layer between LMA and SSEs to improve the interface wettability and further suppress the dendrite-Li growth as a buffer layer. Finally, the ideal SLMBs with high Li-conduct SSEs would exhibit the high energy and power density, which is comparable to liquid LMBs.

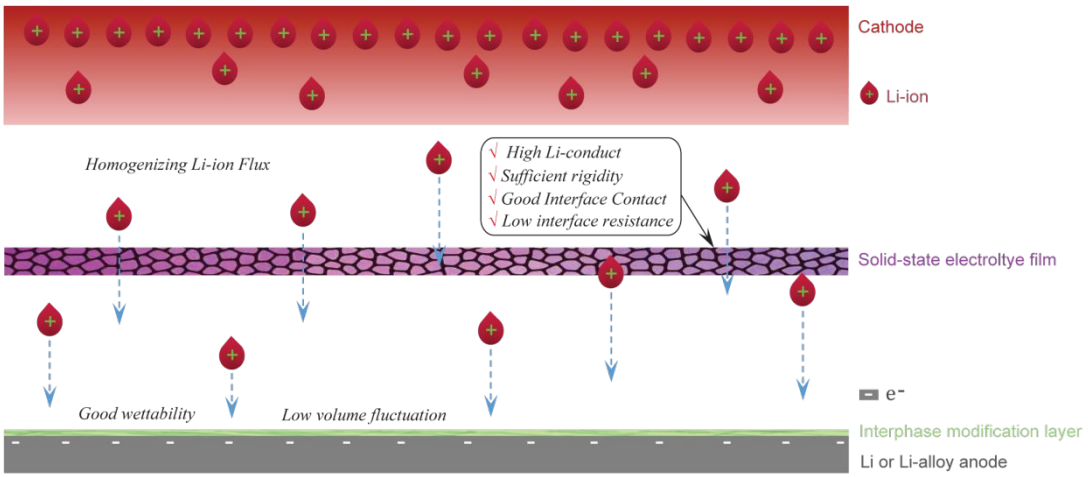

Fig. 20 Schematic illustration of an ideal high-safety SLMBs with superior solid-state electrolyte film.

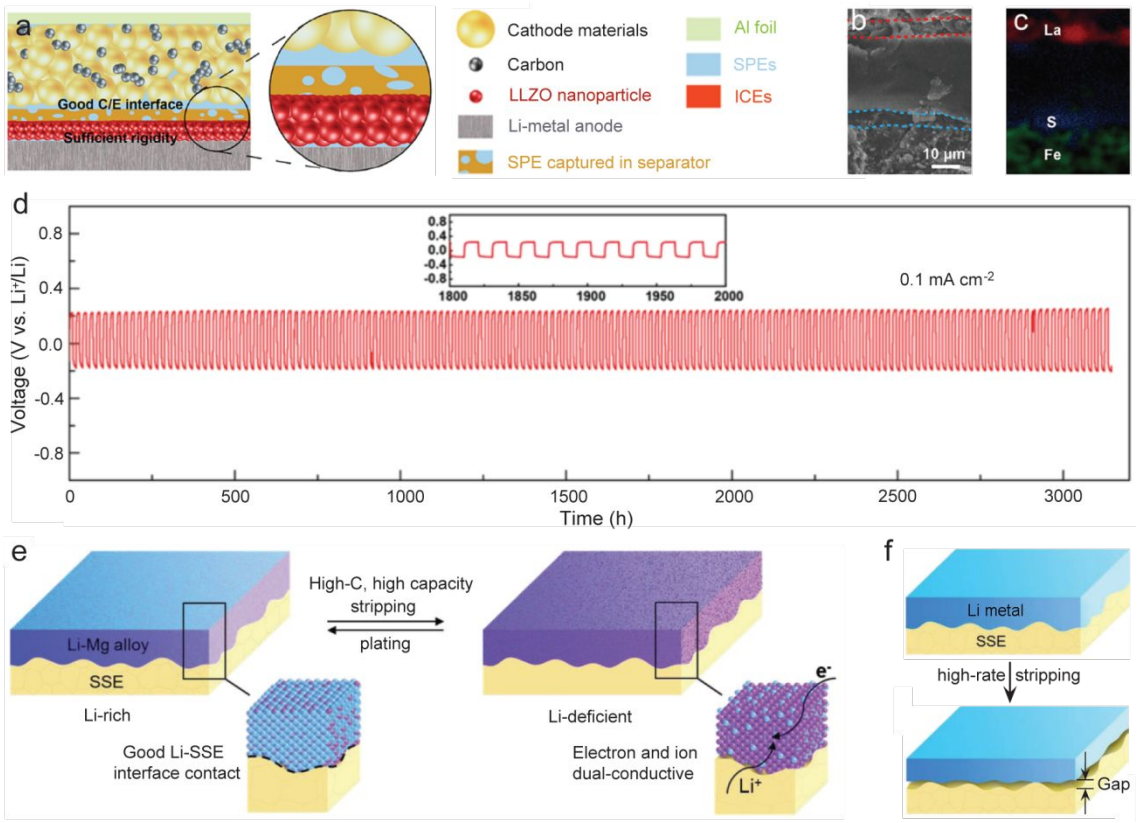

Fig. 21 a) Schematic of ASSE as electrolyte, b) side views and c) EPMA-EDS of the $LiFePO_4$ LLZTO/Li cell, d) the cycle stability of Li/ASE/Li cell.[115] a-d) Reproduced with permission from ref. 115. Copyright 2018, American Chemical Society; Schematics of the interfacial evolution of e) pristine LMA and f) Li-Mg alloy anode during lithium stripping/plating.[152] e and f) Reproduced with permission from ref. 152. Copyright 2019, Wiley-VCH.

3.4.1. A thin asymmetric SSEs with complementary advantages both PSSEs and ICSSEs

Various kinds of SSEs have been put forward to get more safe SLMBs, SSEs can usually be divided into two categories: polymer SSEs (PSSEs) and inorganic ceramic SSEs (ICSSEs).[115] PSSEs with morphology versatility and flexibility exhibit a low electrode/electrolyte interfacial resistance, but its low mechanical strength limits their capability to inhibit lithium dendrite penetration.[63, 115] On the contrary, lithium dendrites will have difficulty penetrating across ICSSEs films because of their robust mechanical rigidity.[91] However, the insufficient contact of ICSSEs and electrodes lead to high resistive interface, which hampered the independent development of ICSSEs in SLMBs.[24, 115]

Given these abovementioned factors, the complementary advantages between PSSEs and ICSSEs are an effective strategy to obtain practical SLMBs free of the aforementioned shortcomings.[115] From this point of view, Guo and co-workers[115] design a thin asymmetric solid-state electrolyte (ASSE) to satisfy the requirements of LMA and electrodes simultaneously (Fig. 21a). The unique ASSE consist of a compact $Li_7La_3Zr_2O_{12}$ (LLZO) layer with polymer electrolyte (PE) on the LMA side and a soft layer of PE on the cathode side, which are confirmed by the energy dispersive spectroscopy maps equipped (Fig. 21b, c). In this ASSE, the LLZO layer on the surface of LMA can effectively hinder the dendrite penetration due to its high elastic modulus, and the soft PE layer on the surface of cathode can form a compact interface contact, which would promote the ion/electron diffusion kinetics. Therefore, the cooperative effect of the PSSEs and ICSSEs provide a good interface contact and dendrite-free LMA, enhancing the life-span and safety of SLMBs (Fig. 21d).

3.4.2. An ion/electron dual-conductive alloy skeleton with seamless interface contact for SLMBs

In order to enhance the poor interface contact between electrodes and SSEs, Hu and co-workers provided a ion/electron dual-conductive solid frame by partly dealloying the Li-Mg in a garnet-type SSEs,[152] which successfully addressed the issues of poor interfacial contact and sluggish ion/electron kinetics (Fig. 21). The interface of pure Li with the garnet electrolyte during Li stripping could produce interface gaps (Fig. 21e), especially at high current density, which lead to the increased interface resistance.[91, 152] On the contrary, the Li-Mg and garnet form a compact interphase without any obvious gaps between the Li-Mg and SSEs (Fig. 21f). The seamless interface contact would improve the interfacial chemistry (including low interface resistance, good electron/ion dual-conductive interface) and provide a stable electron/ion dual-conductive solid skeleton during Li plating/stripping.[152] This strategy of designing a dual electron/ion conductive alloy skeleton provides a possible path to achieve high energy SLMBs.

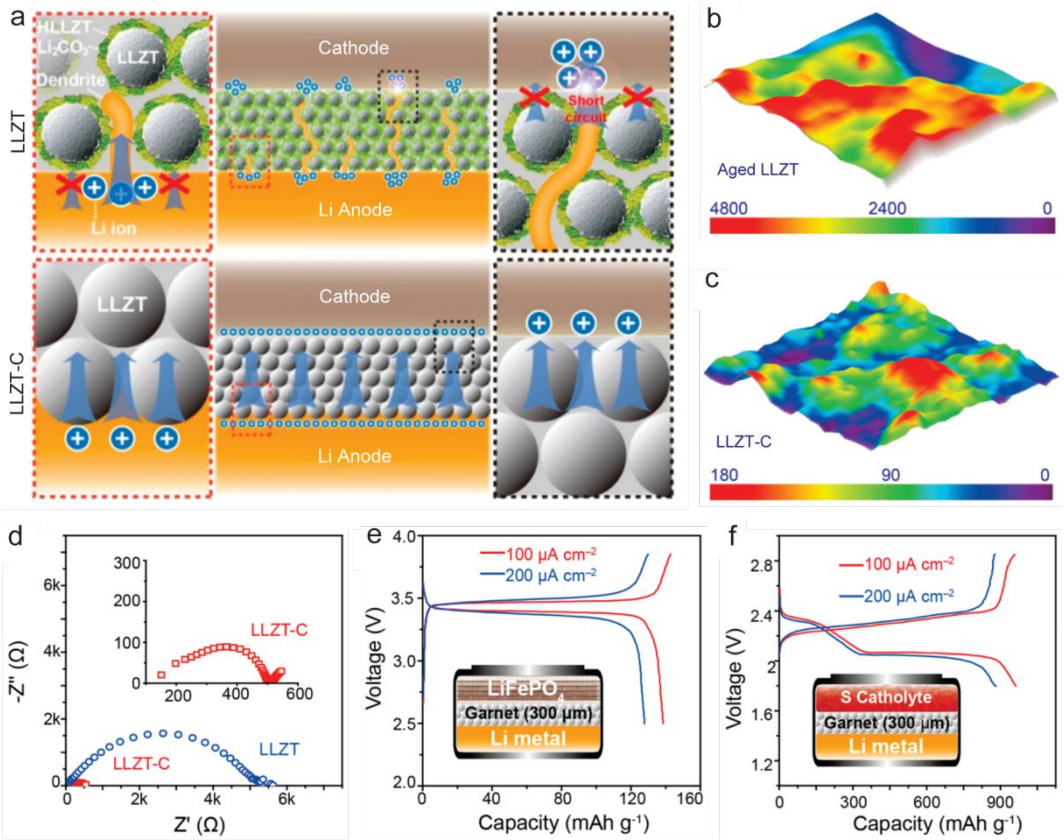

Fig. 22 a) Schematic of Li-ion transport behaviour LMBs with LLZT and carbon-decorated LLZT, Raman mapping of b) LLZT and c) carbon-treated LLZT, d) EIS of LLZT and carbon-modified LLZT, the capacity/voltage curves of e) asymmetric Li/LLZZT-C $LiFePO_4$ and f) Li/LLZZT-C S SLMBs at 65 °C.[100] a-f) Reproduced with permission from ref. 100. Copyright 2018, American Chemical Society.

3.4.3. A modified garnet-type SSEs with ultralow interfacial resistance for SLMBs

Various oxide solid Li-ion conductors have been widely researched due to their large electrochemical window and superior chemical stability against moisture.[91, 115, 153, 154] The typical oxide electrolytes include LIPON (e.g., $Li_{2.9}PO_{0.3}N_{0.46}$),[155]

perovskite (e.g., $Li_{0.33}La_{0.55}TiO_3$),[156] garnet (e.g., $Li_7La_3Zr_2O_{12}$),[154, 157] NASICON (e.g., $Li_{1.3}Al_{0.3}Ti_{1.7}(PO_4)_3$),[105] and antiperovskite (e.g., Li_2OHCl).[156, 158] In these oxide electrolytes, the garnet-type electrolytes with low interfacial resistance are chemically more stable with metallic Li in comparison to other electrolytes. However, a passivation layer could be generated on the interface between garnet LLZO and LMA through contact with each other.[154] Generally, the surface of bare garnet $Li_{6.5}La_3Zr_{1.5}Ta_{0.5}O_{12}$ (LLZT) electrolytes easily forms a Li_2CO_3 layer by H^+/Li^+ exchange and hence decreases the Li^+ conductivity. [157, 159] Furthermore, the insulating Li_2CO_3 layer may irreversibly decompose at 3.2 V ($2\ Li_2CO_3 + C \rightarrow 3\ CO_2 + 4\ Li^+ + 4\ e^-$), which is harmful to the electrochemical window of this garnet-type electrolytes.[159, 160] With this perspective, Goodenough and co-workers developed a carbon-treated garnet LLZT (LLZT-C) electrolyte with an very low interface resistance for SLMBs (Fig. 22a), which has no Li_2CO_3 on the surface of garnet LLZT-C by the contrast experiment of Raman mapping between LLZT (Fig. 22b) and LLZT-C (Fig. 22c).[91] These abovementioned points are vividly depicted in Fig. 22a, a stable garnet LLZT-C framework with high Li-ion conductivity and low interface resistance were formed by a simple yet efficient carbon post-treatment method (Fig. 22d). Most importantly, the good electrochemical performances with high CE and small overpotential of asymmetric Li/LLZZT-C $LiFePO_4$ and Li/LLZZT-C S full cells have preliminary demonstrated their potential applications in the future high safety SLMBs (Fig. 22e and f).

3.4.4. Engineering 3D LMA with flowable interphase for SLMBs

Replacing volatile LE with nonflammable SSEs counterparts is an attractive strategy to restrain Li dendrite growth.[63] However, the low Li-ion conductive, large interface resistance, large volume and poor interfacial contact between SSEs and electrodes are serious hindrances the development of SLMBs, these issues result in uneven current distribution, which may accelerate Li dendrite growth.[154] In addition, unlike LE, SSEs hardly have any fluidity to achieve a successive contact with active materials inside the electrodes.[63] Various strategies have been proposed to enhance the interfacial conglutination and ion/electron dual-conductive properties and interfacial fluctuation between electrodes and SSEs, including engineering the alloy interface layer on the LMA,[101, 152] plasticizing PSSEs,[161, 162] building interfacial buffer layers,[105, 163] and constructing 3D Li-containing composite anode.[63] Although a wide variety of SSEs for LMBs have been proposed in these years, these

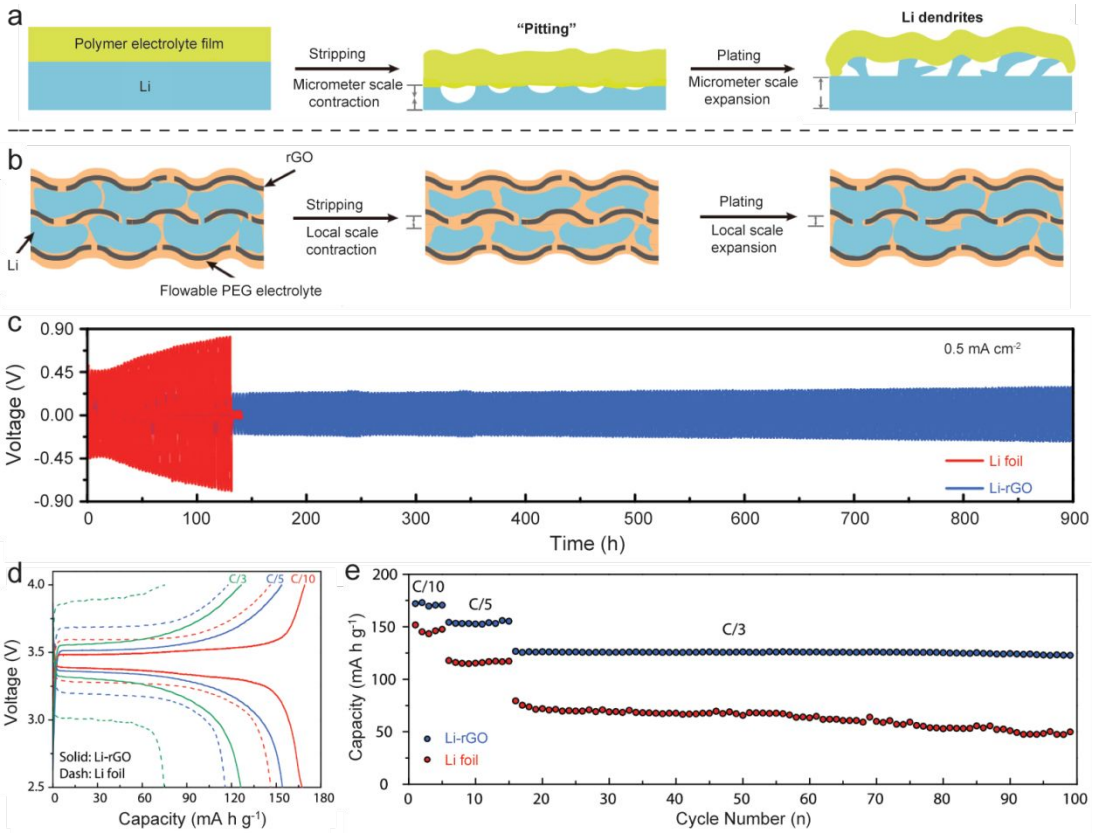

Fig. 23 a) Schematic elaborating the volume shrink/expansion and inhomogeneous lithium stripping/depositing of LMA, b) schematic revealing the superiorities of the flowable Li-rGO in solid LMBs, c) the cycle stability of Li-rGO and fresh LMA electrodes in a symmetric cells, d) galvanostatic curves and e) long cycle performances of full-cells employing $LiFePO_4$ as cathode.[63] a-e) Reproduced with permission from ref. 63. Copyright 2017, AAAS.

technologies are still far from practical application.[154]

In order to address the aforementioned issues and make LMA a feasible technology, Cui and co-workers provided an aradigm shift on the structural design of SLMBs, a 3D LMA composite with flowable interphase (the flowable interfacial cycling) were prepared for SLMBs,[63] it is obvious different from all previous studies where SLMBs were designed using planar Li foil.[60, 62, 164] The planar Li foil have a large volume fluctuation during Li stripping/plating and inhomogeneous Li stripping/plating make it hard to form a good connect between electrodes and SSEs (Fig. 23a).[62, 63] On the contrary, the 3D LMA interface is ionically connected to the bulk SSEs by a flowable PE interphase, which is important for accommodating the interfacial fluctuation to keep a seamless contact during cycling (Fig. 23b).[62, 63] Furthermore, a homogeneous Li layer with a thickness of several hundred nanometers can form in between 2D reduced graphene oxide (rGO) nanosheets after the redox reaction between Li and GO film host.[62] The rich surface functional groups on rGO can generates a good molten Li wettability due to the lithiophilic surface of rGO.[24, 62] Therefore, the solid-state cells (SSCs) with flowable interphase 3D Li-rGO showed more stable cycling performance for at least 900 hours in symmetric cells (Fig. 23c) and much lower charge/discharge polarization and high specific capacity in solid-state Li $LiFePO_4$ batteries (Fig. 23d, e) compared to the conventional SSCs with planar Li foil.[63]

3.5. Other emerging strategies for developing high-energy LMA

3.5.1. Intermittent high-current pulses prevent battery failure

Application of LMAs gives high energy densities in second LMBs, but the continuous growth of lithium dendrites not only consumes Li-ion from electrolyte but also causes failure of the cell due to short circuiting.[4, 165] Employment of intermittent high-current pulses provides a promising path to heal the dendrites and prevents short-circuiting (Fig. 24).[4, 165, 166] This concept of pulse current charging was first applied for lead acid battery to remove undesired components and to extend battery life span.[167] In the past year, Li and co-workers[4] employed a simple physical concepts to capacitate the dendrites to heal themselves. They found that the dendrites undergo self-heating at an appropriate current density, which promote the flux/flow of Li-ion, smooth the dendrites and finally form the equilibrium flat configuration quickly. In addition, the surface transport of Li-ion is mainly temperature-dependent based on the MDS of Li transport process.[4, 166] The processes of self-heating during Li stripping/plating are safe without electrolyte breakdown or thermal damage. For example, cells were

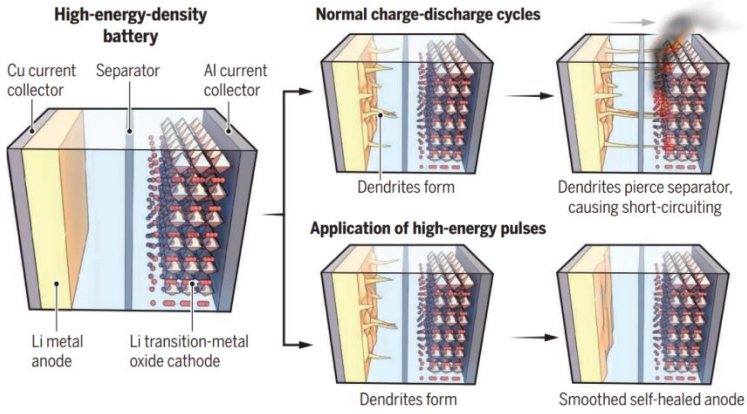

Fig. 24 Schematic of self-healing strategy of LMBs.[165] Reproduced with permission from ref. 165. Copyright 2018, AAAS.

cycled at 15 mA cm^{-2} indicated no occurrence of short circuiting even after long time in symmetrical Li-Li cell. In addition to dendrite healing in symmetrical batteries, the healing processes of dendrites also are suitable to the asymmetrical Li-S full-cells system. The Li-S cell was cycled at ~9.0 mA cm^{-2}, the dendrites will heal themselves into a smooth (film-like) surface. Therefore, the healing strategy is also a reconstruction processes of dendrites surface and SEI, the CE will again regain back to a high value during the healing process.[4] These rational results of this strategy will provide a potential solution to develop high energy LMBs.

3.5.2. Healing Li dendrite of LMA by applying an asymmetrical bidirectional current

The dendrite-free LMA is essential condition to realize high safety LMBs, dendrites are often derived from the non-uniform charge distribution,[4, 165] which result in the SEI fracture and dendritic growth and finally lead to the failure of LMA. In order to suppress the dendritic growth, some emerging strategies of healable LMA are rising, by the means of optimizing charge distribution. For instance, Li and co-workers[4] found that the LMA can be healed by the way of heating-induced nucleation.

Wang and co-workers[168] proposed that a suitable stress distribution also can heal LMA. Recently, Wu and co-workers[169] developed an asymmetrical bidirectional current (ABC) and a shelve time for charge relaxation (STCR) methods to heal LMA. By comparison, the ABC method exhibits the best healing ability among three modes (ABC, CM and STCR) in suppressing dendrite growth (Fig. 25a). The ABC method is an asymmetrical-deposition by inversing current for dendritic elimination, the shelve time of ABC is turned into an inverse current to dissolve the reborn dendrites (Fig. 25b). By this method, the reborn dendrites can be well restrained by the synchronous healing mechanism (Fig. 25c), a smooth interface during Li plating can be kept, and a stable cycling with a low polarization of ~27 mV beyond 1000 h can be obtained (Fig. 25d). These electrochemical performances are obvious superior to the conventional chronoamperometry mode (CM) method in terms

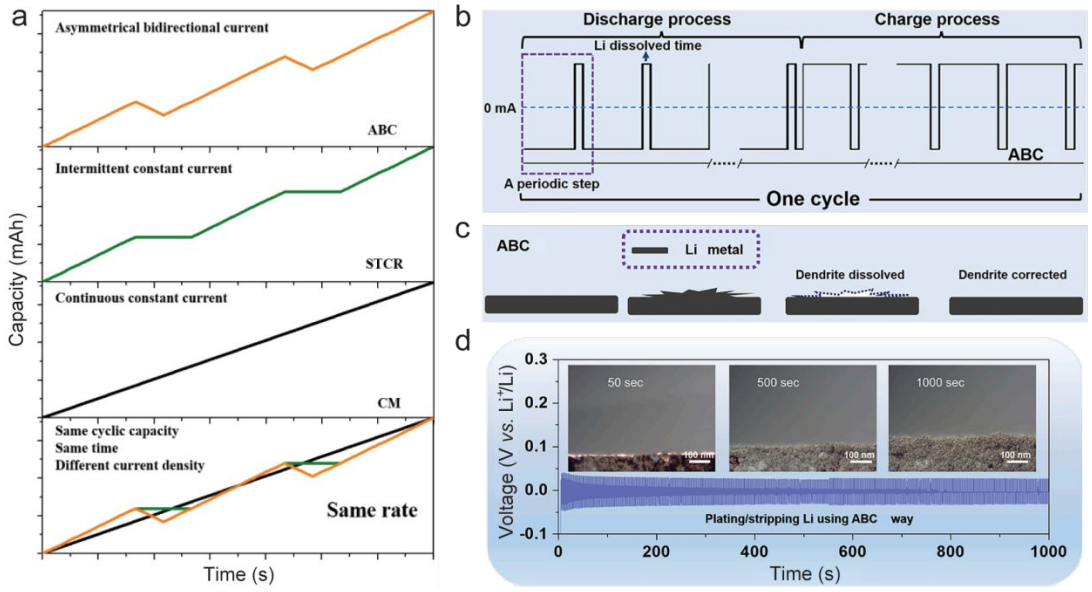

Fig. 25 a) The curves of three charging models, schematic of b) ABC model and c) the interfacial evolution of LMA under ABC model, d) the polarization stability by means of ABC (the three insets are the lithium plating behaviour in Li/Cu system).[169] a-i) Reproduced with permission from ref. 169. Copyright 2020, Cell Press.

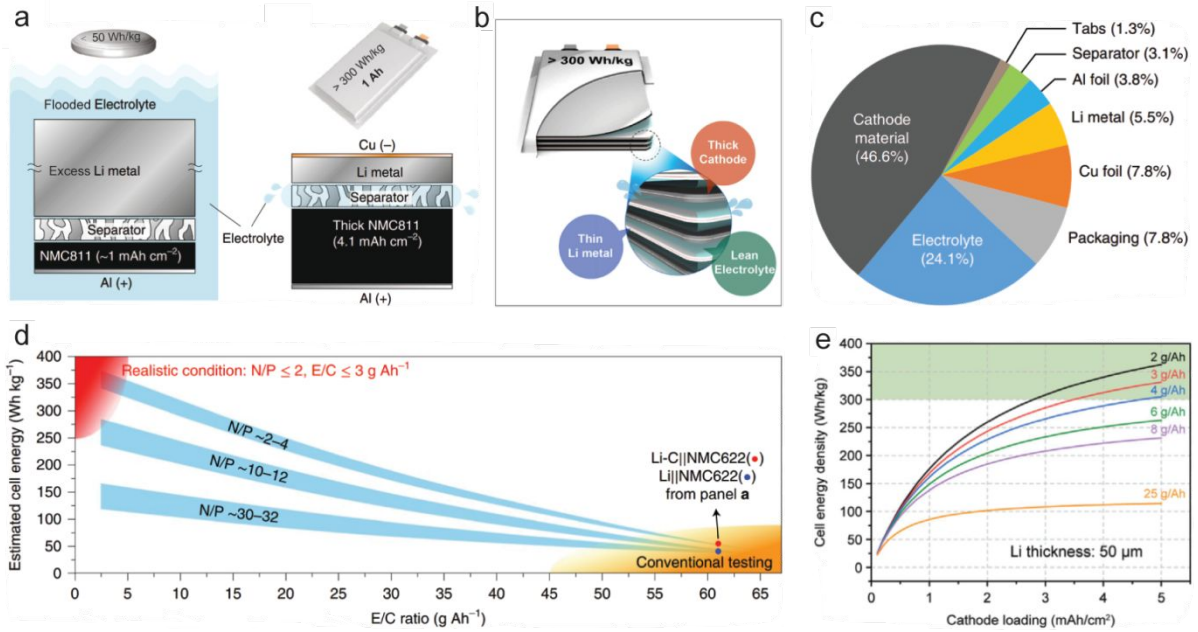

Fig. 26 a) Comparison of the lab cell-level and the high-energy pouch-cell.[170] Reproduced with permission from ref. 170. Copyright 2019, Springer Nature; b) The goal of a pouch-cell is over 300 Wh kg^{-1} with high ACM loading, lean electrolyte and thin LMA.[171] b and e) Reproduced with permission from ref. 171. Copyright 2019, Cell Press; c) The mass distributions of a pouch-cell.[172] Reproduced with permission from ref. 172.

of low polarization, superior stability, long cycle life and stable SEI, indicating ABC is an effective approach to suppress the dendritic growth during repetitive cycling.

3.5.3. Benchmarking the electrochemical performances of LMBs

Generally, it is hard to evaluate to various LMBs performance due to the lack of a standardized benchmark.[8] Recently, scientists have been proposed some benchmark protocols for building high-energy LMBs, which will facilitate the development of LMBs with high specific energy (E_m).[8, 170, 171] Obviously, the conventional coin-cell presents a low E_m (E_m < 50 Wh kg^{-1}) based on the mass of flooded electrolyte, excess LMA and low cathode active material (CAM) loading in most reported articles, which is far from the goal of 300 Wh kg^{-1} (Fig. 26a).[170] Therefore, a practical pouch-cell with lean electrolyte, high CAM loading and thin LMA was proposed, which had a high E_m of over 300 Wh kg^{-1} (Fig. 26b),[171] and the composition of the pouch-cell was presented in Fig. 26c.[172] Distinctly, the mass of CAM loading, LMA and electrolyte mainly determine the E_m of pouch-cell, decreasing the mass percentage of electrolyte and LMA or increasing the ratio of CAM are beneficial to increasing the E_m of cells. Herein, there are mainly four strategies can effective enhance the E_m of pouch-cells:[8, 143, 170] i) decreasing the ratio of N/P (eg. N/P ≤ 2); ii) decreasing the E/C ratio (eg. E/C ≤ 3 g Ah^{-1}); iii) increasing the mass percentage or areal capacity of CAM; iV) using high E_m CAM such as NCM with high-nickel content (eg, NMC622, NMC811 of over 180 mA h g^{-1}), LNCM (> 147 mA h g^{-1}) and Li_2S/S (> 1166 mA h g^{-1}). Liu and co-workers[170] revealed the relationship among E_m, N/P and E/C in a pouch-cell at different conditions, the goal E_m of over 300 Wh kg^{-1} can be achieved only when both N/P ≤ 2 and E/C ≤ 3 g Ah^{-1} in a NMC622 Li pouch-cell (Fig. 26d and e).

From the abovementioned viewpoints, we compared the key electrochemical performances of these advanced strategies represented in this review (Table 1), most of the reported strategies are far from the goal of 300 Wh kg^{-1}. Therefore, the effectiveness of these strategies is somewhat difficult to confirm because some key electrochemical parameters are not carefully limited.[171] For example, the rate and cyclability of LMA and LMBs can be controlled via the mass of electrolyte, CAM loading, LMA thickness and areal capacity in some extent. So it is critical that benchmarking the electrochemical parameters to evaluate the real properties of new materials and realize the high-energy LMBs.[171, 173] From now on, the tested electrochemical performances of LMBs should better obey the benchmark proposed by Liu[170, 171] and Janek[8] to realize the goal of 300-500 Wh kg^{-1} in LMBs.

4. Building better all-solid-state lithium batteries

Li dendrite is relatively easier to form in LEs, which may cause sporadic safety hazard.[75, 93] Various strategies have been proposed to restrain Li-dendrite growth during Li stripping/plating, including interfacial chemistry regulating[14-16, 23-25, 27, 34]

Table 1 Comparison of key electrochemical performances of LMBs in various strategies.

Strategies	Cathode‖Anode	CAM Loading (mg cm^{-2})	Li foil (μm)	Electrol-yte (μL)	*T* (°C)	C-Rate/ Capacity (mA cm^{-2})	N/P	Tap Density (g cm^{-3})	Area capacity (mAh cm^{-2})	E/C (g Ah^{-1})	E_m (Wh kg^{-1})
MCI[25]	NMC532 Li	12.02	500	80	25	2.5	-	-	0.5	-	-
MCI[103]	S LLTO/Li	3.0	20	21.4	25	1.5	-	-	-	-	-
SEI regulation[14]	NMC333 Li-PAA	4.0	50	excess	25	1.0	-	-	3.4	-	-
SEI regulation[108]	$LiFePO_4$ p-Li	2.0	400	30	25	0.5C	-	-	2.4	-	-
Interfacial regulation[109]	NMC532 Li	12.02	500	50	25	0.5C	-	-	-	-	-
Interfacial regulation[34]	S Li	1.5	750	-	25	2	-	-	2	-	-
Li-alloy anode[101]	$LiFePO_4$ Li/Ge-garnet	-	-	-	25	0.1	-	-	-	-	-
Li-alloy anode[99]	$LiFePO_4$ Li_xSi-Li	7.4	590	-	25	0.2C	-	-	1.2	-	-
Li-alloy anode[26]	Li-O_2	0.3	400	70	25	0.3	-	-	-	-	-
gradient interfacial[24]	S GZCNT@Li	2.5	273	-	25	0.6	-	-	3	-	-
optimizing electrolyte[42]	NMC333 Li	10.7	250	70	25	0.1C	-	-	1.7	-	-
optimizing electrolyte[39]	NCA Li	12	-	excess	25	0.5C	-	-	2.5	-	-
Optimizing electrolyte[118]	$LiFePO_4$ p-Li	-	50	25	25	0.1C	-	-	1.0	-	-
Li host[50]	$LiFePO_4$ MIEC/Li	8	-	60	25	0.2C	-	-	1.0	-	-
Li host[51]	NMC532 Li	1.4	-	-	25	1C	-	-	-	-	-
Li-CNT host[52]	$LiFePO_4$ Li-CNT	-	-	40	25	1	-	-	2.5	-	-
Li-NGCF host[53]	$LiFePO_4$ Li-NGCF	13	-	-	25	0.5C	-	-	-	-	-
Li-Ni foam host[54]	$LiFePO_4$ Li-Ni	2.5	-	excess	25	0.2C	-	-	-	-	-
Self-smoothing interface[143]	NMC622 Li-C	22.53	Li-C (100)	13	25	0.3C	1.58	~1.2	4.0	3	353
	NMC811 Li-C	20.82	Li-C (100)	13	25	0.2C	1.5	~1.2	4.2	3	381

Li-Cu host[67]	$LiFePO_4$ Li-Cu	5.8	-	50	25	0.5C	-	-	1	-	-
Li-Cu-Ni host[68]	$LiFePO_4$ Li-Cu-Ni	2.0	-	-	25	2C	-	-	-	-	-
3D-Cu-Li[70]	$LiFePO_4$ 3D-Cu-Li	-	-	30	25	0.1	-	-	1	-	-
Li-alloy/graphene[64]	V_2O_5 Li_xSi-rGO	-	-	-	25	1C	-	-	-	-	-
	$LiFePO_4$ Li_xSi-G	-	-	-	25	1C	-	-	-	-	-
	S Li_xSi-graphene	-	-	-	25	0.5C	-	-	-	-	-
Interfacial design[115]	$LiFePO_4$ LLZTO/Li	2	-	80	55	0.2C	-	-	-	-	-
Modified SSE[100]	$LiFePO_4$ LLZT-C/Li	3	-	-	65	0.1	-	-	-	-	-
	NMC811 LLZT-C/Li	3	-	-	65	0.1	-	-	-	-	-
	S LLZT-C/Li	1	-	-	65	0.1		-	-	-	-
Flowable interphase[63]	$LiFePO_4$ LLZTO/Li-rGO	6	-	-	80	3	-	-	1	-	-
ABC method[169]	$LiCoO_2$ Li	-	65	100	25	0.4C	-	-	-	-	-
Limited anode swelling[172]	NMC622 Li-C	20.5	50	3.3g	25	0.3C	2.6	3.0	3.8	3	313
Pouch Cells[171]	NMC622 Li	19.4	50	3.3g	25	0.1C	2.86	3.0	3.5	3	300

The "-" means there is no data available.

and optimizing electrolyte components (Route 1 in Fig. 27),[39, 42, 43, 110, 115, 141] designing a rational 'host' for LMA[48, 50-54, 66, 68]

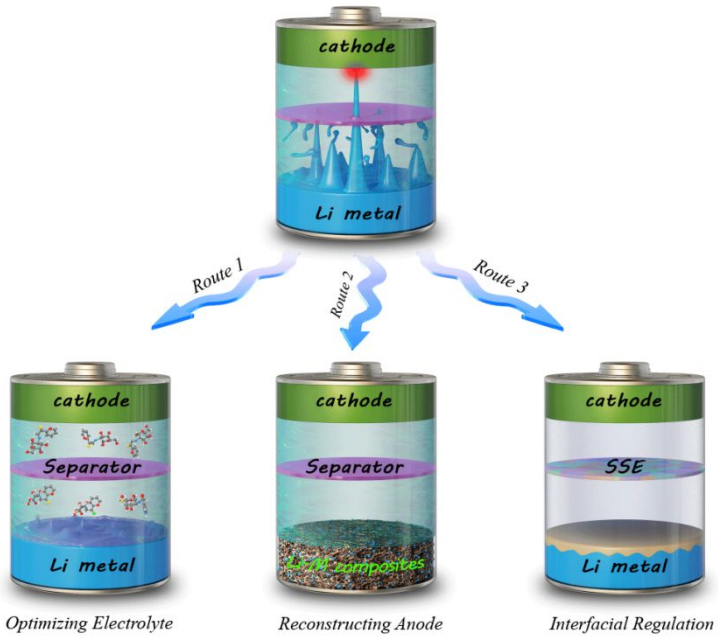

Fig. 27 The main roadmap for developing high-safety LMA in high-energy LMBs. Note that: Li-M is Li-Matrix, SSE is solid-state electrolyte film.

(Route 2 in Fig. 27) and other emerging strategies[4, 7, 57, 64, 165, 174]. While these strategies on LMA protection have been well improved in suppressing the growth of Li dendrites, safety concerns and challenges still remain. SSEs with nonflammable nature and robust mechanical rigidity can well satisfy this point. All-solid-state lithium batteries (ASSLBs) are widely regarded as an ideal battery due to its security, suppressing Li dendrite formation and noncombustible nature,[91, 115, 175] making SSEs the key to build better batteries (Route 3 in Fig. 27). Although the ASSLBs are far from optimized, we believe that it will become a reality by using optimized SSEs to improve the interfacial chemistry (including high ion/electron conductivity, seamless interface contact, ultralow interfacial resistance) between electrodes and SSEs. Furthermore, the electrochemical performances and cycling life of ASSLBs can be further enhanced by engineering a stable 3D Li-containing skeleton[10, 62, 63, 101, 152, 164] such as 3D Li/graphene with flowable interphase[63] or an ion/electron dual-conductive alloy framework.[152]

Generally, SSEs with non-flammable nature are divided into two major categories, polymer-based SSEs (PSSEs) and inorganic-based SSEs (ISSEs). The PSSEs hold a stable interface, easy processing, low conductivity, low tap density and good interface compatibility.[176, 177] Recent years, various PSSEs were rapid developed including ionic PSSEs with flexibility and mechanical integrity, polycarbonate PSSEs with weak Li-ion coordination, high salt concentration PSSEs and their ramification.[177-179] Another class of electrolytes, ISSEs are also widely researched due to its high ionic conductivity, high mechanical strength, high tap density and broad electrochemical windows, but its disadvantages (eg. huge interface

resistance, inferior machinability and poor interface compatibility) hinder its practical application.[145-149] We compared these key electrochemical/physical properties among PSSEs, ISSEs and composite PSSEs/ISSEs (Fig. 28), it is obvious that ISSEs or PSSEs have their own distinctive defects, while the optimized composite/hybrid SSEs consist of inorganic filler and polymer can achieve more superior electrochemical performance than the two class separately. This is in terms of overall ionic conductivity, interface chemistry mechanical strength, batch manufacturing, electrochemical window and dendrite suppression, which demonstrates that the optimized composite/hybrid ISSEs-PSSEs with complementary advantages of both PSSEs and ISSEs is a promising strategy to obtain idea SSEs for future high safety ASSLBs.

These complementary strategies offer very effective channels to improve the interface chemistry of composite SSEs and impede Li dendrite growth in SSEs, some SSEs with distinctive features can be considered such as Garnet-type oxides, NASICON-type, sulfides and nitrides for constructing better composite SSEs.[77, 177, 180-184] For a single component, Zaghib and co-workers[185] found that the PSSEs would gradually become thinner in thickness and decompose with cycling, leading to gas generation, which was responsible for the battery failure. Besides, Wang and co-workers[186] revealed that the origin of Li dendrite formation in Li_3PS_4 and LLZO are attributed to their high electronic conductivity, so researchers should focus on decreasing the electronic conductivity of SSEs with high electronic conductivity in the future, not further increasing. Therefore, it is essential to introduce another component to compensate these defects of single component solid electrolyte, and hence obtain desired solid electrolytes.

The interfacial chemistry of between electrode/SSEs is a huge challenging to build better ASSLBs. Scientists have made great efforts in term of interfacial compatibility,[77, 187] interfacial wettability,[116, 178] mechanical strength[180, 181, 188] and ionic

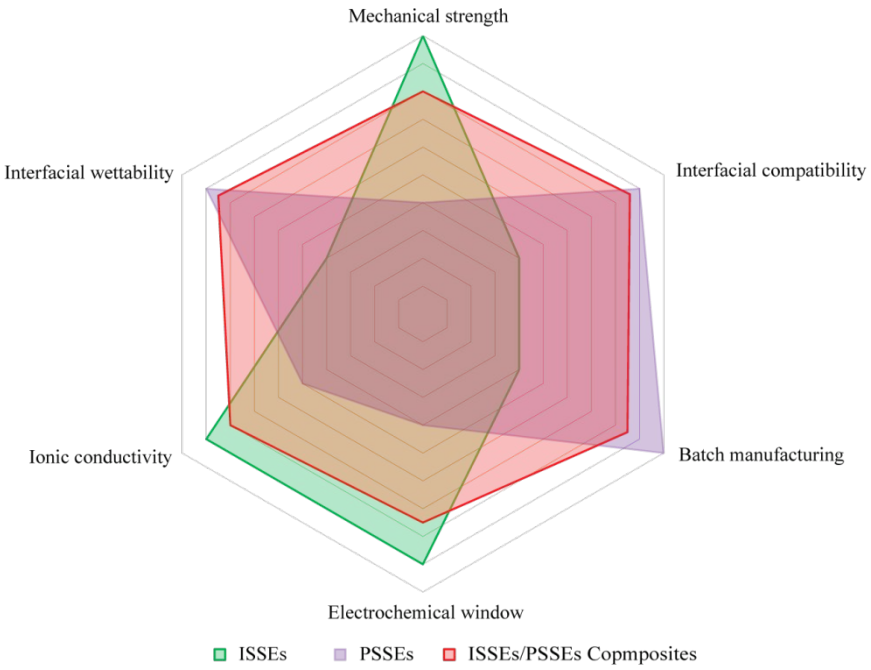

Fig. 28 The spider chart of properties of ISSEs, PSSEs and ISSEs/PSSEs composites.[176-178, 180, 188]

conductivity[179, 182, 189] to improve the chemical/physical properties of the interface between electrode and electrolyte. Some key factors should be considered such as volume expansion/contraction during cycling, which generates a fluctuation in mechanical strain at the interface of electrode and electrolyte, which may result in electron disconnection if the designed interface can't accommodate the volume fluctuation.[2, 190] Therefore, some PSSEs with good interface bonding properties are often introduced into the composite SSEs to address abovementioned issues. Another effective solution is to add a small amount of liquid electrolyte to build a conformal interface, which is also called liquid phase therapy.[191] Finally, the interfacial ionic migration and interfacial reaction with Li should be considered before engineering SSEs, the former decide the rate performances, the latter is closely related to the utilization and consumption of Li.[192] The polymer with superior flexibility and high Li-ion transport with ISSEs content over the percolation threshold present a promising channel to enhance Li conductive, interfacial stability and mechanical strain of the composite/hybrid SSEs.

5. Emerging characterization techniques for LMA in LMBs

To address the challenges of LMBs,[96, 97, 193] our fundamental understanding of the reaction mechanisms is required. However, the complicated physical/chemical processes during cycling still have many unknown properties. Fortunately, various state-of-the-art in situ/operando synchrotron-based X-ray methods are powerful instruments for offering detailed information about the electrochemical mechanisms of LMBs.[96, 97, 194, 195] Moreover, a variety of in situ/operando cell configurations and effective detecting methods for cell design are rapidly developing.[96, 97, 193]

5.1. How is lithium intercalated between bilayer graphene?

The details of these brief intermediate states or non-equilibrium chemical entities are impossible to perform deconvolute by ex situ characterization techniques.[96, 97, 193] The ex situ measurements are likely to involve contamination, relaxation or changes when transferring and handling.[97] On the contrary, in situ characterization can immediately probe the real information at the desired location of a sample, ensuring precision and reliability of the characterization data.[96, 97, 195, 196] Carbon-based materials, especially 2D or 3D graphene-based materials as an optimal host materials for LMA have attracted tremendous attention in LMBs. Therefore, it is necessary to understand its Li-storage behaviour during lithiation/ delithiation.

Various carbon allotropes with high conductivity are widely used as host materials for reversible Li de-/insertion. The details of how Li-ions are stored in these hosts are not trivial to obtain. Generally, the conventional in situ TEM is hard to probe light elements owing to their susceptibility and poor scattering cross-section , especially lithium.[197] Very recently, Kaiser and co-workers[195] revealed lithium atoms to assume multi-layered close-packed order between the two carbon nanosheets by using in situ low-voltage TEM with spherical and chromatic aberration correction (Fig. 29a). The close-packed lithium phase grows laterally between graphene nanosheets during lithiation process, the image time series show that a lateral growth rate of 1 Å s^{-1} can be extracted (Fig. 29b). On the contrary, the close-packed lithium phase gradually vanishes during delithiation process, the bilayer graphene lattice is still remain (Fig. 29c). The high Li-storage capacity is related to the super-dense phase by analyzing the charge distribution and electronic structure, which is far beyond that expected from generation of LiC_6.[195] This point is also demonstrated by both atomistic models of Li crystals obtained from DFT calculations and Li crystal growth. In the miscibility gap over LiC_6, alternative configurations can offer abundant Li-storage sites in layered carbon materials.[53]

5.2. Insight into interface chemistry and dendrite growth in LMBs by Cryo-TEM

The interface chemistry plays a crucial role in LMBs system, which directly affects the cycling stability and electrochemical

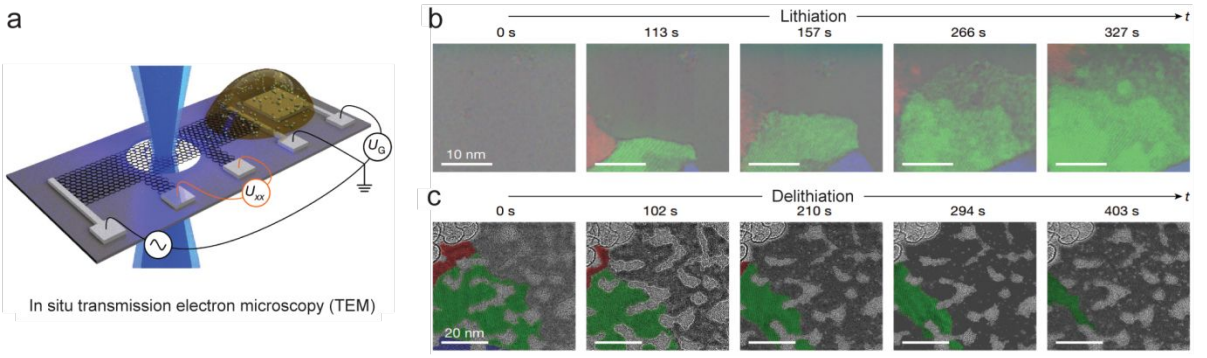

Fig. 29 a) Schematic of the in situ TEM device, TEM images of bilayer graphene during b) lithiation and c) delithiation (grey and black are: graphene; red, blue and green are the different Li phase).[195] a-c) Reproduced with permission from ref. 195. Copyright 2018, Nature Publishing Group.

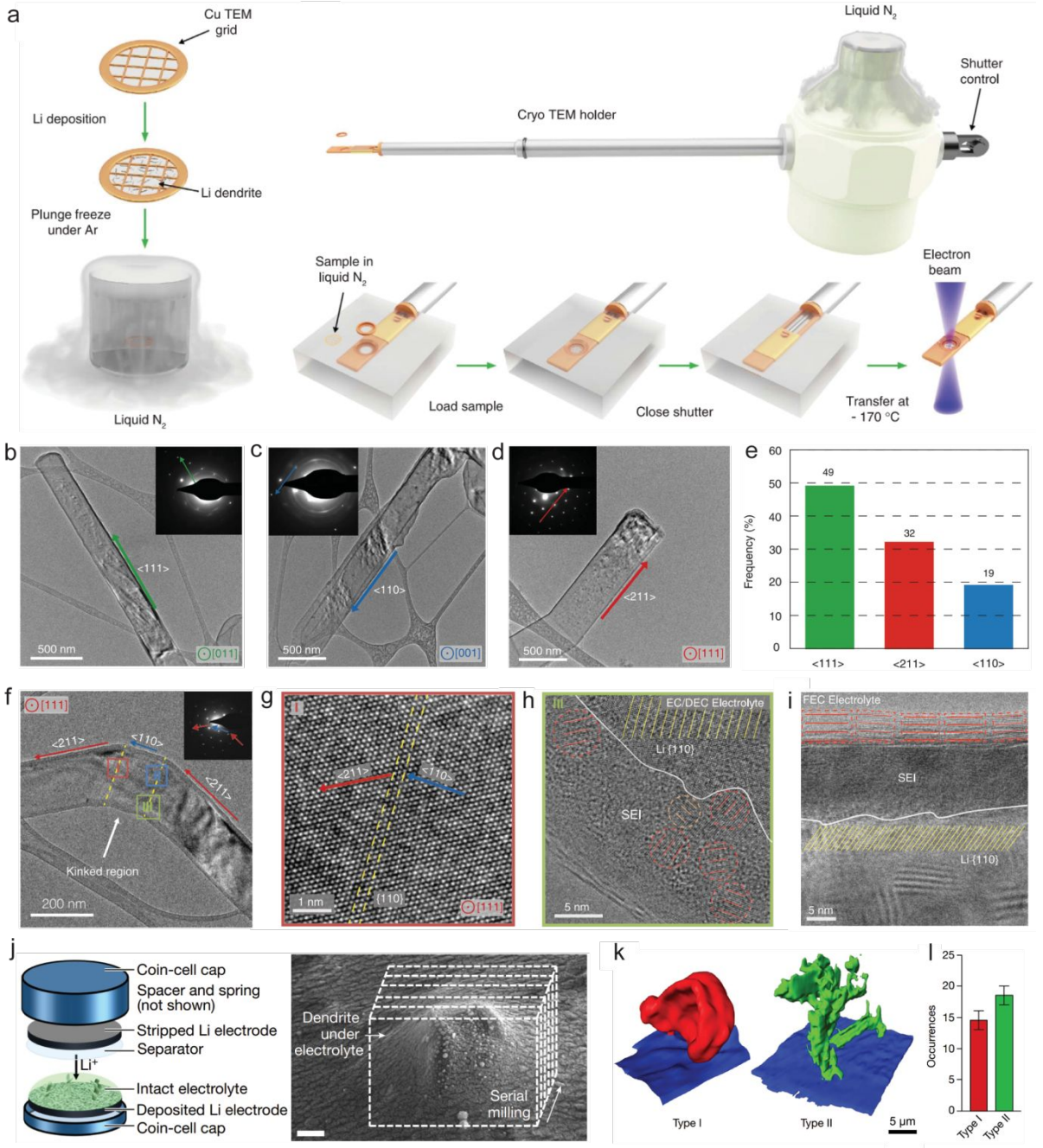

Fig. 30 a) Schematic of preserving LMA by Cryo-TEM device, lithium dendrites grow along b) <111>, c) <110> and d) <211> crystal plane, e) statistics indicating preferential growth direction is <111> crystal plane, f) TEM image of Li whisker transforms from <211> to <110> and again back to <211> crystal plane, g) enlarged region I indicating both kinks, h) high resolution TEM (HRTEM) image of region III disclosing the interfacial components between LMA and SEI, i) atomic-scale HRTEM image of SEI in FEC.[198] a-i) Reproduced with permission from ref. 198. Copyright 2017, AAAS; j) The raised regions can be revealed in a Coin-cell by Cryo-FIB, k) 3D reconstructions of Li dendrite illustrate the morphological distinction, l) Almost equal quantities of the both morphologies were appeared by many coin-cells.[3] j-l) Reproduced with permission from ref. 3. Copyright 2018, Nature Publishing Group.

performance.[24, 91, 194, 198] Moreover, the processes of Li dendrite growth and the formation of SEI layers on the LMA interface are closely related to battery safety and electrochemical performance in high energy LMBs.[3, 198] Although insight into the interfacial chemistry and dendrite are very important for developing feasible solutions to these failure modes in LMBs, these are not well understood due to the lack of advanced in situ high-resolution characterization means.[97, 194]

Given these abovementioned factors, Cui and co-workers[198] developed a Cryo-transfer approach (Fig. 30a) according to Cryo-TEM procedures used in structural biology, and use Cryo-TEM techniques to analysis the structural evolution of LMA and its SEI layer, indicating that atomic-resolution imaging of sensitive electrode material in their native state is feasible at ultralow temperature conditions. The individual dendrite structures can be directly visualized, atomic resolutions of 0.7 Å are available in this characterization. The TEM images with their selected-area electron diffraction images indicate three main growth orientations along <111>, <110> and <211>, in which <111> direction is a preference for Li dendrite growth in carbonate-based electrolyte owing to its appropriate Li surface energies (Fig. 30b-e).[198] Furthermore, the growth direction of Li dendrites don't always follow a straight single-crystalline nanowire, the crystallographic growth orientation will often change as kinks (Fig. 30f). In the kinked region, there are three growth directions of <211>, <110> and <111>. The Li dendrite grows along red arrows from right to left (Fig. 30f), and no any crystal defects are observed at the kinked region (Fig. 30g). The kinked dendrites may owe to the variation of the SEI composition/structure during Li deposition. In the interface of SEI layer, the structure and components between FEC-containing additive and not any additive are different (Fig. 30h and i). Recently, Kourkoutis and co-workers[3] directly observed the real structure and chemistry of dendrites and their interphase in LMBs down to the nanoscale by Cryo-focused ion beam (Cryo-FIB) and Cryo-TEM techniques (Fig. 30j). They found that two dendrite types with different structure and composition on the LMA. One type of dendrites has an extended SEI layer, the other compose of lithium hydride instead of metallic lithium (Fig. 30k). Type II dendrites could become more easy disconnected from electrode than type I dendrites during cycling, both types can contribute disproportionately to capacity attenuation due to the electrochemically disconnection of dead Li (Fig. 30l). There is no doubt that Cryo-FIB and Cryo-TEM techniques are powerful tools for providing detailed nanostructure and atomic-resolution imaging of intact interface between electrode and electrolyte in LMBs, revealing the related information of dendrites growth and SEI layers.

5.3. In situ recording Li microstructure evolution and battery performance fading by synchrotron X-ray tomography

The non-destructive 3D (synchrotron) X-ray tomography technique can provide a direct visual access to inner electrodes, which contribute to well understand the working mechanisms and performance degradation during cycling.[97, 194, 199] Against this background, Sun and co-workers[194] uncover the complicated evolution processes of internal short circuits (ISCs) and electrochemically generated Li microstructure (EG-LMSs, e.g. dendrite,[3, 194] mossy,[24] pellet,[91] whiskers,[3] etc., any shape that differentiates from pristine Li) by synchrotron X-ray tomography technique (Fig. 31a-c). The direct fracture of separator caused by the continuously growing EG-LMSs will lead to ISCs (Fig. 31d-g), the evolution processes of LMSs are also well consistent with its electrochemical curve (Fig. 31h). Moreover, the trilayer Celgard 2325 separator (Fig. 31i) or

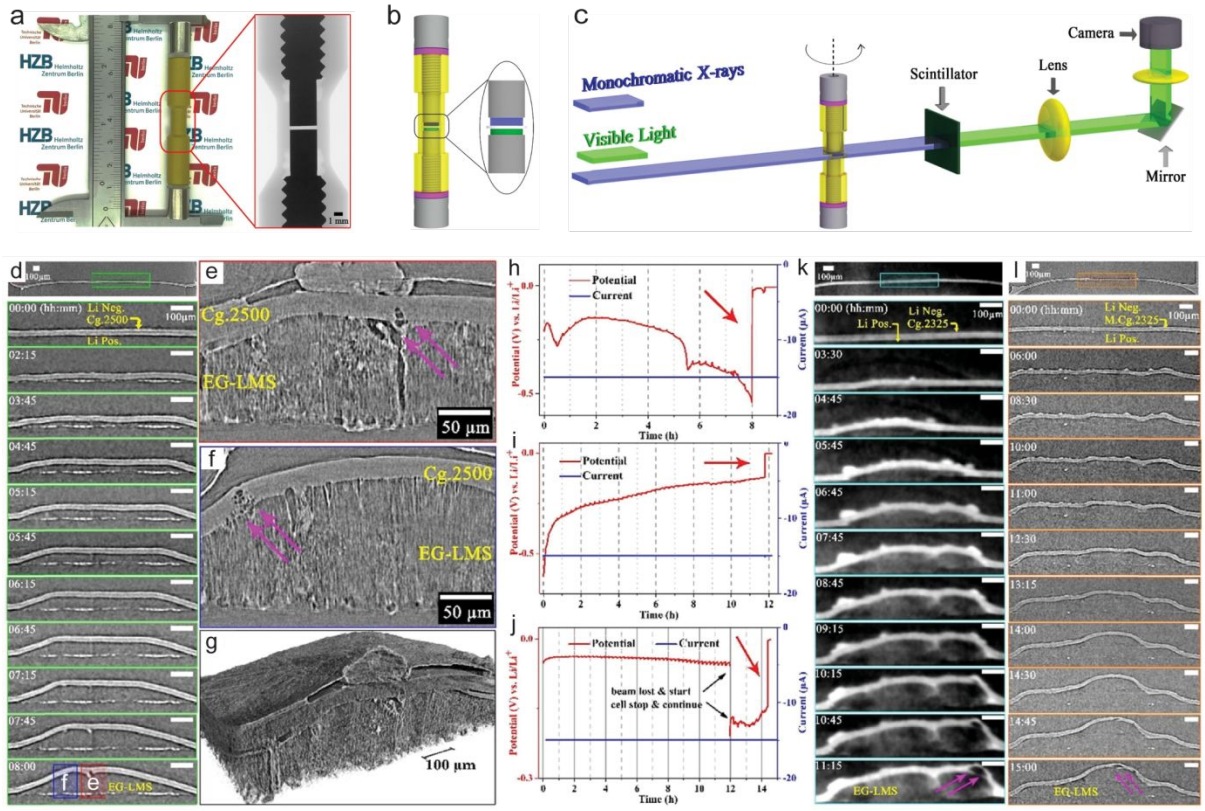

Fig. 31 a) Photograph of the designed cell device, b) the internal structure and compositions of cell, c) schematic of the experimental configuration of the tomography technique, d-h) indicate both the inner morphological evolutions and electrochemical tests of No. 1 cell during discharge, e) and f) are the magnified images of d), g) a 3D microstructure and h) the electrochemical performance, i) and k) indicate the electrochemical property and morphological evolutions of No. 2 cell, j) and l) present the relevant results of No. 3 cell.[194] a-l) Reproduced with permission from ref. 194. Copyright 2019, Elsevier.

Al_2O_3-modified Celgard 2325 separator (Fig. 31j) also display a similar rupture processes. In comparison to monolayer Celgard 2325 separator, the trilayer Celgard 2325 separator (Fig. 31k) and Al_2O_3-modified Celgard 2325 separator (Fig. 31l) show relatively good electrochemical curves, but finally all are ISCs due to the continuously growing EG-LMSs. Therefore, these separators with relatively larger pores and poor mechanical strength are not suitable for LMBs, while the development of SSEs is an effective solution owing to their sufficient mechanical rigidity to protect their integrity and to restrain the EG-LMSs growing-through. Similarly, the real information of LMS and EG-LMSs growth of SLMBs during cycling can be also detailed recorded by this non-destructive in situ/operando characterization technique. In addition, the non-destructive 3D (synchrotron) X-ray tomography technique also can apply to other second alkaline metal batteries in non-/aqueous battery systems, especially beam-sensitive materials.[194, 199]

5.4. Quantifying the inactive Li in LMBs by titration gas chromatography method

As we all known, the inactive ('dead') Li are composed of SEI Li^+ (e.g. LiF, LiO_2, Li_2CO_3 and $ROCO_2Li$) and unreacted Li^o.[3, 67] It is widely believed that the low CE caused by the continuous SEI fractures and increased 'dead' Li during Li stripping/plating.[92] However, the contribution of SEI Li^+ and unreacted metallic Li^o to capacity fading has not been quantified. Therefore, great efforts to differentiate and quantify the SEI Li^+, inactive Li^o and reversible Li are extremely important to better understand the fading mechanisms of capacity. Recently, Meng and co-workers[192] provide an effective method to quantify inactive Li by the titration gas chromatography (TGC) approach (Fig. 32a), the core idea of the quantitation analysis is based on the redox ($2\ Li + 2\ H_2O \rightarrow H_2\uparrow + 2\ LiOH$) between inactive metallic Li^o and protic solvents (e.g. H_2O), the content of inactive metallic Li^o can be accurate calculated based on the generated H_2 obtained by TGC. Therefore, the content of pristine Li and unreacted metallic Li^o can be directly measured via the TGC approach, the SEI Li^+ can be also calculated based on the law of conservation of mass ($Li_{total} = Li_{inactive} + Li_{reversible}$, where $Li_{inactive} = Li_{unreacted} + SEI\ Li^+$), so the CE

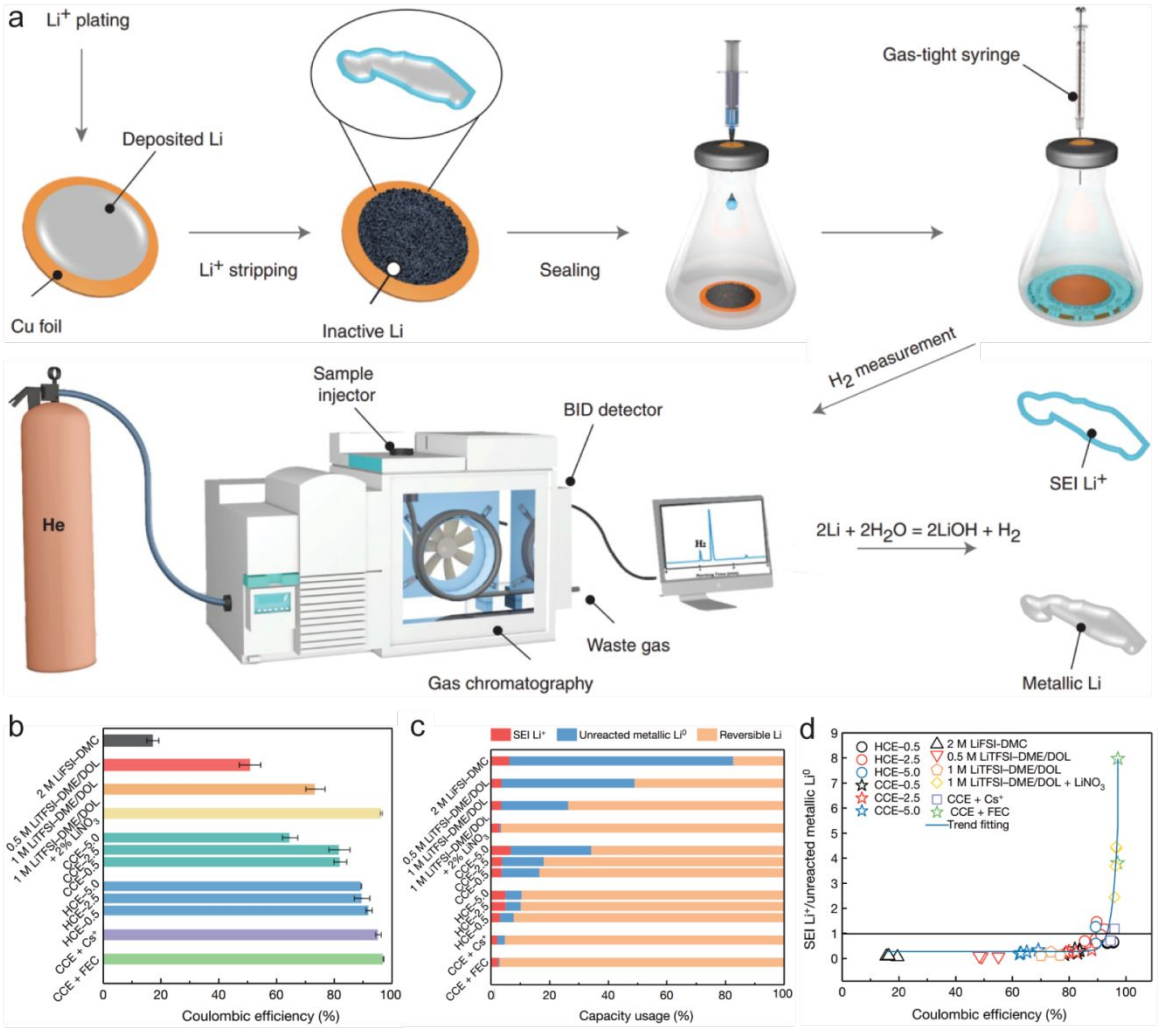

Fig. 32 a) Schematic of quantifying inactive lithium by TGC approach, b) the 1st cycle CE of Li Cu cells in different electrolytes, c) statistics of capacity usage among inactive lithium, SEI Li^+ and reversible lithium in various electrolytes, d) the relationship between CE and SEI Li^+, inactive lithium.[192] a-d) Reproduced with permission from ref. 192. Copyright 2019, Nature Publishing Group.

and capacity usage in different conditions can be quantified based on the calculated SEI Li^+, unreacted metallic Li^0 and reversible Li (Fig. 32b and c). The capacity loss arises from the inactive lithium, which showing a linear relationship with CE (Fig. 32d). Obviously, the CE decay is dominated by the unreacted Li, which shows a linear relationship with CE. Besides, the microstructures and formation mechanism of inactive Li during plating/stripping processes can be also revealed by the advanced Cryo-FIB–scanning electron microscopy and Cryo-TEM techniques.[3, 200] Given these abovementioned conclusions, an advisable strategy is reactivation/ minimization the unreactive metallic Li to improve the CE. Another good strategy is to form a stable SEI with mechanically elastic by optimizing electrolytes or to design a robust artificial SEI membrane on the surface of LMA.

6. Conclusions and Perspectives

It is widely believed that LMBs are promising next-generation high energy density devices, though it is still faced with various challenges. The main challenge is the continuous growth of lithium dendrites during cycling, which could penetrate through the separator and induce cell short circuiting. In liquid-state LMBs, recently emerging strategies and perspectives focus on regulating interface chemistry, optimizing electrolyte components, designing a rational 'host' for lithium metal and using pulse current charging. Although these strategies and perspectives on LMA protection have been well improved in restraining the growth of dendrites, safety concerns and challenges still remain. To reduce this safety problem, SSEs are

considered able to better restrict problematic Li dendrites and build safe SLMBs. In the recent years, tremendous effort have been devoted to address these challenges (including poor interface contact between electrode and SSEs, high interface resistance and low ion/electron conductivity) of SLMBs, such as constructing a thin asymmetric SSEs with complementary advantages both for PSSEs and ICSSEs, designing an ion/electron dual-conductive alloy skeleton with seamless interface contact and engineering 3D LMA with flowable interphase and so on. Therefore, building better SLMBs are crucial for realizing future high safety ESDs. Furthermore, the progress of emerging characterization techniques, nanotechnology-based solutions and interface-based science would promote the Li-based batteries systems, especially Li-S and Li-O_2 batteries. Inspired by the bright prospects of LMBs, we believe that the progress of high-safety LMA will play a crucial role in future high energy density ESDs.

6.1. The main challenges of LMA in high-energy LMBs

The development of LMA is critical to realize the future high-energy LMBs. After being in-depth researched in recent years, LMA has achieved unprecedented progress in restraining Li-dendrite growth and improving cycling life, especially through development of interface-based science, nanotechnology-based solutions and novel characterization tools. However, there is still a long way to go from laboratory to commercial application. The problematic Li-dendrite and 'dead' Li are still remain during the plating/stripping processes, the former may cause potential safety hazards, and the later will lead to low CE, the both main issues greatly hinder LMA's practical application in LMBs. Therefore, the tremendous effort should be devoted towards restraining the Li-dendrite growth and reducing the amount of 'dead' Li through tuning the nanostructure of deposited lithium during the cycling processes.

6.2. The progress of emerging characterization techniques will accelerate the realization of safety LMA

The progress of all kinds of operando/*in situ* characterization techniques (e.g. electron, neutron, X-ray, optical or scanning probes) will facilitate the development of safe LMA and gain an in-depth understanding of the structure evolution, dynamic process and growth mechanism of Li-dendrite during Li plating/stripping processes. The evolution of crystal structures, phase transformations, interfacial properties of LMA during plating/stripping can be precisely detected by operando/*in situ* synchrotron-based X-ray sources combined with neutron-based techniques. The evolution of whole morphology, microstructure, and interface of LMA during discharge/charge processes can be clearly observed through *in situ* TEM or tomographic technique, the HRTEM with atomic level spatial resolution and millisecond temporal resolution can also reveal the crystal growth behavior of Li-dendrite during Li plating/stripping processes. In addition, the development of both time-resolved X-ray diffraction and time-resolved X-ray absorption spectroscopy with very high temporal resolution will also provide the detail dynamic information of LMA anode.

6.3. Advocating the standardized testing protocols to accelerate the LMBs towards practical application

In a large number of many previously published papers, the obtained electrochemical data are based on an excess amount of LMA and of the electrolyte, which is far from the actual demand for commercial applications. Therefore, to better evaluate the performance of electrode or cell in practical application, and optimize cell-level energy density, encouraging researchers to challenge the new test protocol will help promote the application of high-energy LMBs, the advocated standardized testing protocols of LMBs with layered cathode and LMA are presented as below. The mass loading of cathode material should be 3.5 mA h cm^{-2} or more, the current density is 0.3 mA cm^{-2} (certainly, it is not the only option, but depends on the purpose of cell-level's testing), lean electrolyte should not exceed 3 g Ah^{-1} (that is, E/C ≤ 3 g Ah^{-1}), the N/P should be less than 2, the baseline of LMA in thickness is 50 μm or less, and the E_m of a lithium metal pouch cell should be over 300 Wh kg^{-1}. These advocated testing protocols will accelerate the development of new high-energy materials that can be integrated into the realistic battery systems.

6.4. Tuning wettability of LMA through chemical strategy for high-energy LMBs

The poor wettability of LMA is hard to allow it to diffuse across the interface of lithiophobic matrixes, resulting poor interface contact and inferior cycle performance. Thus, tuning the wettability of molten lithium through rational interface design is a highly effective and feasible strategy. For example, lithiophilic coatings with halogen functional groups (e.g. N, P, F, Cl, Br and I) could form new chemical/ionic bond with molten Li and thus improved wettability. Besides, the negative values of Gibbs formation energy for the reactions both molten lithium and lithiophilic substrates (including organic materials, inorganic materials or in-/organic composites) could also improve wettability.

6.5. Developing emerging strategies for improving the safety concerns caused by the problematic Li-dendrite

The main challenge of LMBs is that during charging process, the continuous lithium plating in an irregular manner, forming dendritic/powdery microstructures, which are the root of Li-dendrite and 'dead' Li. The Li-dendrite formation is rooted in

the mass transport of the Li^+, which largely determines the final morphology of electroplated Li-metal, even though this process is usually neglected in analysis of Li-dendrites formation. Besides, the diffusion rate and concentration gradients of Li ions are closely related to the plating behavior of Li-ion in the entire electrode. Worst of all, the dendritic Li reacts with electrolyte, further consuming electrolyte irreversibly. Finally, the continuous accumulation of insulating SEI layers produces 'dead' Li and result in a low CE of Li-metal cells. Therefore, strategy that reactivates 'dead' Li may be beneficial to improve CE.

The strategies of optimizing electrolyte components are an effective channel in suppression Li-dendrite growth. The electrolyte should promote the homogeneous diffusion of Li-ion on the electrode surface and restrain the formation of a larger concentration gradient in the interphase. Besides, some functionalized additives will be also useful to homogenize the concentration gradient. Therefore, an optimized electrolyte should have little or no side reactions with LMA, and thus no 'dead' Li is formed or generated by consuming Li.

Conflicts of interest

There are no conflicts to declare.

Acknowledgements

The authors D.-H. Liu, Z.-Y. Bai and L. Yang appreciate the financial support from the project funded by National Natural Science Foundation of China (51902090, 51922008, 51872075), China Postdoctoral Science Foundation (Grant No. 2019M652546), Henan Province Postdoctoral Start-Up Foundation (Grant No. 1901017), "111" project (Grant No. D17007) and Henan Center for Outstanding Overseas Scientists (Grant No. GZS2018003). The work at Argonne was supported by the U. S. Department of Energy (DOE), Office of Energy Efficiency and Renewable Energy, Vehicle Technologies Office, and Argonne National Laboratory is operated for DOE Office of Science by UChicago Argonne, LLC, under contract number DE-AC02-06CH11357. The authors A. Yu and Z. Chen gratefully acknowledge the Natural Sciences and Engineering Research Council of Canada, the University of Waterloo, and the Waterloo Institute for Nanotechnology, University of Waterloo. We also want to acknowledge the anonymous reviewers who provide a lot of helpful suggestions to enhance this review.

References

1 Y. Zhou, M. Su, X. Yu, Y. Zhang, J. G. Wang, X. Ren, R. Cao, W. Xu, D. R. Baer, Y. Du, O. Borodin, Y. Wang, X. L. Wang, K. Xu, Z. Xu, C. Wang and Z. Zhu, *Nat. Nanotechnol.*, 2020, **15**, 224-230.
2 L. Zhang, T. Yang, C. Du, Q. Liu, Y. Tang, J. Zhao, B. Wang, T. Chen, Y. Sun, P. Jia, H. Li, L. Geng, J. Chen, H. Ye, Z. Wang, Y. Li, H. Sun, X. Li, Q. Dai, Q. Peng, T. Shen, S. Zhang, T. Zhu and J. Huang, *Nat. Nanotechnol.*, 2020, **15**, 94-98.
3 M. J. Zachman, Z. Tu, S. Choudhury, L. A. Archer and L. F. Kourkoutis, *Nature*, 2018, **560**, 345-349.
4 L. Li, S. Basu, Y. Wang, Z. Chen, P. Hundekar, B. Wang, J. Shi, Y. Shi, S. Narayanan and N. Koratkar, *Science*, 2018, **359**, 1513-1516.
5 M. S. Kim, J.-H. Ryu, Deepika, Y. R. Lim, I. W. Nah, K.-R. Lee, L. A. Archer and W. Il Cho, *Nat. Energy*, 2018, **3**, 889-898.
6 Z. P. Cano, D. Banham, S. Ye, A. Hintennach, J. Lu, M. Fowler and Z. Chen, *Nat. Energy*, 2018, **3**, 279-289.
7 J. Wang, Y. Yamada, K. Sodeyama, E. Watanabe, K. Takada, Y. Tateyama and A. Yamada, *Nat. Energy*, 2017, **3**, 22-29.
8 S. Randau, D. A. Weber, O. Kötz, R. Koerver, P. Braun, A. Weber, E. Ivers-Tiffée, T. Adermann, J. Kulisch, W. G. Zeier, F. H. Richter and J. Janek, *Nat. Energy*, 2020, **5**, 259-270.
9 M. S. Kim, M.-S. Kim, V. Do, Young R. Lim, In W. Nah, L. A. Archer and W. I. Cho, *Nano Energy*, 2017, **41**, 573-582.
10 K. Song, D. A. Agyeman, M. Park, J. Yang and Y. M. Kang, *Adv. Mater.*, 2017, **29,** 1606572.
11 J. J. Xu, Q. C. Liu, Y. Yu, J. Wang, J. M. Yan and X. B. Zhang, *Adv. Mater.*, 2017, **29**, 1606552.
12 Y. Liu, Q. Liu, L. Xin, Y. Liu, F. Yang, E. A. Stach and J. Xie, *Nat. Energy,* 2017, **2**, 17083.
13 D. Lin, Y. Liu and Y. Cui, *Nat. Nanotech.*, 2017, **12**, 194.

14 N. W. Li, Y. Shi, Y. X. Yin, X. X. Zeng, J. Y. Li, C. J. Li, L. J. Wan, R. Wen and Y. G. Guo, *Angew. Chem. Int. Ed*., 2018, **57**, 1505-1509.
15 J. Lee, D. A. Kitchaev, D. H. Kwon, C. W. Lee, J. K. Papp, Y. S. Liu, Z. Lun, R. J. Clement, T. Shi, B. D. McCloskey, J. Guo, M. Balasubramanian and G. Ceder, *Nature*, 2018, **556**, 185-190.
16 L. Ma, M. S. Kim and L. A. Archer, *Chem. Mater*., 2017, **29**, 4181-4189.
17 Y. Liu, D. Lin, P. Y. Yuen, K. Liu, J. Xie, R. H. Dauskardt and Y. Cui, *Adv. Mater*., 2017, **29**, 1605531.
18 G. Li, Y. Gao, X. He, Q. Huang, S. Chen, S. H. Kim and D. Wang, *Nat. Commun.*, 2017, **8**, 850.
19 A. C. Kozen, C.-F. Lin, O. Zhao, S. B. Lee, G. W. Rubloff and M. Noked, *Chem. Mater*., 2017, **29**, 6298-6307.
20 N. W. Li, Y. X. Yin, C. P. Yang and Y. G. Guo, *Adv. Mater*., 2016, **28**, 1853-1858.
21 K. K. Fu, Y. Gong, B. Liu, Y. Zhu, S. Xu, Y. Yao, W. Luo, C. Wang, S. D. Lacey, J. Dai, Y. Chen, Y. Mo, E. Wachsman and L. Hu, *Sci. Adv*., 2017, **3**, e1601659.
22 X. Wang, J. Zhuang, M. Liu, C. Wang, Y. Zhong, H. Wang, X. Cheng, S. Liu, G. Cao and W. Li, *J. Mater. Chem. A,* 2019, **7**, 19104-19111.
23 N. D. Trinh, D. Lepage, D. Ayme-Perrot, A. Badia, M. Dolle and D. Rochefort, *Angew. Chem. Int. Ed*., 2018, **57**, 5072-5075.
24 H. Zhang, X. Liao, Y. Guan, Y. Xiang, M. Li, W. Zhang, X. Zhu, H. Ming, L. Lu, J. Qiu, Y. Huang, G. Cao, Y. Yang, L. Mai and Y. Zhao, *Nat. Commun.*, 2018, **9**, 3729.
25 C. Yan, X. B. Cheng, Y. X. Yao, X. Shen, B. Q. Li, W. J. Li, R. Zhang, J. Q. Huang, H. Li and Q. Zhang, *Adv. Mater*., 2018, **30**, 1804461.
26 K. Liao, S. Wu, X. Mu, Q. Lu, M. Han, P. He, Z. Shao and H. Zhou, *Adv. Mater*., 2018, **30**, 1705711.
27 B. Zhu, Y. Jin, X. Hu, Q. Zheng, S. Zhang, Q. Wang and J. Zhu, *Adv. Mater*., 2017, **29**, 1603755.
28 K. Liu, A. Pei, H. R. Lee, B. Kong, N. Liu, D. Lin, Y. Liu, C. Liu, P. C. Hsu, Z. Bao and Y. Cui, *J. Am. Chem. Soc.*, 2017, **139**, 4815-4820.
29 X. Liang, Q. Pang, I. R. Kochetkov, M. S. Sempere, H. Huang, X. Sun and L. F. Nazar, *Nat. Energy*, 2017, **2**, 17119.
30 Y. Gao, Y. Zhao, Y. C. Li, Q. Huang, T. E. Mallouk and D. Wang, *J. Am. Chem. Soc.,* 2017, **139**, 15288-15291.
31 S. Choudhury, Z. Tu, S. Stalin, D. Vu, K. Fawole, D. Gunceler, R. Sundararaman and L. A. Archer, *Angew. Chem. Int. Ed*., 2017, **56**, 13070-13077.
32 W. Yang, Y. Bi, Y. Qin, Y. Liu, X. Zhang, B. Yang, Q. Wu, D. Wang and S. Shi, *J. Power Sources*, 2015, **275**, 785-791.
33 J. Xie, L. Liao, Y. Gong, Y. Li, F. Shi, A. Pei, J. Sun, R. Zhang, B. Kong, R. Subbaraman, J. Christensen and Y. Cui, *Sci. Adv*., 2017, **3**, eaao3170.
34 C. Yan, X. B. Cheng, Y. Tian, X. Chen, X. Q. Zhang, W. J. Li, J. Q. Huang and Q. Zhang, *Adv. Mater*., 2018, **30**, e1707629.
35 Y. Xu, T. Li, L. Wang and Y. Kang, *Adv. Mater*., 2019, **31**, 1901662.
36 M. Ebadi, C. Marchiori, J. Mindemark, D. Brandell, C. Moyses and A. C. Moyses, *J. Mater. Chem. A*, 2019, **7**, 8394-8404.
37 A. Paolella, H. Demers, P. Chevallier, C. Gagnon, G. Girard, N. Delaporte, W. Zhu, A. Vijh, A. Guerfi and K. Zaghib, *J. Power Sources*, 2019, **427**, 201-206.
38 A. Mirsakiyeva, M. Ebadi, C. M. Araujo, D. Brandell, P. Broqvist and J. Kullgren, *J. Phys. Chem. C*, 2019, **123**, 22851-22857.
39 C. Yan, Y. X. Yao, X. Chen, X. B. Cheng, X. Q. Zhang, J. Q. Huang and Q. Zhang, *Angew. Chem. Int. Ed*., 2018, **57**, 14055-14059.
40 B. Zhou, L. Guo, Y. Zhang, J. Wang, L. Ma, W. H. Zhang, Z. Fu and Z. Peng, *Adv. Mater*., 2017, **29**, 1701568.
41 R. Miao, J. Yang, Z. Xu, J. Wang, Y. Nuli and L. Sun, *Sci. Rep.*, 2016, **6**, 21771.
42 S. Jiao, X. Ren, R. Cao, M. H. Engelhard, Y. Liu, D. Hu, D. Mei, J. Zheng, W. Zhao, Q. Li, N. Liu, B. D. Adams, C. Ma, J. Liu, J.-G. Zhang and W. Xu, *Nat. Energy*, 2018, **3**, 739-746.
43 J. Zheng, M. H. Engelhard, D. Mei, S. Jiao, B. J. Polzin, J.-G. Zhang and W. Xu, *Nat. Energy*, 2017, **2**, 17012.
44 H. Wang, M. Matsui, H. Kuwata, H. Sonoki, Y. Matsuda, X. Shang, Y. Takeda, O. Yamamoto and N. Imanishi, *Nat. Commun.*, 2017, **8**, 15106.
45 J. Qian, W. A. Henderson, W. Xu, P. Bhattacharya, M. Engelhard, O. Borodin and J. G. Zhang, *Nat. Commun.*, 2015, **6**, 6362.
46 A. Mauger, C. M. Julien, A. Paolella, M. Armand and K. Zaghib, *Mat. Sci. Eng. R*, 2018, **134**, 1-21.
47 X. B. Cheng, M. Q. Zhao, C. Chen, A. Pentecost, K. Maleski, T. Mathis, X. Q. Zhang, Q. Zhang, J. Jiang and Y. Gogotsi, *Nat. Commun.*, 2017, **8**, 336.

48 W. Zhang, H. L. Zhuang, L. Fan, L. Gao and Y. Lu, *Sci. Adv*., 2018, **4**, eaar4410.
49 A. Basile, A. I. Bhatt and A. P. O'Mullane, *Nat. Commun.*, 2016, **7**, 11794.
50 C. Zhang, S. Liu, G. Li, X. Liu and J. Luo, *Adv. Mater.*, 2018, **30**, 1801328.
51 P. Xue, S. Liu, X. Shi, C. Sun, C. Lai, Y. Zhou, D. Sui, Y. Chen and J. Liang, *Adv. Mater.*, 2018, **30**, 1804165.
52 Z. Sun, S. Jin, H. Jin, Z. Du, Y. Zhu, A. Cao, H. Ji and L. J. Wan, *Adv. Mater*., 2018, **30**, 1800884.
53 L. Liu, Y. X. Yin, J. Y. Li, S. H. Wang, Y. G. Guo and L. J. Wan, *Adv. Mater*., 2018, **30**, 1706216.
54 A. M. Hafez, Y. Jiao, J. Shi, Y. Ma, D. Cao, Y. Liu and H. Zhu, *Adv. Mater*., 2018, **30**, 1802156.
55 H. Shang, Z. Zuo, L. Yu, F. Wang, F. He and Y. Li, *Adv Mater*, 2018, **30**, 1801459.
56 M. Bai, K. Xie, K. Yuan, K. Zhang, N. Li, C. Shen, Y. Lai, R. Vajtai, P. Ajayan and B. Wei, *Adv. Mater.*, 2018, **30**, 1801213.
57 T. T. Zuo, X. W. Wu, C. P. Yang, Y. X. Yin, H. Ye, N. W. Li and Y. G. Guo, *Adv. Mater.*, 2017, **29**, 1700389.
58 H. Ye, S. Xin, Y. X. Yin, J. Y. Li, Y. G. Guo and L. J. Wan, *J. Am. Chem. Soc.*, 2017, **139**, 5916-5922.
59 R. Zhang, X. B. Cheng, C. Z. Zhao, H. J. Peng, J. L. Shi, J. Q. Huang, J. Wang, F. Wei and Q. Zhang, *Adv. Mater.*, 2016, **28**, 2155-2162.
60 Y. Liu, D. Lin, Z. Liang, J. Zhao, K. Yan and Y. Cui, *Nat. Commun.*, 2016, **7**, 10992.
61 R. Mukherjee, A. V. Thomas, D. Datta, E. Singh, J. Li, O. Eksik, V. B. Shenoy and N. Koratkar, *Nat. Commun.*, 2014, **5**, 3710.
62 D. Lin, Y. Liu, Z. Liang, H.-W. Lee, J. Sun, H. Wang, K. Yan, J. Xie and Y. Cui, *Nat. Nanotech*., 2016, **11**, 626.
63 Y. Liu, D. Lin, Y. Jin, K. Liu, X. Tao, Q. Zhang, X. Zhang and Y. Cui, *Sci. Adv*., 2017, **3**, eaao0713.
64 J. Zhao, G. Zhou, K. Yan, J. Xie, Y. Li, L. Liao, Y. Jin, K. Liu, P.-C. Hsu, J. Wang, H.-M. Cheng and Y. Cui, *Nat. Nanotech*., 2017, **12**, 993.
65 G. Zheng, S. Lee, Z. Liang, H.-W. Lee, K. Yan, H. Yao, HaotianWang, W. Li, S. Chu and Y. Cui, *Nat. Nanotech*., 2014, **9**, 618-623.
66 P. Zou, Y. Wang, S. W. Chiang, X. Wang, F. Kang and C. Yang, *Nat. Commun.*, 2018, **9**, 464.
67 S. H. Wang, Y. X. Yin, T. T. Zuo, W. Dong, J. Y. Li, J. L. Shi, C. H. Zhang, N. W. Li, C. J. Li and Y. G. Guo, *Adv. Mater*., 2017, **29**, 1703729.
68 S. Wu, Z. Zhang, M. Lan, S. Yang, J. Cheng, J. Cai, J. Shen, Y. Zhu, K. Zhang and W. Zhang, *Adv. Mater.*, 2018, **30**, 1705830.
69 Q. Yun, Y. B. He, W. Lv, Y. Zhao, B. Li, F. Kang and Q. H. Yang, *Adv. Mater*., 2016, **28**, 6932-6939.
70 C. P. Yang, Y. X. Yin, S. F. Zhang, N. W. Li and Y. G. Guo, *Nat. Commun.*, 2015, **6**, 8058.
71 W. Liu, D. Lin, A. Pei and Y. Cui, *J. Am. Chem. Soc.*, 2016, **138**, 15443-15450.
72 X. B. Cheng, T. Z. Hou, R. Zhang, H. J. Peng, C. Z. Zhao, J. Q. Huang and Q. Zhang, *Adv. Mater*., 2016, **28**, 2888-2895.
73 H. Wang, D. Lin, Y. Liu, Y. Li and Y. Cui, *Sci. Adv*., 2017, **3**, e1701301.
74 Y. Guo, H. Li and T. Zhai, *Adv. Mater*., 2017, **29**, 1700007.
75 C. Yang, K. Fu, Y. Zhang, E. Hitz and L. Hu, *Adv. Mater*., 2017, **29**, 1701169.
76 K. K. Fu, Y. Gong, Z. Fu, H. Xie, Y. Yao, B. Liu, M. Carter, E. Wachsman and L. Hu, *Angew. Chem. Int. Ed*., 2017, **56**, 14942-14947.
77 J. Duan, W. Wu, A. M. Nolan, T. Wang, J. Wen, C. Hu, Y. Mo, W. Luo and Y. Huang, *Adv. Mater*., 2019, **31**, 1807243.
78 A. Mauger, C. M. Julien, A. Paolella, M. Armand and K. Zaghib, *Mater*., 2019, **12**, 3892.
79 N. Delaporte, A. Guerfi, H. Demers, H. Lorrmann, A. Paolella and K. Zaghib, *ChemistryOpen*, 2019, **8**, 192-195.
80 A. Kushima, K. P. So, C. Su, P. Bai, N. Kuriyama, T. Maebashi, Y. Fujiwara, M. Z. Bazant and J. Li, *Nano Energy,* 2017, **32**, 271-279.
81 C. von Lüders, J. Keil, M. Webersberger and A. Jossen, *J. Power Sources*, 2019, **414**, 41-47.
82 Q. Li, T. Yi, X. Wang, H. Pan, B. Quan, T. Liang, X. Guo, X. Yu, H. Wang, X. Huang, L. Chen and H. Li, *Nano Energy*, 2019, **63**, 103895.
83 M. Golozar, P. Hovington, A. Paolella, S. Bessette, M. Lagace, P. Bouchard, H. Demers, R. Gauvin and K. Zaghib, *Nano Lett*., 2018, **18**, 7583-7589.
84 Y. He, X. Ren, Y. Xu, M. H. Engelhard, X. Li, J. Xiao, J. Liu, J. G. Zhang, W. Xu and C. Wang, *Nat. Commun.*, 2019, **14**, 1042-1047.
85 H. Liu, X. B. Cheng, R. Xu, X. Q. Zhang, C. Yan, J. Q. Huang and Q. Zhang, *Adv. Energy Mater*., 2019, **9**, 1902254.
86 K. Yan, J. Wang, S. Zhao, D. Zhou, B. Sun, Y. Cui and G. Wang, *Angew. Chem*., 2019, **58**, 11364-11368.
87 J. Ko and Y. S. Yoon, *Ceram. Int.*, 2019, **45**, 30-49.

88 A. Jana, S. I. Woo, K. S. N. Vikrant and R. E. Garcı´a, *Energy Environ. Sci*., 2019, **12**, 3595-3607.
89 X. Cao, X. Ren, L. Zou, M. H. Engelhard, W. Huang, H. Wang, B. E. Matthews, H. Lee, C. Niu, B. W. Arey, Y. Cui, C. Wang, J. Xiao, J. Liu, W. Xu and J.-G. Zhang, *Nat. Energy,* 2019, **4**, 796-805.
90 S. H. Yu, X. Huang, J. D. Brock and H. D. Abruna, *J. Am. Chem. Soc*., 2019, **141**, 8441-8449.
91 A. Wang, S. Kadam, H. Li, S. Shi and Y. Qi, *NPJ Comput. Mater.*, 2018, **4**, 15.
92 Y. Zhang, Y. Shi, X. C. Hu, W. P. Wang, R. Wen, S. Xin and Y. G. Guo, *Adv. Energy Mater.*, 2019, **10**, 1903325.
93 F. Wu, Y.-X. Yuan, X.-B. Cheng, Y. Bai, Y. Li, C. Wu and Q. Zhang, *Energy Storage Mater*., 2018, **15**, 148-170.
94 L. Liu, Y.-X. Yin, J.-Y. Li, N.-W. Li, X.-X. Zeng, H. Ye, Y.-G. Guo and L.-J. Wan, *Joule*, 2017, **1**, 563-575.
95 E. Paled, *J. Electrochem. Soc*., 1979, **126**, 2047-2051.
96 S. Lv, T. Verhallen, A. Vasileiadis, F. Ooms, Y. Xu, Z. Li and M. Wagemaker, *Nat. Commun.*, 2018, **9**, 2152.
97 S.-M. Bak, Z. Shadike, R. Lin, X. Yu and X.-Q. Yang, *NPG Asia Mater*., 2018, **10**, 563-580.
98 Z. Tu, M. J. Zachman, S. Choudhury, S. Wei, L. Ma, Y. Yang, L. F. Kourkoutis and L. A. Archer, *Adv. Energy Mater.*, 2017, **7**, 1602367.
99 W. Tang, X. Yin, S. Kang, Z. Chen, B. Tian, S. L. Teo, X. Wang, X. Chi, K. P. Loh, H. W. Lee and G. W. Zheng, *Adv. Mater.*, 2018, **30**, 1801745.
100 Y. Li, X. Chen, A. Dolocan, Z. Cui, S. Xin, L. Xue, H. Xu, K. Park and J. B. Goodenough, *J. Am. Chem. Soc*., 2018, **140**, 6448-6455.
101 W. Luo, Y. Gong, Y. Zhu, Y. Li, Y. Yao, Y. Zhang, K. K. Fu, G. Pastel, C. F. Lin, Y. Mo, E. D. Wachsman and L. Hu, *Adv. Mater*., 2017, **29**, 1606042.
102 S.-J. Tan, J. Yue, X.-C. Hu, Z.-Z. Shen, W.-P. Wang, J.-Y. Li, T.-T. Zuo, H. Duan, Y. Xiao, Y.-X. Yin, R. Wen and Y.-G. Guo, *Angew. Chem. Int. Ed*., 2019, **131**, 7884-7889.
103 J. Yan, J. Yu and B. Ding, *Adv. Mater*., 2018, **30**, 1705105.
104 Y. Liu, D. Lin, P. Y. Yuen, K. Liu, J. Xie, R. H. Dauskardt and Y. Cui, *Adv. Mater*., 2017, **29**, 1605531.
105 W. Zhou, S. Wang, Y. Li, S. Xin, A. Manthiram and J. B. Goodenough, *J. Am. Chem. Soc.,* 2016, **138**, 9385-9388.
106 J. Lopez, A. Pei, J. Y. Oh, G. N. Wang, Y. Cui and Z. Bao, *J. Am. Chem. Soc*., 2018, **140**, 11735-11744.
107 G. Li, Q. Huang, X. He, Y. Gao, D. Wang and S. H. Kim, *ACS Nano*, 2018, **12**, 1500-1507.
108 Y. Zhao, G. Li, Y. Gao, D. Wang, Q. Huang and D. Wang, *ACS Energy Lett*., 2019, **4**, 1271-1278.
109 Y. Gu, W. W. Wang, Y. J. Li, Q. H. Wu, S. Tang, J. W. Yan, M. S. Zheng, D. Y. Wu, C. H. Fan, W. Q. Hu, Z. B. Chen, Y. Fang, Q. H. Zhang, Q. F. Dong and B. W. Mao, *Nat. Commun.*, 2018, **9**, 1339.
110 X.-Q. Zhang, X.-B. Cheng, X. Chen, C. Yan and Q. Zhang, *Adv. Funct. Mater*., 2017, **27**, 1605989.
111 J. M. Martinez de la Hoz, F. A. Soto and P. B. Balbuena, *J. Phys. Chem. C*, 2015, **119**, 7060-7068.
112 P. G. Bruce, S. A. Freunberger, L. J. Hardwick and J. M. Tarascon, *Nat. Mater.*, 2011, **11**, 19-29.
113 J. Dai, C. Yang, C. Wang, G. Pastel and L. Hu, *Adv. Mater*., 2018, **30**, 1802068.
114 A. Ostadhossein, J. Guo, F. Simeski and M. Ihme, *Commun. Chem*., 2019, **2**, 95.
115 H. Duan, Y. X. Yin, Y. Shi, P. F. Wang, X. D. Zhang, C. P. Yang, J. L. Shi, R. Wen, Y. G. Guo and L. J. Wan, *J. Am. Chem. Soc*., 2018, **140**, 82-85.
116 S. H. Wang, J. Yue, W. Dong, T. T. Zuo, J. Y. Li, X. Liu, X. D. Zhang, L. Liu, J. L. Shi, Y. X. Yin and Y. G. Guo, *Nat. Commun.*, 2019, **10**, 4930.
117 J. Pu, J. Li, K. Zhang, T. Zhang, C. Li, H. Ma, J. Zhu, P. V. Braun, J. Lu and H. Zhang, *Nat. Commun.*, 2019, **10**, 1896.
118 X.-Q. Zhang, X. Chen, X.-B. Cheng, B.-Q. Li, X. Shen, C. Yan, J.-Q. Huang and Q. Zhang, *Angew. Chem. Int. Ed*., 2018, **57**, 5301-5305.
119 K. Matsumoto, K. Inoue, K. Nakahara, R. Yuge, T. Noguchi and K. Utsugi, *J. Power Sources*, 2013, **231**, 234-238.
120 K. Yoshida, M. Nakamura, Y. Kazue, N. Tachikawa, S. Tsuzuki, S. Seki, K. Dokko and M. Watanabe, *J. Am. Chem. Soc*., 2011, **133**, 13121-13129.
121 K.-H. Chen, K. N. Wood, E. Kazyak, W. S. LePage, A. L. Davis, A. J. Sanchez and N. P. Dasgupta, *J. Mater. Chem*. A, 2017, **5**, 11671-11681.
122 Z. L. Brown, S. Jurng, C. C. Nguyen and B. L. Lucht, *ACS Appl. Energy Mater*., 2018, **1**, 3057-3062.
123 E. A. Olivetti, G. Ceder, G. G. Gaustad and X. Fu, *Joule*, 2017, **1**, 229-243.
124 J. F. Wishart, *Energy Environ. Sci*., 2009, **2**, 956.
125 U. Ulissi, G. A. Elia, S. Jeong, F. Mueller, J. Reiter, N. Tsiouvaras, Y. K. Sun, B. Scrosati, S. Passerini and J. Hassoun, *ChemSusChem*, 2018, **11**, 229-236.
126 S. S. Moganty, N. Jayaprakash, J. L. Nugent, J. Shen and L. A. Archer, *Angew. Chem*., 2010, **122**, 9344-9347.

127 G. G. Yadav, J. W. Gallaway, D. E. Turney, M. Nyce, J. Huang, X. Wei and S. Banerjee, *Nat. Commun.*, 2017, **8**, 14424.
128 J.-S. Kim, H. Choi, J.-N. Lee, H. Kang, D. Ima and H. Kim, *RSC Adv*., 2017, **7**, 24679-24682.
129 K. Yoo, A. Deshpande, S. Banerjee and P. Dutta, *Electrochim. Acta*, 2015, **176**, 301-310.
130 J. Tong, S. Wu, N. von Solms, X. Liang, F. Huo, Q. Zhou, H. He and S. Zhang, *Front. Chem.*, 2019, **7**, 945.
131 D. Bedrov, J. P. Piquemal, O. Borodin, A. D. MacKerell, Jr., B. Roux and C. Schroder, *Chem. Rev.*, 2019, **119**, 7940-7995.
132 Y. Yang, D. M. Davies, Y. Yin, O. Borodin, J. Z. Lee, C. Fang, M. Olguin, Y. Zhang, E. S. Sablina, X. Wang, C. S. Rustomji and Y. S. Meng, *Joule*, 2019, **3**, 1986-2000.
133 B. Garcia, S. Lavallée, G. Perron, C. Michot and M. Armand, *Electrochim. Acta*, 2004, **49**, 4583-4588.
134 Y. Zhou, M. Su, X. Yu, Y. Zhang, J. G. Wang, X. Ren, R. Cao, W. Xu, D. R. Baer, Y. Du, O. Borodin, Y. Wang, X. L. Wang, K. Xu, Z. Xu, C. Wang and Z. Zhu, *Nat. Nanotechnol*., 2020, **15**, 224-230.
135 T. Li, X.-Q. Zhang, P. Shi and Q. Zhang, *Joule*, 2019, **3**, 2647-2661.
136 N. Ohba, S. Ogata and R. Asahi, *J. Phys. Chem. C*, 2019, **123**, 9673-9679.
137 L. A. Selis and J. M. Seminario, *RSC Adv.*, 2019, **9**, 27835.
138 L. Xu, B. Wang, F. Han, S. Liu, P. Sheng, H. Li, G. Zhao, X. Chen, H. Bai, T. Li and C. He, *Chem. Phys. Lett*., 2020, **744**, 137210.
139 T. Xie, A. France-Lanord, Y. Wang, Y. Shao-Horn and J. C. Grossman, *Nat. Commun.*, 2019, **10**, 2667.
140 B. V. Merinov, S. Naserifar, S. V. Zybin, S. V. Zybin, W. A. G. III, J. Lee, J. H. Lee, H. E. Han, Y. C. Choi and S. H. Kim, *J. Chem. Phys*., 2020, **152**, 031101.
141 B. Wu, G. Zhang, M. Yan, T. Xiong, P. He, L. He, X. Xu and L. Mai, *Small*, 2018, **14**, 1703850.
142 S. Matsuda, Y. Kubo, K. Uosaki and S. Nakanishi, *Carbon*, 2017, **119**, 119-123.
143 C. Niu, H. Pan, W. Xu, J. Xiao, J. G. Zhang, L. Luo, C. Wang, D. Mei, J. Meng, X. Wang, Z. Liu, L. Mai and J. Liu, *Nat. Nanotechnol.*, 2019, **14**, 594-601.
144 F. Zheng, Y. Yang and Q. Chen, *Nat. Commun.*, 2014, **5**, 5261.
145 T. Ichikawa, N. Hanada, S. Isobe, H. Leng and H. Fujii, *J. Phys. Chem. B*, 2004, **108**, 7887-7892.
146 H. K. Christenson, *CrystEngComm*, 2013, **15**, 2030.
147 E. Cha, M. D. Patel, J. Park, J. Hwang, V. Prasad, K. Cho and W. Choi, *Nat. Nanotechnol.*, 2018, **13**, 337-344.
148 Z. Cao, B. Li and S. Yang, *Adv. Mater.*, 2019, **31**, 1901310.
149 Q. Li, B. Quan, W. Li, J. Lu, J. Zheng, X. Yu, J. Li and H. Li, *Nano Energy*, 2018, **45**, 463-470.
150 H. Duan, J. Zhang, X. Chen, X. D. Zhang, J. Y. Li, L. B. Huang, X. Zhang, J. L. Shi, Y. X. Yin, Q. Zhang, Y. G. Guo, L. Jiang and L. J. Wan, *J. Am. Chem. Soc*., 2018, **140**, 18051-18057.
151 H. H. Chang, *Phys. Rev. E*, 2008, **78**, 056704.
152 C. Yang, H. Xie, W. Ping, K. Fu, B. Liu, J. Rao, J. Dai, C. Wang, G. Pastel and L. Hu, *Adv. Mater.*, 2019, **31**, 1804815.
153 E. Quartarone and P. Mustarelli, *Chem. Soc. Rev.*, 2011, **40**, 2525-2540.
154 V. Thangadurai, S. Narayanan and D. Pinzaru, *Chem. Soc. Rev.*, 2014, **43**, 4714-4727.
155 G.-y. Adachi, N. Imanaka and H. Aono, *Adv. Mater*., 1996, **8**, 127-135.
156 Z. D. Hood, H. Wang, A. Samuthira Pandian, J. K. Keum and C. Liang, *J. Am. Chem. Soc*., 2016, **138**, 1768-1771.
157 C. Galven, J.-L. Fourquet, M.-P. Crosnier-Lopez and F. o. Le Berre, *Chem. Mater.*, 2011, **23**, 1892-1900.
158 C. Ma, Y. Cheng, K. Yin, J. Luo, A. Sharafi, J. Sakamoto, J. Li, K. L. More, N. J. Dudney and M. Chi, *Nano Lett.*, 2016, **16**, 7030-7036.
159 Z. Zhang, Q. Zhang, Y. Chen, J. Bao, X. Zhou, Z. Xie, J. Wei and Z. Zhou, *Angew. Chem. Int. Ed.*, 2015, **54**, 6550-6553.
160 W. D. Richards, L. J. Miara, Y. Wang, J. C. Kim and G. Ceder, *Chem. Mater.*, 2015, **28**, 266-273.
161 X.-X. Zeng, Y.-X. Yin, N.-W. Li, W.-C. Du, Y.-G. Guo and L.-J. Wan, *J. Am. Chem. Soc*., 2016, **138**, 15825-15828.
162 L. Porcarelli, C. Gerbaldi, F. Bella and J. R. Nair, *Sci. Rep.*, 2016, **6**, 19892.
163 P. R. Chinnam and S. L. Wunder, *ACS Energy Lett.*, 2016, **2**, 134-138.
164 X. Han, Y. Gong, K. K. Fu, X. He, G. T. Hitz, J. Dai, A. Pearse, B. Liu, HowardWang, G. Rubloff, Y. Mo, V. Thangadurai, E. D.Wachsman and L. Hu, *Nat. Mater.*, 2016, **16**, 572.
165 A. Mukhopadhyay and M. K. Jangid, *Science*, 2018, **359**, 1463.
166 L. Zhou, K. Zhang, J. Sheng, Q. An, Z. Tao, Y.-M. Kang, J. Chen and L. Mai, *Nano Energy*, 2017, **35**, 281-289.
167 A. Kirchev, A. Delaille, M. Perrin, E. Lemaire and F. Mattera, *J. Power Sources*, 2007, **170**, 495-512.

168 X. Wang, W. Zeng, L. Hong, W. Xu, H. Yang, F. Wang, H. Duan, M. Tang and H. Jiang, *Nat. Energy*, 2018, **3**, 227-235.
169 D. Wang, C. Qin, X. Li, G. Song, Y. Liu, M. Cao, L. Huang and Y. Wu, *iScience*, 2020, **23**, 100781.
170 J. Liu, Z. Bao, Y. Cui, E. J. Dufek, J. B. Goodenough, P. Khalifah, Q. Li, B. Y. Liaw, P. Liu, A. Manthiram, Y. S. Meng, V. R. Subramanian, M. F. Toney, V. V. Viswanathan, M. S. Whittingham, J. Xiao, W. Xu, J. Yang, X.-Q. Yang and J.-G. Zhang, *Nat. Energy*, 2019, **4**, 180-186.
171 S. Chen, C. Niu, H. Lee, Q. Li, L. Yu, W. Xu, J.-G. Zhang, E. J. Dufek, M. S. Whittingham, S. Meng, J. Xiao and J. Liu, *Joule*, 2019, **3**, 1094-1105.
172 C. Niu, H. Lee, S. Chen, Q. Li, J. Du, W. Xu, J.-G. Zhang, M. S. Whittingham, J. Xiao and J. Liu, *Nat. Energy*, 2019, **4**, 551-559.
173 V. Pellegrini, S. Bodoardo, D. Brandell and K. Edström, *Solid State Commun*., 2019, 303-304, 113733.
174 Y. Jin, K. Liu, J. Lang, D. Zhuo, Z. Huang, C.-a. Wang, H. Wu and Y. Cui, *Nat. Energy*, 2018, **3**, 732-738.
175 Y. Li, W. Zhou, X. Chen, X. Lu, Z. Cui, S. Xin, L. Xue, Q. Jia and J. B. Goodenough, *Proc. Natl. Acad. Sci. U. S. A.*, 2016, **113**, 13313-13317.
176 X. Wang, R. Kerr, F. Chen, N. Goujon, J. M. Pringle, D. Mecerreyes, M. Forsyth and P. C. Howlett, *Adv. Mater.*, 2020, **32**, 1905219.
177 B. Commarieu, A. Paolella, J.-C. Daigle and K. Zaghib, *Cur. Opin. Electrochem*., 2018, **9**, 56-63.
178 J. Zhang, B. Sun, Y. Zhao, A. Tkacheva, Z. Liu, K. Yan, X. Guo, A. M. McDonagh, D. Shanmukaraj, C. Wang, T. Rojo, M. Armand, Z. Peng and G. Wang, *Nat. Commun*., 2019, **10**, 602.
179 Q. Zhao, X. Liu, S. Stalin, K. Khan and L. A. Archer, *Nat. Energy*, 2019, **4**, 365-373.
180 N. Zhao, W. Khokhar, Z. Bi, C. Shi, X. Guo, L.-Z. Fan and C.-W. Nan, *Joule*, 2019, **3**, 1190-1199.
181 C. Yan, P. Zhu, H. Jia, Z. Du, J. Zhu, R. Orenstein, H. Cheng, N. Wu, M. Dirican and X. Zhang, *Energy Storage Mater*., 2020, **26**, 448-456.
182 H. Huo, Y. Chen, R. Li, N. Zhao, J. Luo, J. G. Pereira da Silva, R. Mücke, P. Kaghazchi, X. Guo and X. Sun, *Energy Environ. Sci.*, 2020, **13**, 127-134.
183 F. Zhou, Z. Li, Y. Y. Lu, B. Shen, Y. Guan, X. X. Wang, Y. C. Yin, B. S. Zhu, L. L. Lu, Y. Ni, Y. Cui, H. B. Yao and S. H. Yu, *Nat. Commun*., 2019, **10**, 2482.
184 Y. Gao, Z. Yan, J. L. Gray, X. He, D. Wang, T. Chen, Q. Huang, Y. C. Li, H. Wang, S. H. Kim and T. E. Mallouk, *Nat. Mater.*, 2019, **18**, 384-389.
185 S. Kaboli, H. Demers, A. Paolella, A. Darwiche, M. Dontigny, D. Clement, A. Guerfi, M. L. Trudeau, J. B. Goodenough and K. Zaghib, *Nano Lett.*, 2020, **20**, 1607-1613.
186 F. Han, A. S. Westover, J. Yue, X. Fan, F. Wang, M. Chi, D. N. Leonard, N. J. Dudney, H. Wang and C. Wang, *Nat. Energy*, 2019, **4**, 187-196.
187 C. Sångeland, J. Mindemark, R. Younesi and D. Brandell, *Solid State Ionics*, 2019, **343**, 115068.
188 T. Krauskopf, R. Dippel, H. Hartmann, K. Peppler, B. Mogwitz, F. H. Richter, W. G. Zeier and J. Janek, *Joule*, 2019, **3**, 2030-2049.
189 S. Kim, H. Oguchi, N. Toyama, T. Sato, S. Takagi, T. Otomo, D. Arunkumar, N. Kuwata, J. Kawamura and S. I. Orimo, *Nat. Commun.*, 2019, **10**, 1081.
190 Y.-G. Lee, S. Fujiki, C. Jung, N. Suzuki, N. Yashiro, R. Omoda, D.-S. Ko, T. Shiratsuchi, T. Sugimoto, S. Ryu, J. H. Ku, T. Watanabe, Y. Park, Y. Aihara, D. Im and I. T. Han, *Nat. Energy*, 2020, **5**, 299-308.
191 C.-Z. Zhao, B.-C. Zhao, C. Yan, X.-Q. Zhang, J.-Q. Huang, Y. Mo, X. Xu, H. Li and Q. Zhang, *Energy Storage Mater.*, 2020, **24**, 75-84.
192 C. Fang, J. Li, M. Zhang, Y. Zhang, F. Yang, J. Z. Lee, M. H. Lee, J. Alvarado, M. A. Schroeder, Y. Yang, B. Lu, N. Williams, M. Ceja, L. Yang, M. Cai, J. Gu, K. Xu, X. Wang and Y. S. Meng, *Nature*, 2019, **572**, 511-515.
193 C. Wang, Y. Gong, J. Dai, L. Zhang, H. Xie, G. Pastel, B. Liu, E. Wachsman, H. Wang and L. Hu, *J. Am. Chem. Soc*., 2017, **139**, 14257-14264.
194 F. Sun, X. He, X. Jiang, M. Osenberg, J. Li, D. Zhou, K. Dong, A. Hilger, X. Zhu, R. Gao, X. Liu, K. Huang, D. Ning, H. Markötter, L. Zhang, F. Wilde, Y. Cao, M. Winter and I. Manke, *Mater. Today*, 2019, **27**, 21-32.
195 M. Kuhne, F. Borrnert, S. Fecher, M. Ghorbani-Asl, J. Biskupek, D. Samuelis, A. V. Krasheninnikov, U. Kaiser and J. H. Smet, *Nature*, 2018, **564**, 234-239.
196 G. E. Ice, J. D. Budai and J. W. Pang, *Science*, 2011, **334**, 1234-1239.
197 Oshima and Yoshifumi, *Microscopy*, 2017, **66**, 1-2.
198 Y. Li, Y. Li, A. Pei, K. Yan, Y. Sun, C.-L. Wu, L.-M. Joubert, R. Chin, A. L. Koh, Y. Yu, J. Perrino, B. Butz, S. Chu and Y. Cui, *Science*, 2017, **358**, 506-510.

199 F. Sun, R. Gao, D. Zhou, M. Osenberg, K. Dong, N. Kardjilov, A. Hilger, H. Markötter, P. M. Bieker, X. Liu and I. Manke, *ACS Energy Lett.*, 2019, **4**, 306-316.

200 D. Liu, Z. Shadike, R. Lin, K. Qian, H. Li, K. Li, S. Wang, Q. Yu, M. Liu, S. Ganapathy, X. Qin, Q. H. Yang, M. Wagemaker, F. Kang, X. Q. Yang and B. Li, *Adv. Mater.*, 2019, **31**, 1806620.